

NASA-CR-114593

Available to the Public

STUDY OF POROUS SURFACE MICROPHONES FOR ACOUSTIC MEASUREMENTS IN WIND TUNNELS

D.U. Noiseux

BBN Report No. 2539

PRICES SUBJECT TO CHANGE

April 1973

REPRODUCED BY
NATIONAL TECHNICAL
INFORMATION SERVICE
U. S. DEPARTMENT OF COMMERCE
SPRINGFIELD, VA. 22161

Submitted to:

NASA
Ames Research Center
Moffett Field, California 94035

Attn: Mr. Paul Soderman

(NASA-CR-114593) STUDY OF POROUS SURFACE
MICROPHONES FOR ACOUSTIC MEASUREMENTS IN
WIND TUNNELS (Bolt, Beranek, and Newman,
Inc.) 101 p CSCL 09A

G3/09 Unclas
02824

N73-23289

NAS 2-6844

STUDY OF POROUS SURFACE MICROPHONES FOR ACOUSTIC MEASUREMENTS
IN WIND TUNNELS

D.U. Noiseux

BBN Report No. 2539

April 1973

Submitted to:

NASA
Ames Research Center
Moffett Field, California 94035

Attn: Mr. Paul Soderman

TABLE OF CONTENTS

	page
I. INTRODUCTION	1
II. RESULTS	4
III. CONCLUSIONS	7
APPENDIX 1: TOLERANCES OF THE POROUS PIPE MICROPHONE	8
1. INTRODUCTION	8
2. MEAN AND VARIANCE	10
3. DISCUSSION	13
APPENDIX 2: CALIBRATION OF FOUR POROUS PIPE MICROPHONES ...	17
1. FLOW RESISTANCE AND SWR	17
2. RESPONSE	19
3. CONCLUSIONS	26
APPENDIX 3: EFFECT OF THE REACTIVE COMPONENT OF THE IMPEDANCE OF THE POROUS SURFACE ON THE RESPONSE OF A POROUS SURFACE SENSOR	28
1. ANALYSIS	28
2. SPECIFIC ACOUSTIC IMPEDANCE OF A POROUS SURFACE .	38
2.1 Sintered Porous Surface	40
APPENDIX 4: DESIGN AND PRELIMINARY RESULTS OF A POROUS SURFACE MICROPHONE IN AN AEROFOIL	42
1. EXPERIMENTAL RESULTS	46
APPENDIX 5: FREQUENCY RESPONSE AND DIRECTIVITY OF THE POROUS STRIP SENSOR IN AN AEROFOIL. DIRECTIVITY OF THE POROUS PIPE SENSOR	50

TABLE OF CONTENTS (Cont.)

	page
APPENDIX 6: WIND TUNNEL TESTS IN A QUIET FLOW	70
1. INTRODUCTION	70
2. WIND TUNNEL	70
3. RESULTS	71
4. CONCLUSION	82
APPENDIX 7: WIND TUNNEL TESTS IN A SPOILED FLOW	84
1. INTRODUCTION	84
2. FLOW SPOILER	85
3. RESULTS	89
4. DISCUSSION	89
5. CONCLUSIONS FROM THE TESTS IN THE SPOILED FLOW ..	95

I. INTRODUCTION

This report considers porous surface sensors acting as directional microphones in subsonic airflow.

The first part of the report deals with the design of a Porous Strip Sensor set in an aerofoil. The second part presents the experimental results of frequency response, directivity, and flow noise of a Porous Pipe Sensor and a Porous Strip sensor. For flow noise, these sensors are compared with the Bruel and Kjaer half-inch condenser microphone with a nose cone. The flow noise is examined under two conditions of flow: in a very quiet flow where the turbulence is approximately 0.3% and in a spoiled flow where the turbulence is approximately 5%.

The sensitivity $W(\omega, k_1)$ of a porous surface sensor is defined as the ratio of the pressure p_m on the surface of the microphone element to the pressure p on the porous surface,

$$\frac{p_m(\omega)}{p(\omega, k_1)} = W(\omega, k_1) \quad (1)$$

where ω is the frequency in radians per second, and k_1 is the wavenumber component of the pressure field along the axis of the sensor. The sensitivity could be separated into two factors

$$W(\omega, k_1) = H(\omega) w(k_1) \quad (2)$$

where $H(\omega)$ depends only on frequency and is called the frequency response and $w(k_1)$ depends only on the wavenumber k_1 and is called the directivity function.

For an ideal porous surface sensor¹ the frequency response is unity, and the directivity function is

$$w(k_1) = \frac{\sin(k_1 - k_0) L/2}{(k_1 - k_0) L/2} \quad (3)$$

where k_1 is the wavenumber of the gas inside the sensor and L is the length of porous surface.

A real porous surface sensor has a frequency response which decreases with frequency. The causes of this decrease are not fully understood. The viscous boundary layer at the inside surfaces of the sensor contributes to the drop in the frequency response; the reactive component of the acoustic impedance of the porous surface also contributes to the drop in the frequency response.

The directivity function of the ideal porous surface sensor, for a plane acoustic wave, where

$$k_1 = k_0 \cos \theta \quad (4a)$$

and for a sensor having air in its cavity,

$$k_1 = k_0 \quad (4b)$$

becomes

$$w(k_0 \cos \theta) = \frac{\sin[k_0(1 - \cos \theta)L/2]}{k_0(1 - \cos \theta)L/2} \quad (4c)$$

¹ D.U. Noiseux and T. Horwath, "Design of a Porous Pipe Microphone for the Rejection of Axial Flow Noise", in preparation.

k_0 being the acoustic wavenumber in air. Eq. (4c) is used to plot the directivity pattern in polar coordinate θ .

The directivity function of a real porous surface sensor follows the directivity of the ideal sensor, for its main lobe; the minor lobes deteriorate gradually, the deterioration depending primarily on the non-uniformity of the porosity (or acoustic impedance) of the porous surface.

The main feature of the porous surface sensor is that its directivity function $w(k_1)$ given by (3) extends well into the subsonic region: $|k_1| > k_0$; therefore the porous surface sensors have the property of filtering out those components of the pressure field which are predominantly subsonic, like those associated with a turbulent flow. The directivity function in the sonic region could also be useful in discriminating against unwanted sonic signals, like those in a reverberant acoustic field.

II. RESULTS

The results are presented in a set of seven Appendices which were originally written as memos during the course of this investigation. Appendices No. 1, 3 and 4 deal with the design of the aerodynamic Porous Strip Sensor; Appendices No. 2, 4 and 5 show the acoustic calibration of a Porous Pipe Sensor and an aerodynamic Porous Strip Sensor. Appendices No. 6 and 7 give the experimental results of flow noise in wind tunnel tests. Each appendix is reviewed in the following paragraphs.

Appendix No. 1 examines the non-uniformity of the porous surface for its effect on the directivity function. The main result is that the directivity function is bounded between the two limits $\pm\gamma$,

$$|w(k_1)| \leq \gamma \quad (5a)$$

given by

$$\gamma = \left| \frac{R_0}{s_0} \right|^{1/2} \sqrt{2 X_0/L} \quad (5b)$$

where s_0 is the mean value of the porosity of the porous surface, R_0 is the spatial correlation of the non-uniformities, and X_0 is the correlation length of the non-uniformities.

This limitation to the directivity function is, of course, undesirable because it tends to increase the flow noise sensed by the sensor. Eq. (5b) is used as a criterion for the tolerances in the selection of the porous surface.

Appendix No. 2 gives the acoustic calibration of a set of Porous Pipe Sensors, one of which was selected for later tests in the wind tunnel.

Appendix No. 3 considers the reactive component of the acoustic impedance of the porous surface and its effect on the frequency response and directivity function of a porous surface sensor. It shows that the reactive component should cause a significant drop in the frequency response. The reactive component of the porous surfaces has not been measured.

Appendix No. 4 presents the design of the Aerodynamic Porous Strip sensor and the measurement of its acoustic sensitivity.

Appendix No. 5 shows in considerable detail the directivity function, for a plane acoustic wave, of Porous Pipe and of the Aerodynamic Porous Strip sensors. The results are given in the familiar format of directivity patterns as a function of the angles of the direction of propagation of the plane wave with respect to the coordinates of the porous sensors.

The porous surface sensors are shown to follow the ideal directivity function for the main lobe of directivity, with a gradual deterioration of the minor lobes which is consistent with the analysis of Appendix 1.

Appendices No. 6 and 7 give the experimental results of flow noise sensed by the following three sensors in the BBN wind tunnel:

- Bruel & Kjaer half-inch condenser microphone with nose cone.
- Porous Pipe Sensor.
- Porous Strip Sensor in an aerofoil.

The wind tunnel has exhaust diameter of 24 inches and a maximum flow velocity of approximately 70 feet per second.

The first series of tests, given in Appendix No. 6, were made in a very quiet flow, the turbulence level being approximately 0.3%. All three sensors experience a low flow noise which increases as the angle ϕ between the axis of sensors and the flow direction is increased. The Porous Strip Sensor is quieter than the Porous Pipe or the Bruel & Kjaer microphone with a nose cone, for the same angle ϕ . However, the B&K sensor, being essentially omnidirectional, would always be oriented in the direction of flow, $\phi = 0$. The B&K sensor at $\phi = 0$, is quieter than the Porous Strip sensors at $\phi > 30^\circ$ but not as quiet for $\phi < 30^\circ$. In this condition of quiet flow the Porous Strip Sensor in an aerofoil would be advantageous only if its directivity is used to discriminate against unwanted *acoustic* noises, like those of a reverberant acoustic field.

The second series of tests, given in Appendix No. 7, were made in a turbulent flow, the turbulence level being approximately 5%. This turbulence is created by a Flow Spoiler which maintains a small ratio of acoustic noise to overall pressure fluctuations. In this turbulent flow the Porous Strip Sensor is quieter than the other two sensors at the same angle ϕ . In addition, the Porous Strip Sensor at all angles $0 \leq \phi \leq 90^\circ$ is quieter than the B&K sensor at $\phi = 0^\circ$.

III. CONCLUSIONS

The results obtained point to the superiority of the Porous Strip Sensor in an aerofoil over the Porous Pipe Sensor. This superiority is clear in the frequency response. For the flow noise the superiority is not a complete one. In certain regions of the angle ϕ , ($\phi \geq 60^\circ$), of the air flow with respect to the axis of the sensors and in a certain frequency region (around 4 kHz) both sensors have essentially the same flow noise; outside these regions the Porous Strip Sensor is superior. However, this excess flow noise in the Porous Strip Sensor can probably be reduced by a modification of the aerofoil.

In a very quiet flow the Porous Strip Sensor in an aerofoil at angles $\phi > 30^\circ$ senses a larger flow noise than the Bruel & Kjaer microphone with a Nose Cone when the latter one is operated only at $\phi = 0^\circ$. The only advantages of the Porous Strip Sensor are in its operation at $\phi \leq 30^\circ$ and its directivity to acoustic signals. In some applications this directivity may be more important than the level of flow noise: for example in discriminating the direct field from the reverberant field in the reverberant space of a wind tunnel.

In a turbulent flow the Porous Strip Sensor in an aerofoil, operated at all angles $0 \leq \phi \leq 90^\circ$, has a lower flow noise than the Bruel & Kjaer microphone with a nose cone operated only at $\phi = 0^\circ$. The results of the tests in a spoiled flow are an example. Again, the Porous Strip Sensor has the additional property of directivity to acoustic signals.

APPENDIX 1: TOLERANCES OF THE POROUS PIPE MICROPHONE

1. INTRODUCTION

All the components of the porous pipe microphone, except the porosity on the surface, are very well controlled; dimensions of the internal cone of the porous pipe, sensitivity of the condenser microphone. The specific flow resistance of the porous surface enters directly in the design equations, and is assumed to be uniform. In practice this specific flow resistance varies along the surface and becomes the main cause of variability of the response of the porous pipe microphone.

In this Memo we examine the effects of the tolerances of the specific flow resistance $r(x)$ on the response of the porous pipe microphone. This is done by assuming that the local sensitivity $s(x)$ of the porous pipe microphone, at a position x along the axis is exclusively dependent on the local specific flow resistance. This assumption is not quite correct, as will be shown later by examining the design procedure; however, it allows rather simple and useful criteria. Thus, our assumption is

$$s(x) \approx r(x) \quad (1)$$

and the results obtained in terms of $s(x)$ will be transferred to $r(x)$.

The local sensitivity $s(x)$ has an average component s_0 and a varying component $s'(x)$;

$$s(x) = s_0 + s'(x) . \quad (2)$$

The response $w(k_1)$ of the porous pipe microphone, normalized to unity at its maximum is

$$w(k_1) = \frac{1}{s_0 L} \int_{-L/2}^{+L/2} s(x) e^{-i(k_i - k_1)x} dx \quad (3)$$

where L is the length of the porous pipe sensor, k_i is the wave-number of the gas (air) inside the porous pipe, k_1 is the projection of the acoustic wavenumber vector \underline{k}_0 of a plane wave along the axis of the pipe

$$k_1 = |\underline{k}_0| \cos\theta . \quad (4)$$

For the ideal case where the sensitivity $s(x)$ is uniform, $s'(x) = 0$ in Eq. 2, we get the ideal response $w_0(k_1)$, using the subscript 0 to identify this ideal response:

$$w_0(k_1) = \frac{\sin(k_i - k_1)L/2}{(k_i - k_1)L/2} . \quad (5)$$

In practice we have the same gas inside and outside the porous pipe microphone:

$$k_i = k_0 \quad (6)$$

and Eq. 5 becomes

$$w_0(k_0 \cos\theta) = \frac{\sin[k_0(1 - \cos\theta)L/2]}{k_0(1 - \cos\theta)L/2} . \quad (7)$$

Equation 7 is the directivity pattern of the ideal porous pipe microphone in terms of the angle θ of the direction of the incident plane wave with respect to the axis of the porous pipe.

2. MEAN AND VARIANCE

The ensemble mean and variance of $w(k_1)$ will be evaluated in terms of the mean and variance of the local sensitivity $s(x)$.

Let the ensemble mean of $w(k_1)$ be $\langle w(k_1) \rangle$, the angular brackets indicating ensemble average; similarly, let the ensemble mean square value of $|w(k_1)|$ be $\langle |w(k_1)|^2 \rangle$. The variance γ^2 of the response is

$$\gamma^2 = \langle |w(k_1)|^2 \rangle - |\langle w(k_1) \rangle|^2 \quad (8)$$

The variance of the response will be related to the variance of the local sensitivity $s(x)$.

From Eq. 3, the ensemble mean is

$$\begin{aligned} \langle w(k_1) \rangle &= \frac{1}{s_0 L} \left\langle \int_{-L/2}^{+L/2} s(x) e^{-k(k_1 - k_1)x} dx \right\rangle \\ &= \frac{1}{s_0 L} \int_{-L/2}^{+L/2} \langle s(x) \rangle e^{-k(k_1 - k_1)x} dx \quad (9) \end{aligned}$$

The ensemble mean $\langle s(x) \rangle$ is s_0 , defined in Eq. 2. Hence, Eq. 9 becomes the ideal response $w_0(k_1)$:

$$\langle w_1(k_1) \rangle = w_0(k_1) \quad (10)$$

The ensemble mean square value of the magnitude of the response is

$$\begin{aligned}
\langle |w(k_1)|^2 \rangle &= \left\langle \frac{1}{s_0^2 L^2} \int_{-L/2}^{+L/2} s(x) e^{-i(k_1 - k_1)x} dx \right. \\
&\quad \times \left. \int_{-L/2}^{+L/2} s^*(x') e^{i(k_1 - k_1)x'} dx' \right\rangle \\
&= \frac{1}{s_0^2 L^2} \int_{-L/2}^{+L/2} dx \int_{-L/2}^{+L/2} \langle s(x)s^*(x') \rangle e^{-i(k_1 - k_1)(x-x')} dx'
\end{aligned} \tag{11}$$

where * means complex conjugate. Changing variables,

$$x - x' = x''$$

and modifying the limits of integration, we obtain

$$\langle |w(k_1)|^2 \rangle = \frac{1}{s_0^2 L^2} \int_{-L/2}^{+L/2} dx \int_{x-L/2}^{x+L/2} \langle s(x)s^*(x-x'') \rangle e^{-i(k_1 - k_1)x''} dx'' \tag{12}$$

The quantity $\langle s(x)s^*(x-x'') \rangle$ is the correlation function of the spatial variation of the local sensitivity. From Eq. 2 we obtain

$$\begin{aligned}
\langle s(x)s^*(x-x'') \rangle &= s_0^2 + \langle s'(x)s'^*(x-x'') \rangle \\
&= s_0^2 + R'(x, x'')
\end{aligned} \tag{13}$$

where $R'(x, x'')$ is the correlation function of the variable part of $s(x)$. The term s_0^2 will contribute exactly the value $|\langle w(k_1) \rangle|^2$ in Eq. 12. Hence, from Eq. 8 we get

$$\gamma^2 = \frac{1}{s_0^2 L^2} \int_{-L/2}^{+L/2} dx \int_{x-L/2}^{x+L/2} R'(x, x'') e^{-i(k_i - k_1)x''} dx'' . \quad (14)$$

Equation 14 is the main result: the variance γ^2 of the normalized response is related to the spatial correlation $R'(x, x'')$ of the variation of local sensitivity.

In order to evaluate Eq. 14 we will introduce some assumption about the character of the variability of $s'(x)$. Actual measurements of the variation of specific flow resistance of the porous surface suggest that the variations are almost random. Hence, we will assume that the variable part $s'(x)$ of $s(x)$ follows a random process, each porous pipe representing a sample of that process. We will further assume that this process is homogeneous, in the sense that the correlation function $R'(x, x'')$ does not depend on the location x on the porous surface but only on the spatial shift x'' , therefore

$$R'(x, x'') \rightarrow R'(x'') . \quad (15)$$

As a specific random process we choose a process characterized by a correlation distance x_0 :

$$R'(x'') = R'_0 e^{-|x''|/x_0} . \quad (16)$$

The correlation distance x_0 is a measure of the spatial scale of the variation of $s(x)$; Eq. 16 also implies that the local sensitivity $s(x)$ is real.

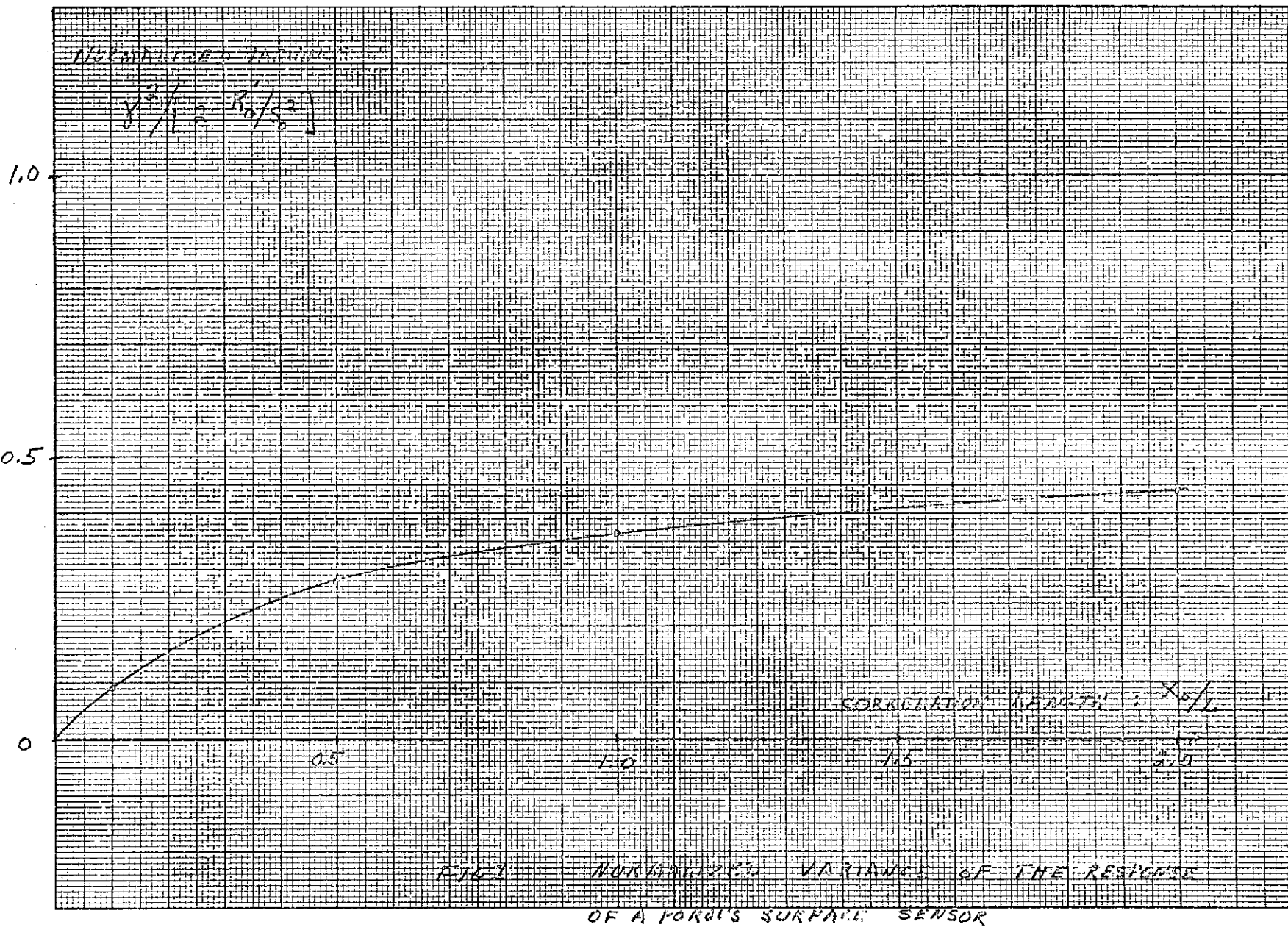
An upper limit to γ^2 is readily obtained with the assumption 16, by retaining only the modulus of the integrand in Eq. 14;

$$\begin{aligned}
\gamma^2 &\leq \frac{R'_0}{s_0^2 L^2} \int_{-L/2}^{+L/2} dx \int_{x-L/2}^{x+L/2} e^{-|x''|/x_0} dx'' \\
&\leq \frac{R'_0}{s_0^2 L^2} \int_{-L/2}^{+L/2} dx \left[\int_{x-L/2}^0 e^{-x''/x_0} dx'' + \int_0^{x+L/2} e^{-x''/x_0} dx'' \right] \\
&\leq \frac{2R'_0}{s_0^2} \frac{x_0}{L} \left[1 - \frac{x_0}{L} \left(1 - e^{-L/x_0} \right) \right] . \tag{17}
\end{aligned}$$

3. DISCUSSION

Equation 17 is the main result. R'_0 is the variance of the variable part of $s(x)$; R'_0/s_0^2 is the variance of the variable part $s(x)$, normalized to the square of the mean value s_0 of $s(x)$; x_0/L is the scale of variation of $s(x)$ normalized to the length L of the porous pipe. Equation 17 is plotted in Fig. 1, it shows that γ^2 increases linearly with the scale x_0/L of the variation of $s'(x)$. It follows that, in order to maintain a small variance γ^2 of the response of the sensor, we should have 1) a small variance R'_0/s_0^2 of the local sensitivity of the sensor, and 2) a small scale x_0/L of this variance.

The result 17 is independent of the wavenumber k_1 ; hence, this upper limit of the variance applies everywhere to the response $w(k_1)$. At large values of $w(k_1)$, near unity, the main lobe of the directivity is hardly affected provided γ^2 is relatively small; at small values of $w(k_1)$ the relative importance of the variance γ^2 becomes progressively larger until it dominates the response when $|w_1(k)|$ becomes comparable with γ . We could emphasize this result by assuming that the variation of $|w_1(k)|$ is



normally distributed. Therefore we would write

$$|w(k_1)| = |w_0(k_1)| \pm 2\gamma \quad (18)$$

with 95% confidence. When the ideal response $|w_0(k)|$ becomes very small, we see from Eq. 18 that $|w(k_1)|$ becomes limited to the standard deviation γ . Thus, if we want to realize low values of $|w(k_1)|$, we must achieve a low standard deviation γ , which means that both the standard deviation $\sqrt{R_0}/s_0$ of the local sensitivity $s(x)$ and the scale x_0/L of the variations in sensitivity must be kept small.

For example $w_0(k_1)$, given by Eq. 7, decreases with the argument $(k_1 - k_1)$, as shown in Fig. 2; at low values of $w_0(k_1)$, Eq. 18 indicates that the possible value of $|w_1(k)|$ may fall anywhere within the band zero to 2γ irrespective of the ideal value $w_0(k)$, provided it is less than 2γ .

A useful approximation of Eq. 17 for low values of x_0/L is

$$\gamma \leq \left(\frac{R_0}{s_0^2}\right)^{1/2} \times \sqrt{2 \frac{x_0}{L}} \quad (19)$$

This result will be used together with the interpretation of Fig. 2, to set the tolerances on the specific flow resistance of the porous surface.

APPENDIX 2: CALIBRATION OF FOUR POROUS PIPE MICROPHONES

Four porous pipe microphones have been calibrated including unit #3 which is the sensor used previously by Dave Bies (BBN) and István Vér (BBN) in the measurement of wind tunnel noise.

The purpose of these calibrations is to select the unit having the best response and use it later for comparison with the new porous surface microphone being designed under this contract.

The four sensors were subjected to the following measurements

- flow resistance of the open end of the sensor
- acoustic standing wave ratio (SWR)
- forward (0°) and backward (180°) frequency response.

The porous pipes sensors have 1/2" OD and a sensitive length of 12 inches.

1. FLOW RESISTANCE AND SWR

The flow resistance is measured at very small pressure drops, of the order of 0.5 inch of water, in order to simulate the low acoustic pressures. The porous surface has a constant flow resistance up to at least 5 inches of water.

The SWR is measured with a small impedance tube having the same inside diameter as the porous pipe. A small probe microphone traverses the impedances tube.

The experimental results are combined in the following table. The ideal value of the specific flow resistance z_0 at the open end of the sensors should be $1.0 \rho c$. The actual values vary from $1.15 \rho c$ up to $1.4 \rho c$ for the older sensor #3. These porous pipes have been selected for having a flow resistance closest to $1.0 \rho c$.

The SWR, at low frequencies, should closely relate to z_0 :

$$\text{SWR} = \frac{1 + \Gamma}{1 - \Gamma}$$
$$\Gamma = \left| \frac{z_0/\rho c - 1}{z_0/\rho c + 1} \right| .$$

If we assume that z_0 is purely real, then

$$\text{SWR} = z_0/\rho c$$

For example, if $z_0/\rho c = 1.2$, then $\text{SWR} = 1.2$ or 1.6 dB at low frequencies. At higher frequencies the SWR becomes a function of frequency, depending on the local variations of the porosity at the surface.

The SWR increases with frequency, indicating that $|z_0/\rho c|$ increases with frequency, probably due to a reactive component in z_0 . However, the accuracy of the measurements of SWR at higher frequencies are somewhat suspicious because the probe microphone is not sufficiently small to make the scattering of probe negligible.

Flow Resistance and SWR

Sensor #	Specific Flow Resistance of Open End: r/pc	SWR, dB				
		Frequency, Hz				
		200	400	800	1600	3200
3*	1.43	2.5 dB	0	1.8	2.4	2.5
30	1.17	2.0 dB	1.2	1.4	1.5	2.5
32	1.15	1.3 dB	0.9	1.0	1.9	2.5
65	1.2	1.2 dB	1.2	1.3	2.0	2.5

* Older BBN unit.

2. RESPONSE

The ideal response $W(\omega, k_1)$ of a sensor is separable into a frequency dependent factor and a wavenumber dependent factor:

$$W(\omega, k_1) = H(\omega)w(k_1)$$

$$w(k_0 \cos \theta) = \frac{\sin[k_0(1-\cos\theta)L/2]}{k_0(1-\cos\theta)L/2}$$

The factor $H(\omega)$ represents the frequency response; the factor $w(k_1)$ represents the directivity function; θ is the angle of incidence of a plane wave with respect to the axis of the pipe; k_0 is the acoustic wavenumber.

The frequency response $H(\omega)$ is measured by setting the angle of incidence θ to 0° ; the directivity function becomes unity. The directivity function is found by setting θ to 180° ; the sensor response becomes

$$W(-k_0) = H(\omega) \frac{\sin k_0 L}{k_0 L}$$

The difference, in dB, of the response at 0° and 180° gives the directivity function in dB.

The ideal directivity function has nulls at the wavenumbers

$$k_0 L = m\pi; m = 1, 2, 3, \dots$$

corresponding to frequencies

$$f = \frac{mc_0}{2L}; m = 1, 2, 3.$$

For these sensors we get the following frequencies of the nulls:

f	m
565 Hz	1
1130	2
1695	3

The maxima of the ideal directivity function and their frequencies are

$$w(k) \Big|_{\max} \begin{cases} = 1 & k_0 = 0 \\ = \frac{1}{k_0 L} & ; k_0 \neq 0 \end{cases}$$

which occur at wavenumbers $k_0 L = (2n-1)\pi/2$; $n = 2, 3, \dots$ and the corresponding frequencies $f = (2n-1) \frac{c}{4L}$:

f	max	n	
0 Hz	0 dB		main lobe
845	-13	2	1st minor lobe
1410	-18	3	2nd minor lobe
1980	-21	4	3rd minor lobe

The responses of the four sensors were measured in the anechoic room. Figures 1a to 1d show the response at 0° and 180° for each sensor.

The responses at 0°, giving the frequency function $H(\omega)$, decrease gradually with frequency. The recent sensors, #30, #32, #65, have a smaller drop at 10 kHz than the older sensor #3, a difference of 6 dB due to the higher flow resistance of sensor #3 compared with the recent sensors. However, the main cause of the decrease in frequency response of the sensors is not yet fully understood. It is due in part to the shear viscous layer of the inside surfaces of the sensors and, in part, to the increase with frequency of the specific impedance of the porous surface; this increase being attributed to a reactive component gradually dominating the sensitive component. This latter effect may be corrected by using a material which is thinner and has a lower porosity.

The directivity function follows approximately the maxima and nulls of the ideal directivity function, at least at low frequencies; the first and second minor lobes are approximately 13 dB and 18 dB down from the main lobe. The next minor lobes become limited to approximately 20 dB. (The response at 180° is limited by acoustic noise in the anechoic room and electrical noise in the region of 10 kHz.) This limitation of the minor



Brüel & Kjær

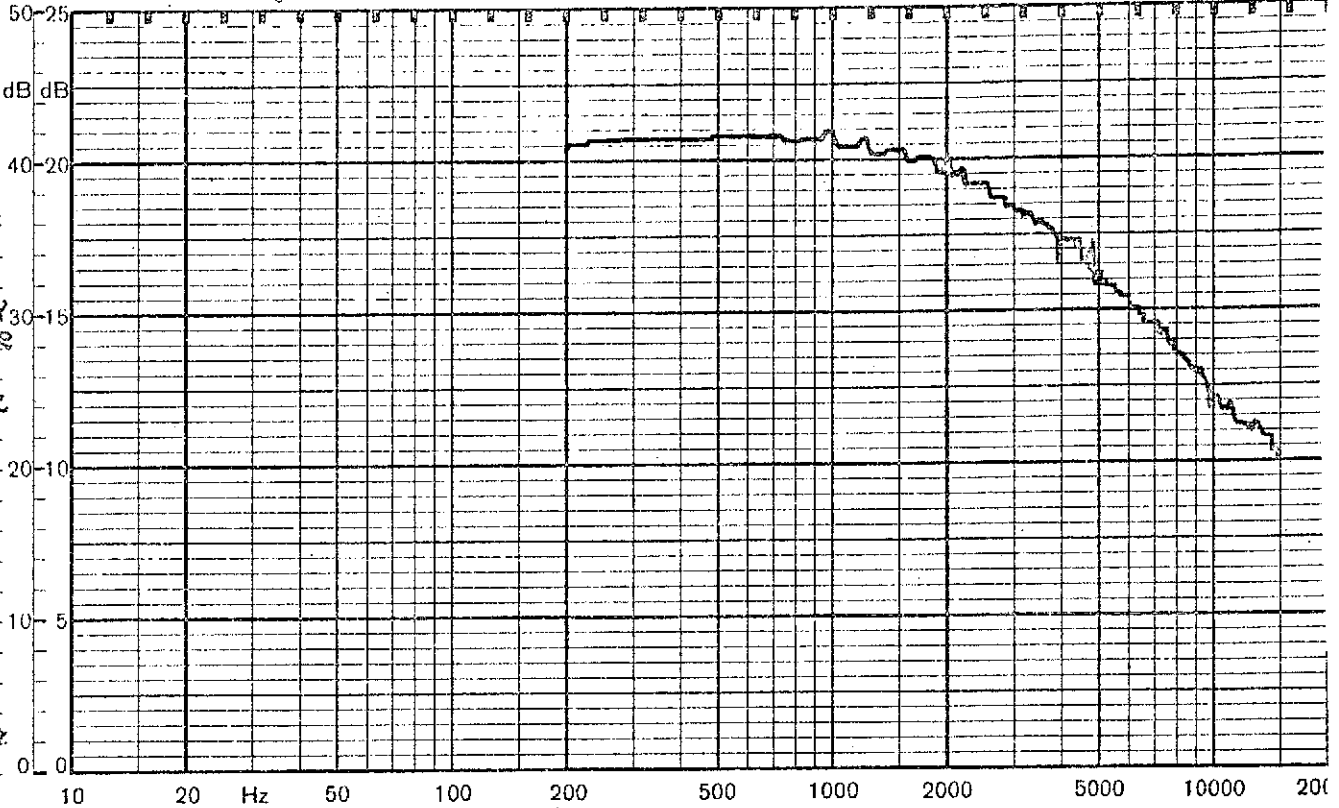
Brüel & Kjær

Brüel & Kjær

Brüel & Kjær

Potentiometer Range: 5.0 dB Rectifier: RMS Lower Lim. Freq.: 200 Hz Wr. Speed: 100 mm/sec

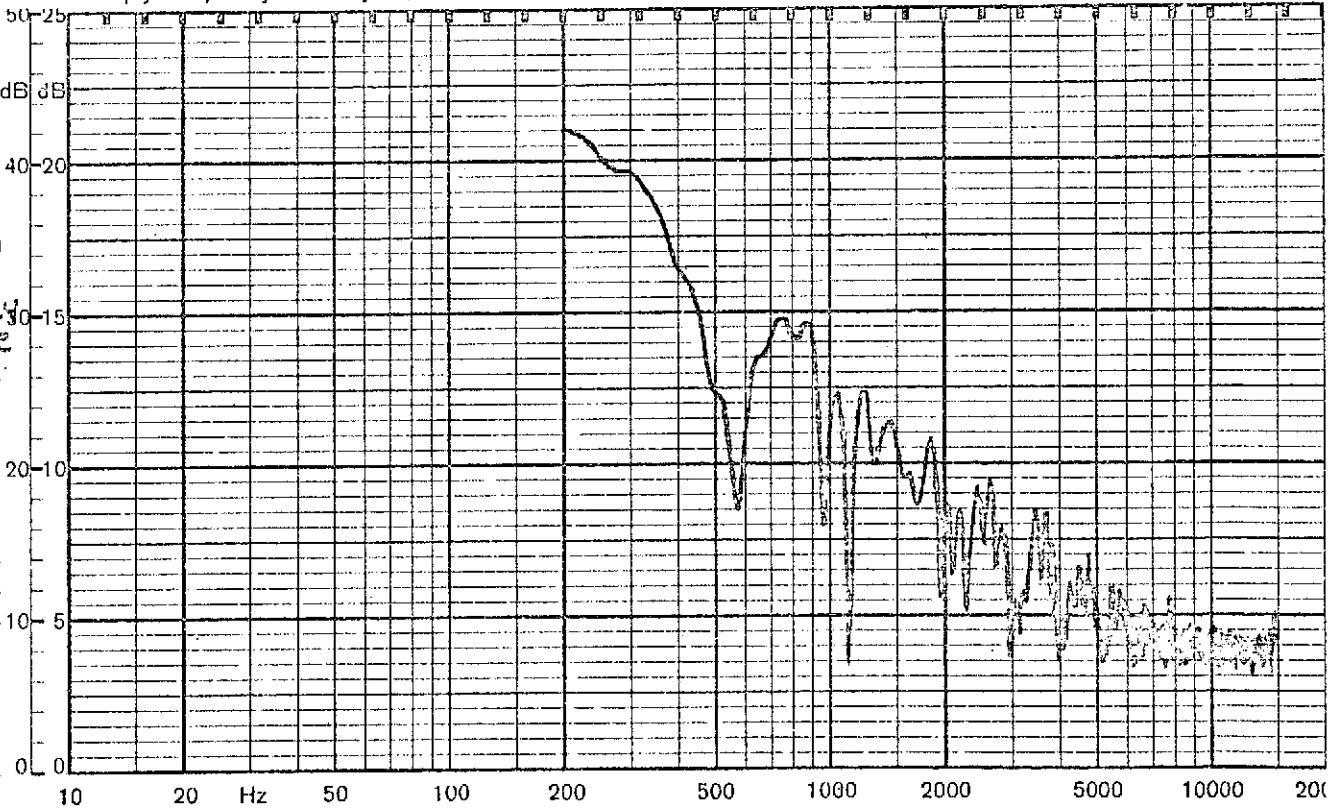
Copenhagen



QP 1124

Multiply Frequency Scale by 1 Zero Level: 3 (1612/21)

Copenhagen



QP 1124

Multiply Frequency Scale by 1 Zero Level: 8 (1612/21)

SPECIFIC FLOW RESISTANCE

510 MKS W/4L

STANDING WAVE RATIO 400 cps

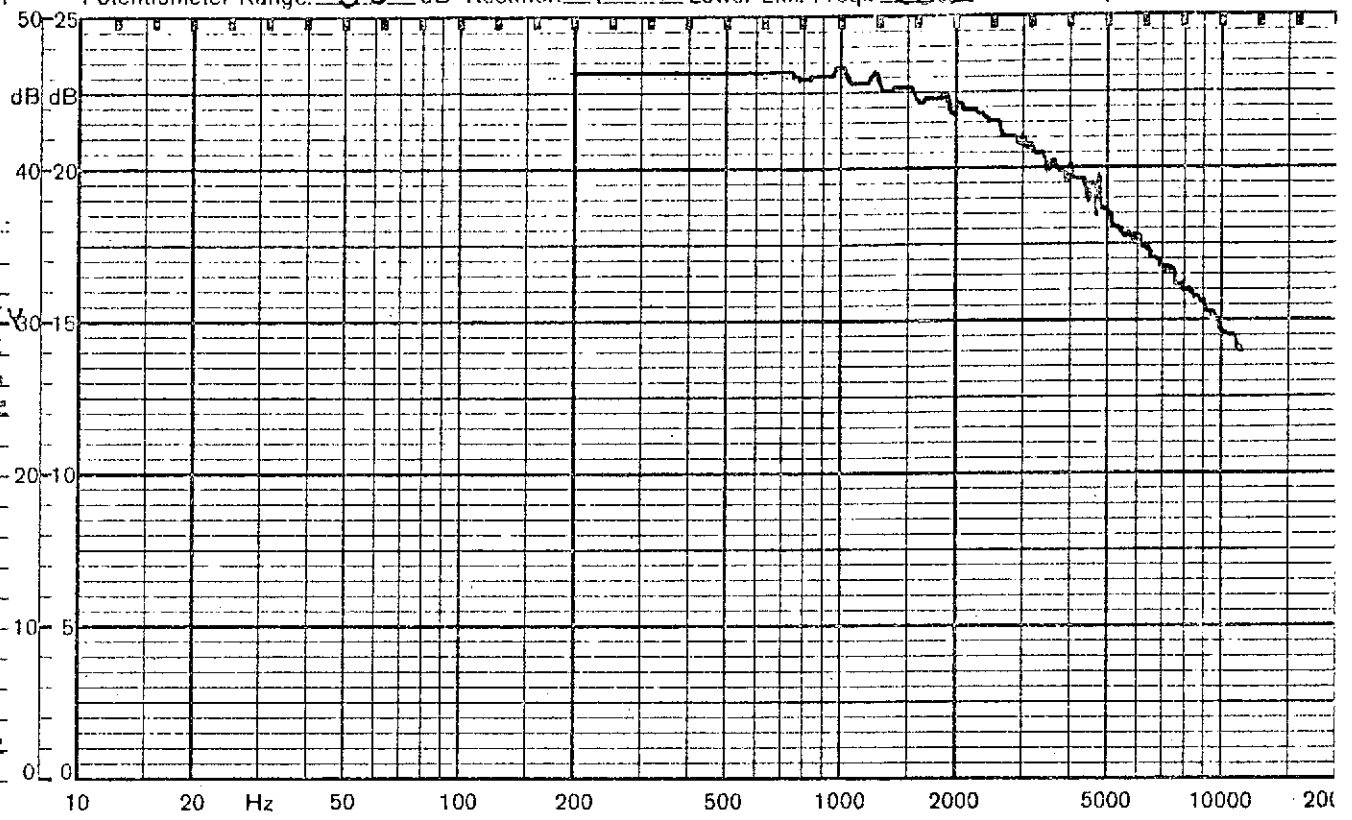
1.2 db

Brüel & Kjær
Copenhagen

Potentiometer Range: 50 dB Rectifier: V_{rms} Lower Lim. Freq.: 200 Hz Wr. Speed: _____ mm/sec

Measuring Obj.:
PIPE 32
0°
FREQUENCY
RESPONSE
50 db
range

Rec. No.:
Date: 6/9/72
Sign.: RS



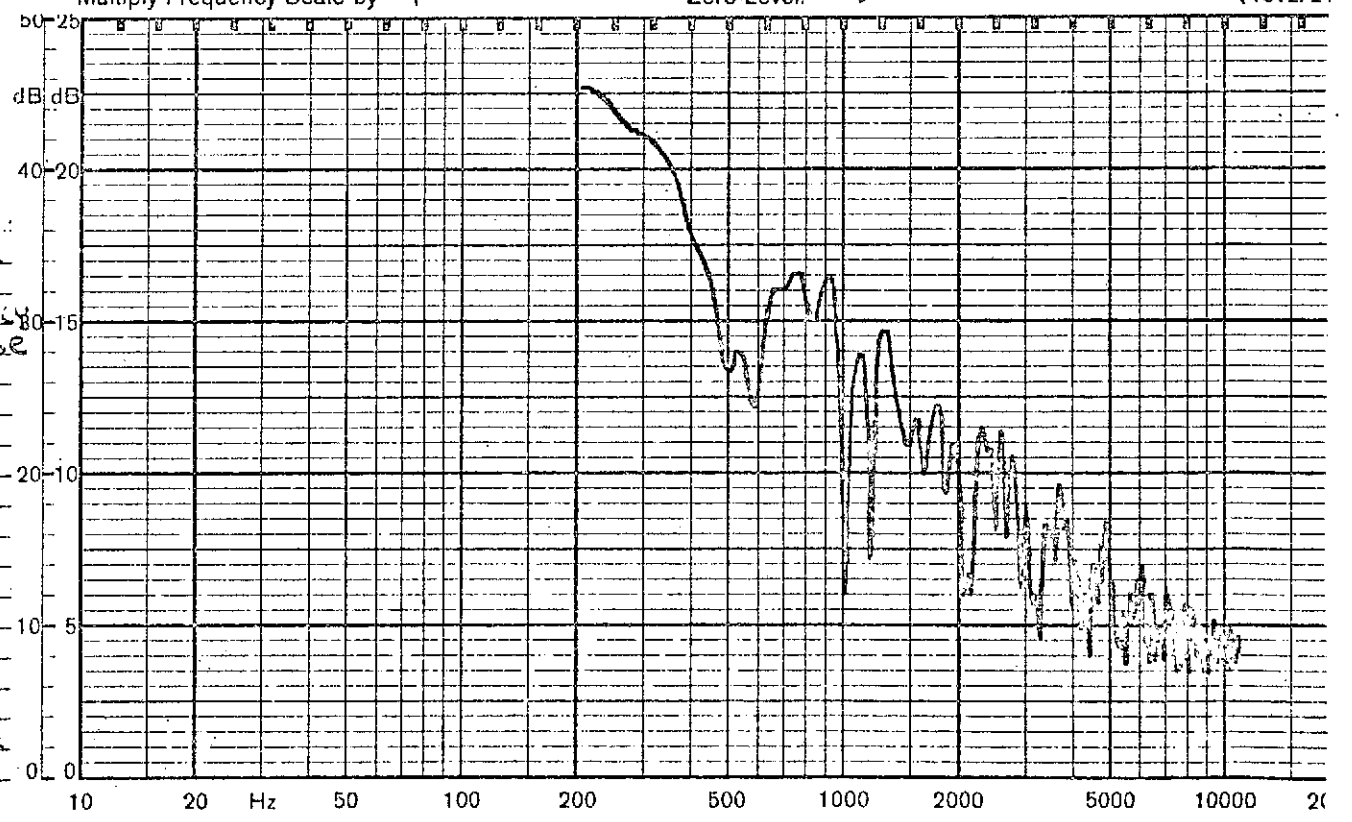
QP 1124

Multiply Frequency Scale by 1 Zero Level: 8 (1612/21)

Copenhagen

Measuring Obj.:
PIPE 32
180°
FREQUENCY
RESPONSE
50 db
range

Rec. No.:
Date: 6/9/72
Sign.: N²



QP 1124

Multiply Frequency Scale by 1 Zero Level: 8 (1612/2)

SPECIFIC FLOW RESISTANCE 482 mks rayl
STANDING WAVE RATIO 400 cps .9 db



Brüel & Kjær

Brüel & Kjær

Brüel & Kjær

Brüel & Kjær

Potentiometer Range: _____ dB Rectifier: _____ Lower Lim. Freq.: _____ Hz Wr. Speed: _____ mm/sec

Copenhagen



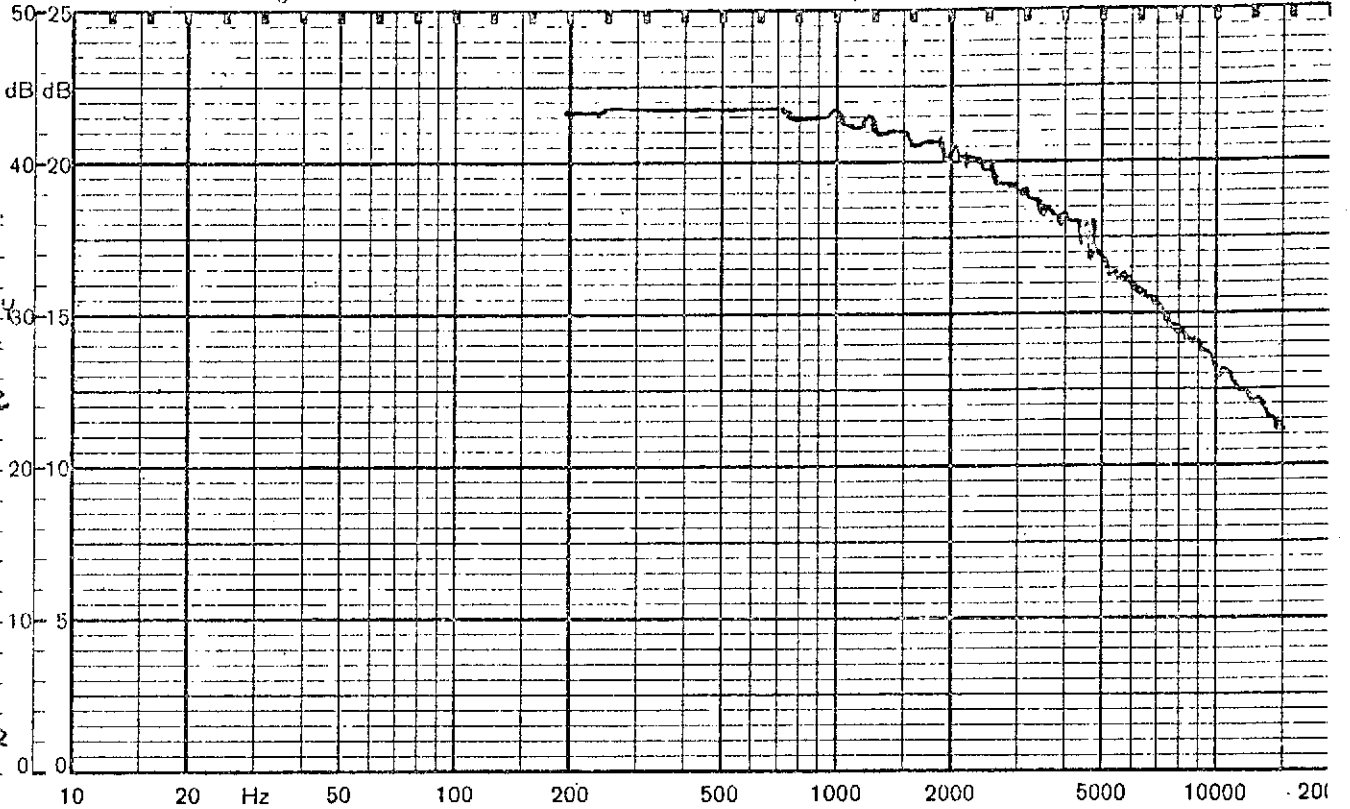
Measuring Obj.:

PIPE 65
0°
FREQUENCY
RESPONSE
50 db
range

Rec. No.:

Date: 6/9/72

Sign.: N



QP 1124

Multiply Frequency Scale by _____

Zero Level: 0

(1612/21)

Copenhagen



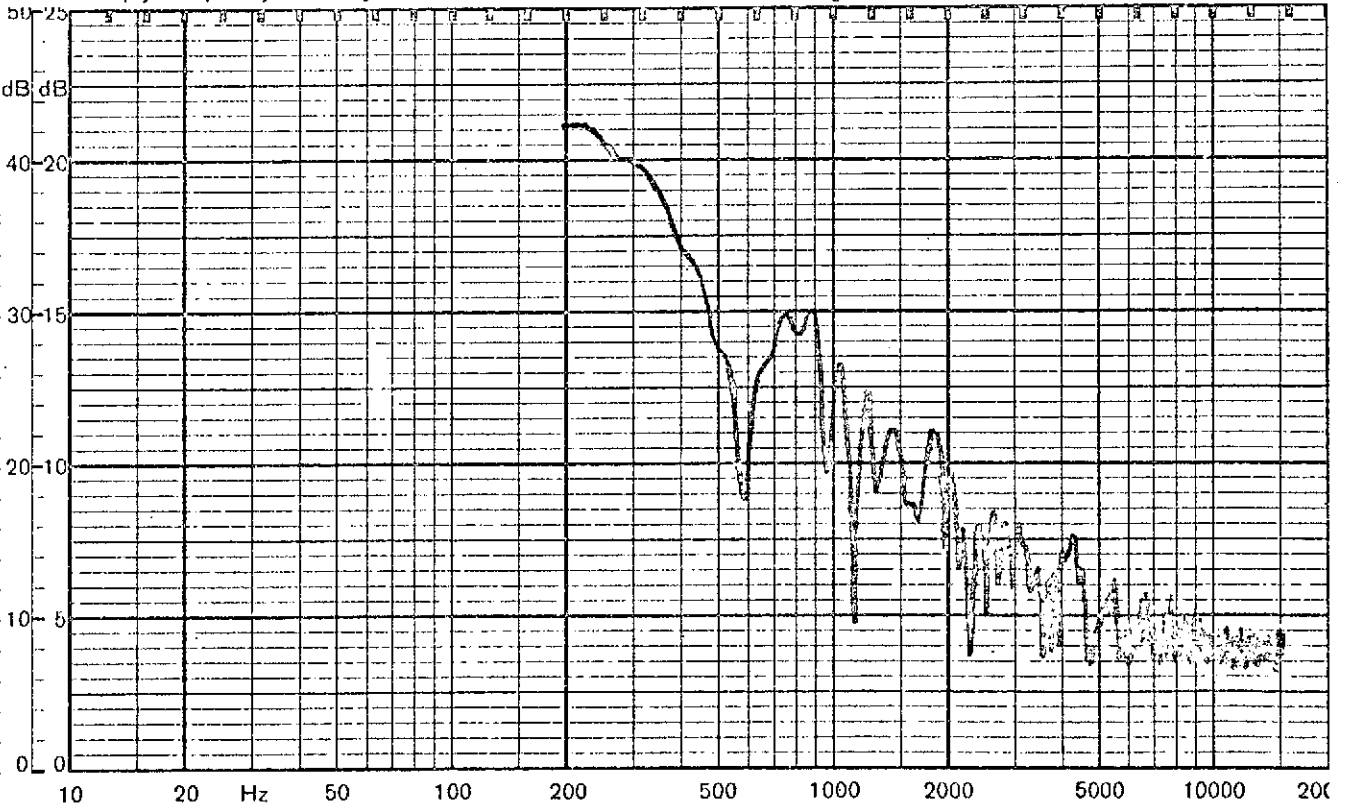
Measuring Obj.:

PIPE 65
180°
FREQUENCY
RESPONSE
50 db
range

Rec. No.:

Date: 6/9/72

Sign.: N



QP 1124

Multiply Frequency Scale by _____

Zero Level: _____

(1612/21)

SPECIFIC FLOW RESISTANCE

502 MKS rayl

STANDING WAVE RATIO 400 cps

1.2 db

Brüel & Kjær

Potentiometer Range: _____ dB Rectifier: _____ Lower Lim. Freq.: _____ Hz Wr. Speed: _____ mm/sec

Copenhagen



Measuring Obj.:

BBN III
STD.

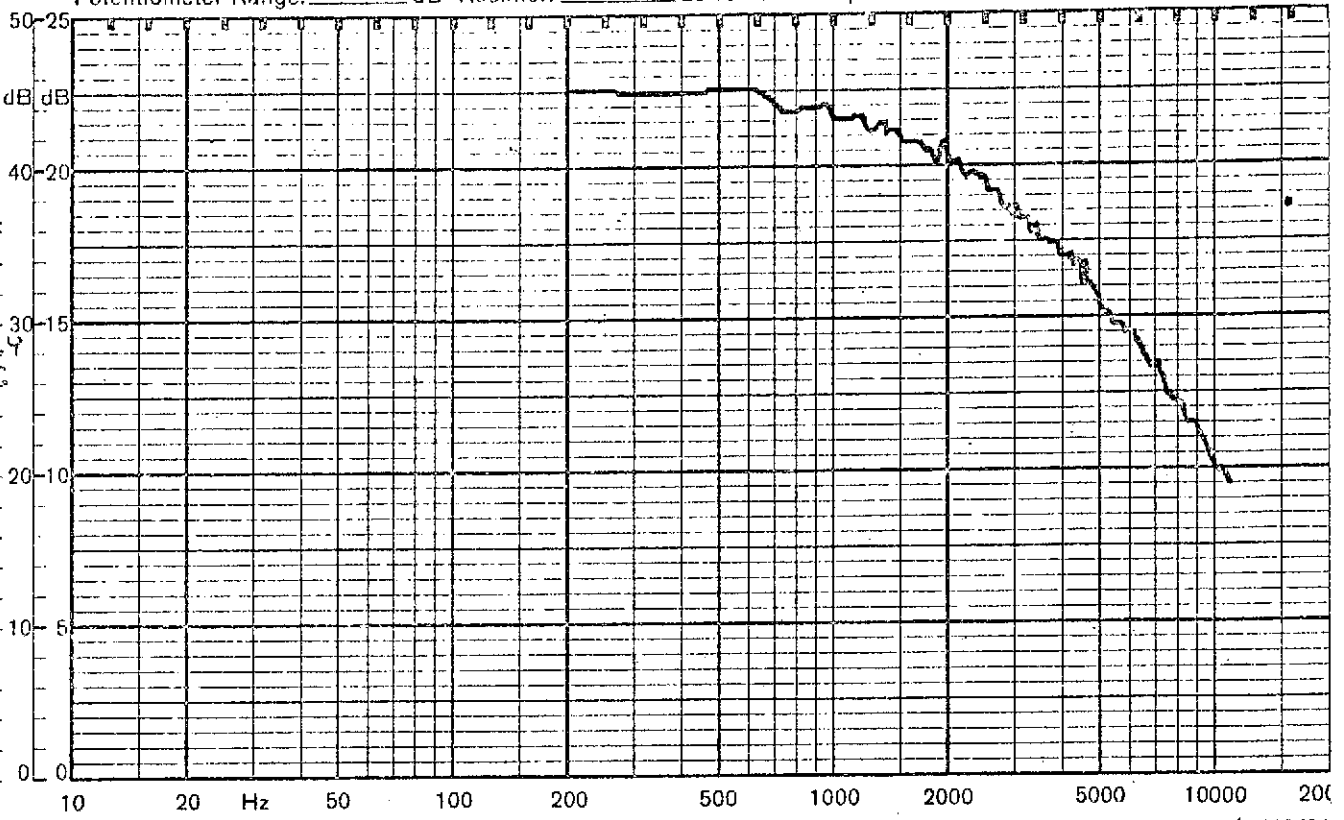
Al cone
Frequency
response

0°
50 db
range

Rec. No.:

Date: 6/9/72

Sign.: *N*



QP 1124

Multiply Frequency Scale by _____

Zero Level: _____

(1612/21)

Copenhagen



Measuring Obj.:

BBN III
Std

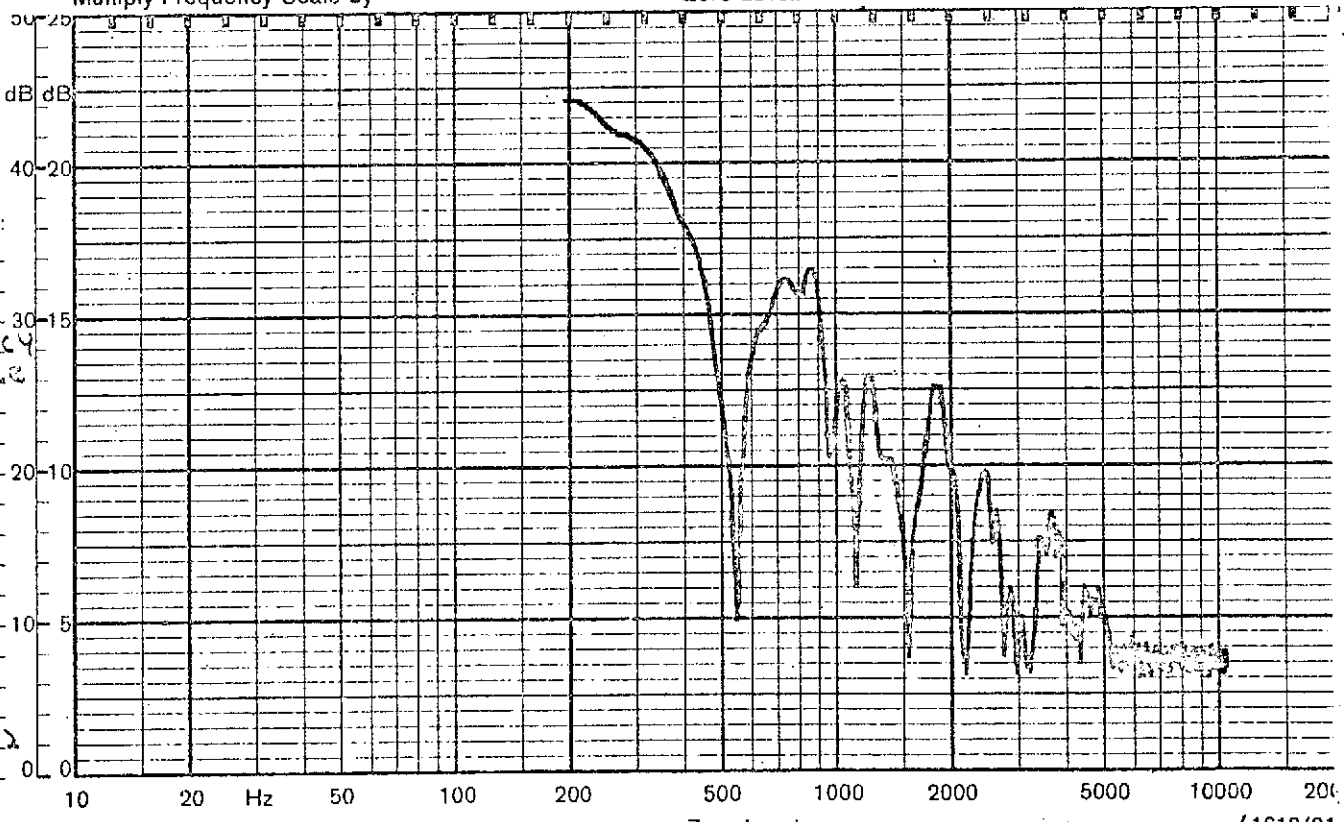
Al cone
Frequency
response

50 db
range

Rec. No.:

Date: 6/9/72

Sign.: *N*



QP 1124

Multiply Frequency Scale by _____

Zero Level: _____

(1612/21)

SPECIFIC FLOW RESISTANCE 595 mks rayl
 STANDING WAVE RATIO 400 cps 0 db

e

lobes is attributed to the variations of the specific flow resistance along the length of the porous pipes. See Memo No. 1, Eq. (19): allowing a variation $\sqrt{R_0}/s_0$ of 10% and a correlation length $x_0/L = 1/4$, the limit to the responses of the minor lobes becomes 2γ , which is approximately -17 dB. Thus, the levels of the minor lobes could be as high as -17 dB with respect to the main lobes, where the ideal response should be less than -20 dB.

3. CONCLUSIONS

1. The directivity function $w(k_1)$ of the real porous pipe microphone appears to be limited to approximately -20 dB. This limitation is not serious for acoustic signals (in the acoustic wavenumber range $-k_0$ to $+k_0$); however, it is more serious for subsonic wavenumbers (which have values of k_1 larger than k_0). For example, the turbulent boundary layer on the surface of the pipe for axial flow has a wavenumber spectrum k_1 showing a maximum in the vicinity of $\omega/0.7U_\infty$ where U_∞ is the free flow velocity. This maximum, occurring at $k_0(0.7M)^{-1}$, where M is the Mach number, corresponds to large values of k_1 where the directivity function is limited. Hence, the real sensor will not have as good a rejection of flow noise as the ideal one. Nevertheless, the rejection of flow noise is substantial.

In order to achieve a better rejection of flow noise, the specific flow resistance of the porous surface should be more uniform, as discussed in Memo No. 1.

2. Improving the frequency response function $H(\omega)$ demands a sensor with very smooth inner surfaces; also the specific surface impedance of the porous pipe should have a smaller reactive component.

These improvements are being considered for the new porous surface sensor being developed.

3. The sensors #30, #32, #65 are preferred to the older sensor #3; their frequency response $H(\omega)$ is higher at 10 kHz. The directivity functions $w(k_1)$ of sensor #3 has an excessive peak near 2 kHz.

APPENDIX 3: EFFECT OF THE REACTIVE COMPONENT OF THE IMPEDANCE
OF THE POROUS SURFACE ON THE RESPONSE OF A POROUS
SURFACE SENSOR

We re-examine the wave equation in a leaky horn¹, introducing the complex surface impedance of the porous surface.

We show that the reactive component of the surface impedance of the porous surface accounts for a major portion of the drop in the frequency response of the sensor.

The first part presents the analysis. In the second part we apply the results of the analysis to a sintered porous surface.

1. ANALYSIS

The wave equation in a leaky horn should be written in terms of the specific impedance $Z_w(x)$ of the porous surface, allowing this impedance to be complex. The conditions for anechoic termination in the +x direction is then rewritten as

$$S(x) (k_i^2 - k^2) - ik \frac{\partial S(x)}{\partial x} - ik_i y_w(x) \rho_i c_i C(x) = 0 \quad (1)$$

where again the viscous boundary layer *inside* the porous sensor is neglected; $y_w(\omega)$ is the specific admittance of the porous surface

¹ D.U. Noiseux and T.G. Horwath, "Design of a Porous Pipe Microphone for the Rejection of Axial Flow Noise." In preparation; to be submitted to JASA.

$$\begin{aligned}
 y_w(x) &= [z_w(x)]^{-1} \\
 &= g_w - ib_w .
 \end{aligned} \tag{2}$$

The reactive part b_w will be negative when z_w has a mass reactance component;

$$z_w = r_w + i\omega m , \tag{3}$$

$$y_w = \frac{r_w - i\omega m}{r_w^2 + (\omega m)^2} . \tag{4}$$

The real and imaginary parts of Eq. 1 are equated separately to zero, giving

$$S(x) (k_i^2 - k^2) - b_w(x) k_i \rho_i c_i C(x) = 0 \tag{5a}$$

$$k \frac{\partial S(x)}{\partial x} + g_w(x) k_i \rho_i c_i C(x) = 0 . \tag{5b}$$

If the reactive part ωm of the specific impedance z_w is zero,

$$z_w = r_w \tag{6a}$$

the first Eq. 5a reduces to

$$k = k_i \tag{6b}$$

and the second Eq. 5b gives

$$\frac{\partial S(x)}{\partial x} = - \frac{\rho_i c_i}{r_w(x)} C(x) . \tag{6c}$$

Equations 6 are the basic equations for the design of the porous surface sensor for the ideal case where the impedance of the porous surface is purely real.

When $b_w(x)$ is nonzero in Eq. 5a, we can approximate its effect by a perturbation method. We consider the case of an unshaded sensor where the ratio $C(x)/r_w(x)$ is a constant

$$C(x)/r_w(x) = \text{constant} , \quad (7a)$$

giving in Eq. 5b,

$$S(x) = S_0(1 - x/L) \quad (7b)$$

satisfying the boundary conditions $S(0) = S_0$, $S(L) = 0$. For a flat porous strip sensor

$$S_0 = wh_0 \quad (8a)$$

$$C(x) = w \quad (8b)$$

$$r_w = \rho_i c_i L/h_0 , \quad (8c)$$

where h_0 is the height of the base of the wedge and L is its length.

The ideal solution (7) and (8) is introduced in Eq. 5a to yield

$$k^2 - k_1^2 + \frac{b_w k_1 \rho_i c_i C}{S_0(1-x/L)} = 0 \quad (9a)$$

$$k^2 \cong k_1^2 \left(1 - \frac{\beta}{1-x/L} \right) \quad (9b)$$

where

$$\beta = \frac{m\rho_i c_i^2 C}{[r_w^2 + (\omega m)^2] S_0} \quad (10)$$

is the error in wavenumber caused by the presence of a reactive component in the specific impedance z_w of the porous surface. Beyond the cut-off frequency ω_c ,

$$\omega_c = \frac{r_w}{m} \quad (11)$$

the value of β decreases rapidly with frequency. Hence the effect of β on the free propagating wavenumber k is significant only for frequencies up to ω_c . We can examine this effect in more details as follows.

The condition for anechoic termination (1) is also used, by reciprocity, to obtain the sensitivity and directivity of the sensor. When the reactive component of z_w is zero, that is $m = 0$, the sensitivity and directivity is given by the integral

$$\left| \frac{1}{L} \int_0^L e^{-i(k_i - k_1)x} dx \right| = \frac{\sin(k_i - k_1)L/2}{(k_i - k_1)L/2} \quad (12a)$$

where k_1 is the axial component of the wavenumber vector of a plane incident wave of wavenumber k_0 :

$$k_1 = k_0 \cos\theta \quad (12b)$$

θ being the angle of the direction of propagation of the plane wave with the axis of the sensor.

When the modified wavenumber k of Eq. 9b is introduced in place of k_1 in Eq. 12 we get the modified directivity I :

$$I = \frac{1}{L} \int_0^L e^{-i \left[k_1 \left(1 - \frac{\beta}{1-x/L} \right)^{1/2} - k_1 \right] x} dx . \quad (13a)$$

The presence of a reactive component of z_w appears to affect both the frequency response and the directivity of the sensor; writing

$$I = I(\omega, k_1) \quad (13b)$$

we do not see offhand how to separate I into two independent factors; one representing the frequency response, the other representing the directivity function.

Equation 13 has not been evaluated in its complete form. A first approximation is to assume that the term

$$\frac{\beta}{1-x/L} \ll 1 \quad (14a)$$

is much smaller than unity; although β will, in practice, be very small, the term becomes very large when x/L is near unity, at the end of the porous sensor.

With the approximation 14a, the internal wavenumber k in Eq. 9b becomes

$$k \cong k_1 \left[1 - \frac{\beta}{2(1-x/L)} \right] . \quad (14b)$$

Using Eq. 14b we can now solve I for the special case where $\theta = 0$ and the gas inside the sensor is the same as the outside gas:

$$k_1 = k_0 \quad (14c)$$

$$I(\omega, k_0) = \frac{1}{L} \int_0^L e^{+i \frac{k_1 \beta x}{2(1-x/L)}} dx \quad (14d)$$

If the same case $\theta = 0$, and $k_1 = k_0$ is applied to the ideal response of Eq. 12, this ideal response would be unity. However the real response (Eq. 14d) becomes a function of frequency because k_1 ,

$$k_1 = \omega/c_1 \quad (15)$$

is a function of frequency. The response (Eq. 14d) may be considered as the frequency response of the sensor, in a rather loose sense.

The effect of the reactive component in z_w is to *decrease* the internal wavenumber k_1 by at least the factor $(1 - \beta)$, the decrease becoming larger as x/L goes to unity, that is as we reach the far end of the porous surface. It follows that perfect matching of the internal and external wavenumbers is not possible; hence the apparent drop in frequency response.

We now solve Eq. 14: introduce the new variable

$$\frac{x/L}{1-x/L} = y - 1 \quad (16)$$

into Eq. 14:

$$I(\omega, k_0) = e^{-ik_1 \beta L/2} \int_1^L \frac{e^{i(k_1 \beta L/2)y}}{y^2} dy \quad (17a)$$

$$= 1 + ik_1 \beta L/2 e^{-ik_1 \beta L/2} \int_{k_1 \beta L/2}^L \frac{e^{it}}{t} dt \quad (17b)$$

$$= 1 - i(k_1 \beta L/2) e^{-ik_1 \beta L/2} [Ci(k_1 \beta L/2) + i(Si(k_1 \beta L/2) - \pi/2)] \quad (17c)$$

where $Ci(u)$ and $Si(u)$ are the cosine and sine integrals,

$$Ci(u) = - \int_u^L \frac{\cos t}{t} dt \quad (18a)$$

$$Si(u) - \pi/2 = - \int_u^L \frac{\sin t}{t} dt \quad (18b)$$

which are tabulated².

At small values of $(k\beta L/2)$ Eq. 17c goes to unity.

Combining separately the real and imaginary parts of Eq. 17 we obtain

$$I(\omega, k_0) = 1 + p\{[Si(p) - \pi/2]\cos p - Ci(p)\sin p\} - ip\{[Si(p) - \pi/2]\sin p + Ci(p)\cos p\} \quad (19a)$$

$$p = \beta k_1 L/2 \quad (19b)$$

At low values of p we can use the approximations

²Abramovitz and Stegun, *Handbook of Mathematical Functions*, Dover Publications, Chapter V.

$$\sin p \cong p \dots$$

$$\cos p \cong 1 \dots$$

$$\text{Si}(p) \cong p \dots$$

$$\text{Ci}(p) \cong \gamma + \ln p \dots$$

and Eq. 19 reduces to

$$\begin{aligned} I(\omega, k_0) &\cong 1 + p[(p - \pi/2) - (\gamma + \ln p)p] \\ &\quad - ip[(p - \pi/2)p + (\gamma + \ln p)] \\ &\cong 1 - \pi/2 p - i(\gamma + \ln p)p ; \quad p \ll 1 \end{aligned} \quad (20)$$

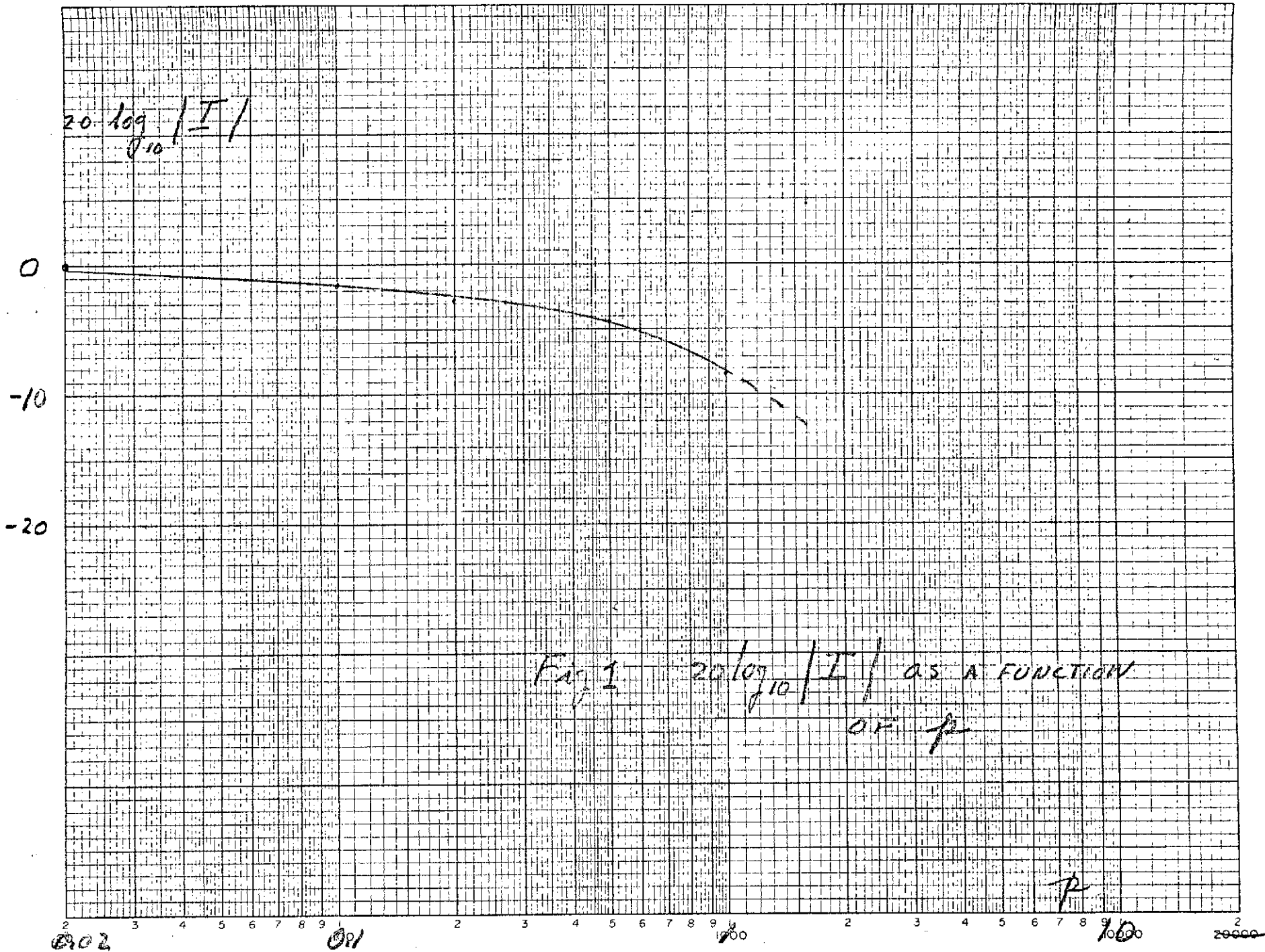
where γ is Euler's constant.

The value of $|I|$ is shown in Fig. 1 as a function of the parameter p . We should recall that p is a function of frequency,

$$\begin{aligned} p &= \beta k_1 L/2 \\ &= \frac{\omega m \rho_i c_i C L/2}{[r_w^2 + (\omega m)^2] S_0} \\ &= \frac{\rho_i c_i C_0 L/2}{r_w S_0} \left[\frac{\omega/\omega_c}{1 + (\omega/\omega_c)^2} \right]. \end{aligned} \quad (21)$$

It increases with frequency up to a maximum at $\omega/\omega_c = 1$ and decreases afterwards; see the sketch in Fig. 2.

The curve of Fig. 1 indicates that the reactive part of the impedance z_w of the porous surface could account for most of the drop in frequency response ($\theta = 0$), of the porous sensor. Typical values of β and p will be examined in the next section.



$20 \log \frac{p}{p_0}$

10 dB

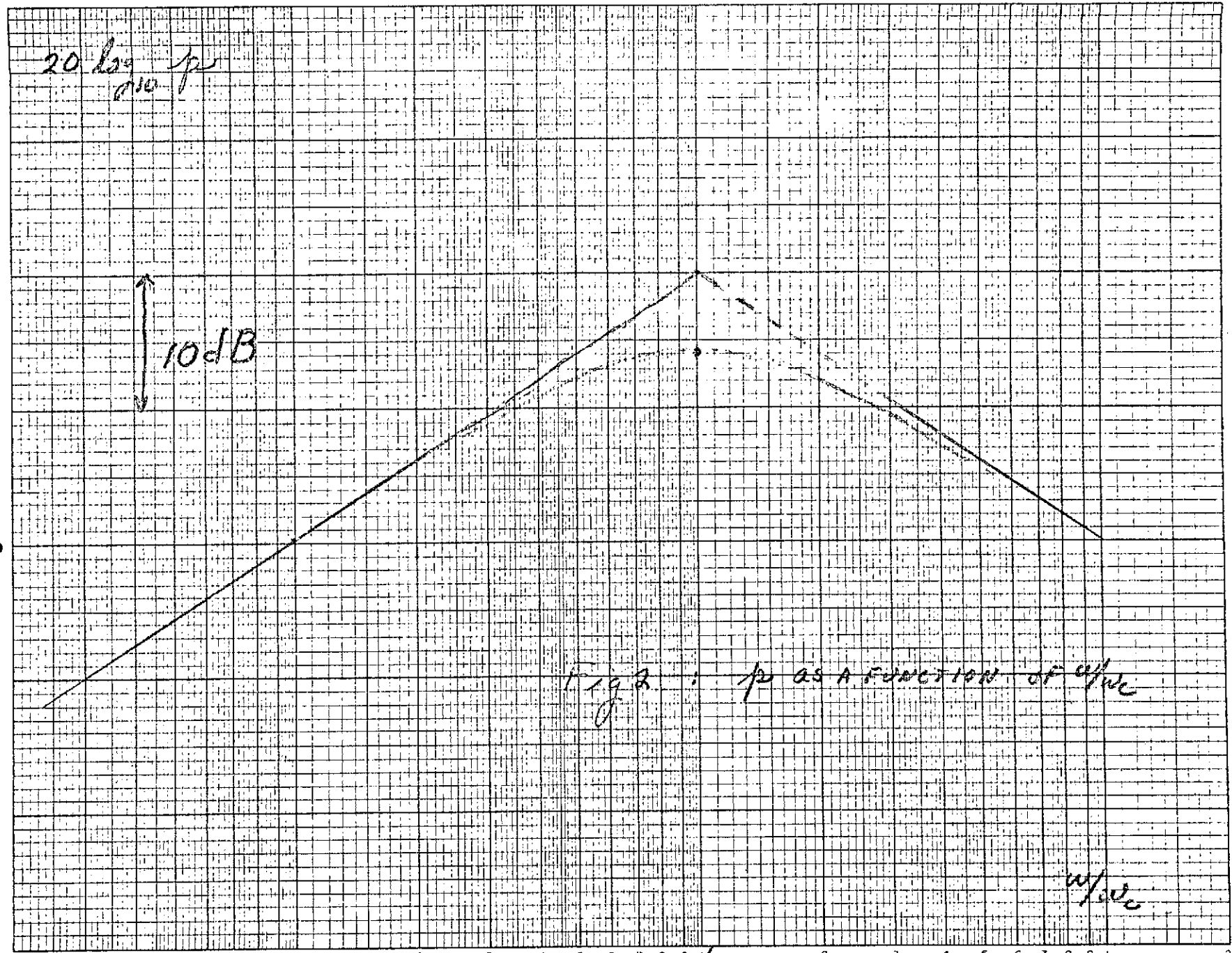
Fig 3: p AS A FUNCTION OF ω/ω_c

ω/ω_c

20 2 3 4 5 6 7 8 9 1000 2 3 4 5 6 7 8 9 10000 20000

FREQUENCY IN CYCLES PER SECOND

37



Finally, the evaluation of I in Eqs. 14 is an approximate one subject to the approximation 14a. In fact, this approximation *over estimates* the true value of I . In other words the true value of I should be lower than the values shown in Fig. 1.

2. SPECIFIC ACOUSTIC IMPEDANCE OF A POROUS SURFACE

The porous surface is a set of small holes connecting one face to the other. The holes may also be interconnected within the porous material; however we will neglect the interconnections. The cross-section of the holes vary considerably from hole to hole. We will show that the larger holes dominate the specific impedance of the surface.

For simplicity we could represent the holes either as circular or as rectangular, depending on the actual porous surface. For example, it appears that a porous surface made of sintered particles have a ratio of circumference to cross-section which is closer to that of a circular hole. Other porous materials made of compressed fibers may have holes which approach a very narrow rectangular hole.

The acoustic impedances Z_A of a circular and narrow rectangular holes³, each of length l , are

³ L.L. Beranek, *Acoustics*, Chap. V.

$$\left. \begin{aligned}
 {}_1Z &= \frac{8\eta\ell}{\pi a^4} + i\omega \frac{4}{3} \frac{\rho_0 \ell}{\pi a^2} \\
 \omega_{c1} &= \frac{6\eta}{a^2 \rho_0}
 \end{aligned} \right\} \text{circular hole}$$

$$\left. \begin{aligned}
 {}_2Z &= \frac{12\eta\ell}{t^3 w} + i\omega \frac{6\rho_0 \ell}{5wt} \\
 \omega_{c2} &= \frac{10\eta}{t^2 \rho_0}
 \end{aligned} \right\} \text{rectangular hole}$$

where η = coefficient of viscosity for the gas,
 a = radius of circular hole,
 t = thickness of rectangular hole,
 w = width of rectangular hole.

In a unit area there are N holes. Hence, the specific acoustic impedance z of the surface becomes

$$z = \left[\sum_{n=1}^N Z_n^{-1} \right]^{-1}$$

where Z_n is the acoustic impedance of the n th hole. Since the conductance of a circular hole increases as the fourth power of the radius it is clear that amongst the N holes per unit surface the large holes will have a dominant role.

The frequency ω_c is the cut-off frequency at which the reactive part equals the resistance part of the acoustic impedance. In order to achieve a high cut-off frequency, the circular holes must have a very small radius "a"; the rectangular holes must

have a very small thickness. If the aspect ratio w/t of the rectangular holes is large, then rectangular holes could have a higher cut-off frequency than the circular holes.

2.1 Sintered Porous Surface

In the following discussion we will assume that the holes of the porous surface are closer to circular holes than to thin rectangular holes. Furthermore, we consider that the holes have a uniform radius "a", which will mark the highest value in the distribution of hole radii. With these simplifications and letting

$$r_w = \frac{1}{N} \frac{8\eta\ell}{\pi a^4}$$

we have

$$z_w = r_w (1 + i\omega/\omega_c) .$$

For a real porous surface, the value of ℓ is roughly equal to the thickness of the surface. Examining the porous surface of the sintered material used we find that the effective hole radii varies from below 10 microns to slightly larger than 25 microns. For the purpose of numerical calculations we will assume that the value of "a" is 30 microns. The cut-off frequency ω_c for circular holes, 30 micron radius, becomes

$$a = 30 \text{ microns}$$

$$\omega_c = 0.95 \times 10^5 \text{ rad/sec}$$

$$f_c = 15 \text{ kHz} .$$

This cut-off frequency is rather low for our applications. It means that in the region of 10 kHz the frequency response of the porous sensor will drop significantly. We can verify this conclusion by evaluating the value of the parameter p given in Eq. 21 for the case of a porous strip sensor of width w :

$$C = w$$

$$S_0 = h_0 w$$

$$\frac{r_w}{\rho_i c_i} = L/h_0$$

$$p = \frac{\rho_i c_i}{r_w} \frac{C_0 L/2}{S_0} \left[\frac{\omega/\omega_c}{1 + (\omega/\omega_c)^2} \right]$$

$$= \frac{1}{2} \left[\frac{\omega/\omega_c}{1 + (\omega/\omega_c)^2} \right]$$

Hence at $\omega = \omega_c = 15$ kHz, p has a maximum value of $1/4$; from Fig. 4 the frequency response should have dropped by more than 3 dB; we recall that the curve of Fig. 1 is conservative.

The same factor $1/2$ in front of the bracket applies also to a porous pipe.

If the hole size has been underestimated, the cut-off frequency would be lower and the drop in frequency response in the 10 kHz would also be larger, primarily because the calculations leading to Fig. 1 are too conservative.

We conclude that the reactive part in the specific acoustic impedance plays a role in decreasing the value of the response of the sensor at high frequencies. This role may be a dominant one.

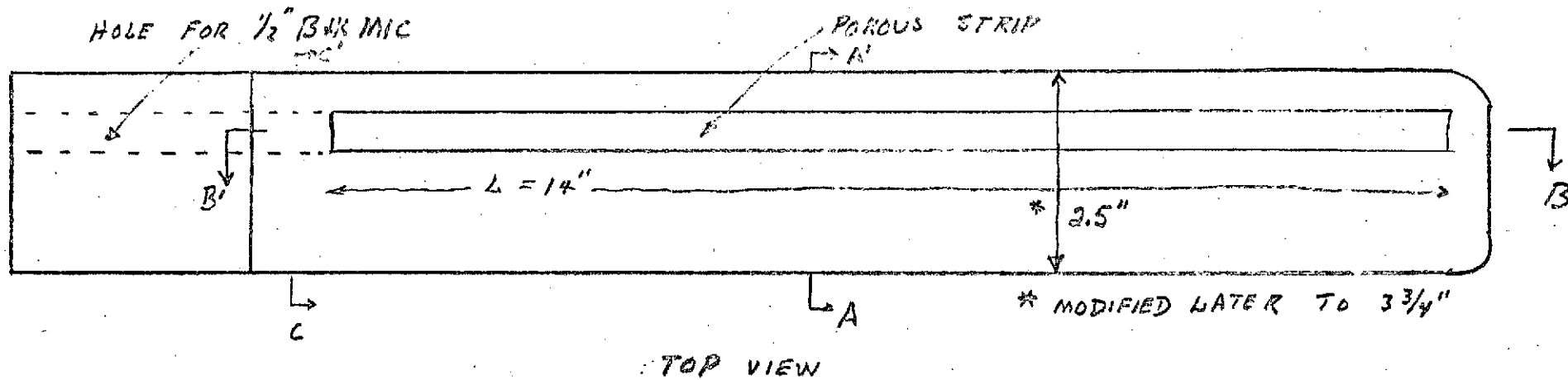
APPENDIX 4: DESIGN AND PRELIMINARY RESULTS OF A POROUS SURFACE MICROPHONE IN AN AEROFOIL

The acoustic design of the porous surface microphone in an aerofoil is sketched in Fig. 1. Two porous surfaces are active, one on each side of the aerofoil; these two surfaces being further separated than the two half surfaces of a porous pipe should sense flow noise which is less correlated from surface to surface; hence the net flow noise sensed by the microphone on the present design could be less than on the porous pipe microphone by at most 3 dB.

The two sensing surfaces in Fig. 1 should have sensitivities well matched in modulus and phase. This means a careful selection of the porous surfaces. The specific flow resistance of the porous surfaces selected is shown in Fig. 2. Each porous surface is made of two shorter strips. These strips were selected from a group of approximately 30 strips which were calibrated acoustically. Most of the strips had variations in excess of 5 dB. The strips shown in Fig. 2 have nearly the same average specific flow resistance of $+1.5 \text{ dB re } (50 \rho_i c_i)$, or $60 \rho_i c_i$. The standard deviation of the variations of specific flow resistance, normalized to the mean is approximately 0.1. The correlation length is roughly 1.5 in. The results,

K - BASE

POROUS SURFACE MICROPHONE



43

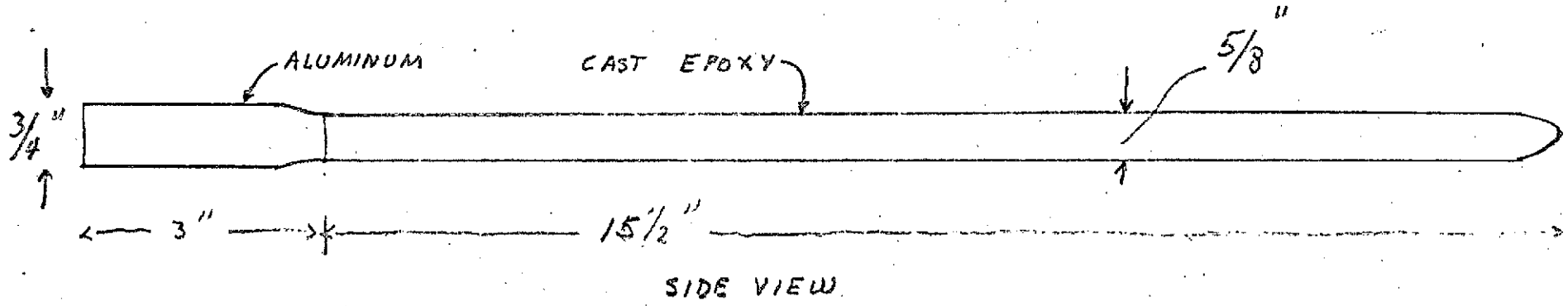


FIG-1-A POROUS SURFACE MICROPHONE IN AERFOIL

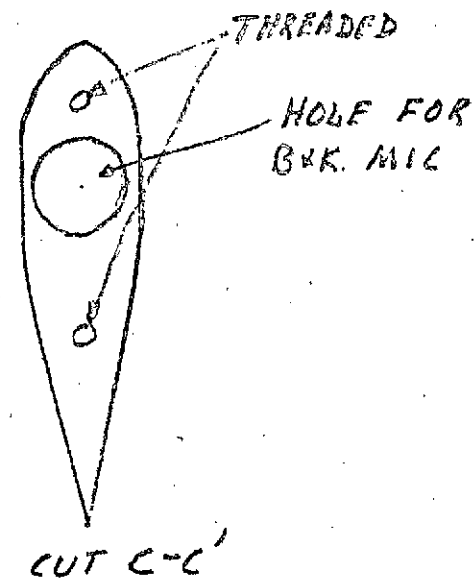
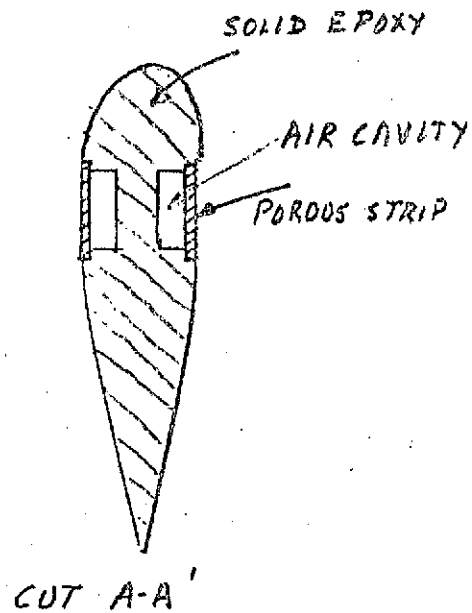
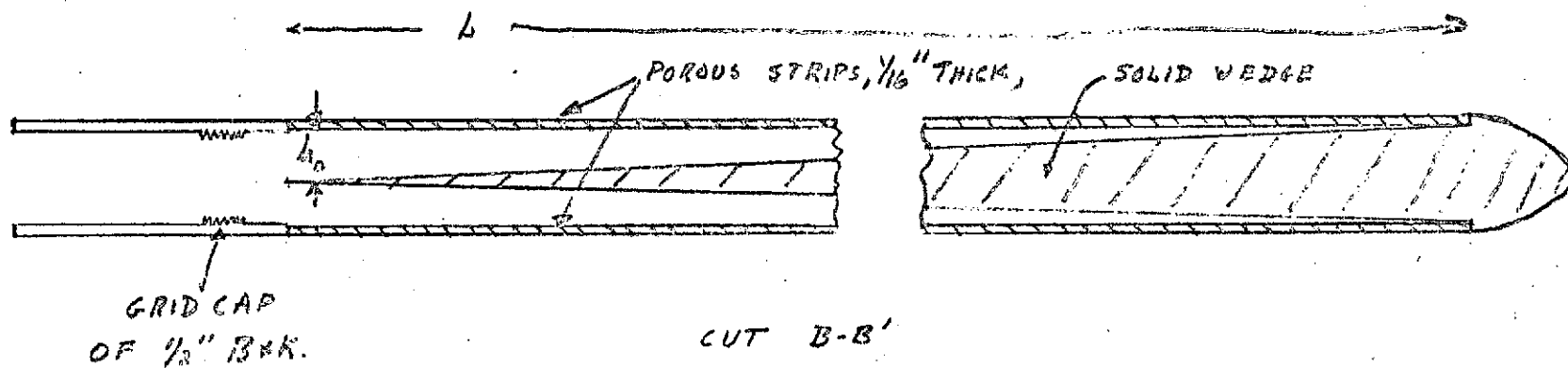
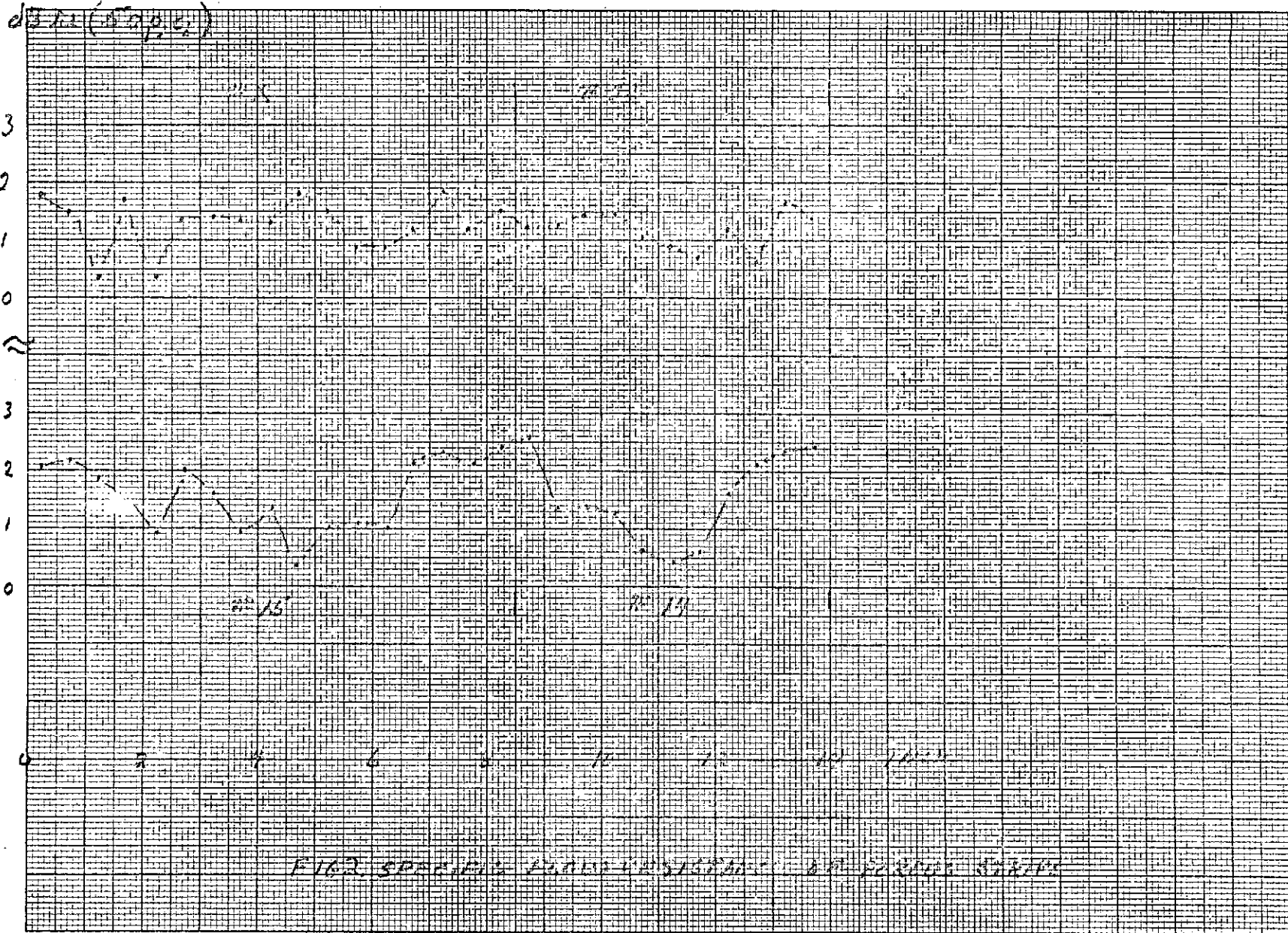


FIG. 1 B CROSS-SECTIONS OF POROUS SURFACE MICROPHONE



45



$$\left(\frac{R_0}{S_0^2}\right)^{1/2} = 0.1$$

$$\frac{x_0}{L} = \frac{1.5}{14}$$

introduced into Eq. 19 of Memo No. 1 gives a standard deviation γ of the response which is

$$\begin{aligned} \gamma &= \left(\frac{R_0}{S_0^2}\right)^{1/2} \sqrt{2 \frac{x_0}{L}} \\ &\approx 4.6 \times 10^{-2} . \end{aligned}$$

The side lobe levels will be limited to 2γ , or 9.2×10^{-2} which is roughly -21 dB with respect to the main lobe.

1. EXPERIMENTAL RESULTS

The sensor sketched in Fig. 1 and the porous strips measured in Fig. 2 were assembled and preliminary measurements made.

The specific flow resistance at the microphone should be $\rho_i c_i$; we measured $0.95 \rho_i c_i$.

The frequency response of the sensor measured for 0° and 180° orientation of its axis with respect to an acoustic source is shown in Fig. 3. Comparing the 0° response of this sensor with a porous pipe we find that the response as a function of frequency does not drop faster; in fact, a slight improvement of a few dB is observed at 10 kHz. The difference between the two curves of Fig. 3 show that the side lobe levels tend to be limited to not less than -20 dB.

47



Brüel & Kjær

Brüel & Kjær

Brüel & Kjær

Brüel & Kjær

Potentiometer Range: _____ dB Rectifier: _____ Lower Lim. Freq.: _____ Hz Wr. Speed: _____ mm/sec. Paper Speed: _____ mm/sec.

Copenhagen



dB

dB

dB

60

40

8

Measuring Obj.:

POROUS STRIP MIC (Model 1)

180° INCIDENCE

45

30

6

30

20

4

Rec. No.:

Aug 8 72

Sign: [Signature]

0

0

10 20 Hz 50 100 200 500 1000 2000 5000 10000 20000 40000 D A B C Lin.

QP 1124

Multiply Frequency Scale by

Zero Level:

(1612/2112)

A B C Lin.

0 -13

-10

-20

-30

NOISE FLOOR

FIG-3B. RESPONSE OF POROUS STRIP MICROPHONE ; 180° INCIDENCE

These preliminary results already indicate that the acoustic response of the present sensor is nearly the same as that of a porous pipe sensor. The directivity of the present sensor in the horizontal plane, when the main chord of the aerofoil is also in the horizontal plane, should be the same as found in a porous pipe sensor of the same length. When the main chord of the aerofoil is vertical, the horizontal directivity will be somewhat different than found for a porous pipe because the scattering cross-section will be larger.

APPENDIX 5: FREQUENCY RESPONSE AND DIRECTIVITY OF THE POROUS STRIP SENSOR IN AN AEROFOIL. DIRECTIVITY OF THE POROUS PIPE SENSOR

The preliminary design of the porous strip sensor reported in Memo No. 4 has been completed and a final sensor assembled and tested. The present Memo gives the final frequency response of this sensor and its directivity patterns; for comparison the directivity patterns of a porous pipe sensor are added.

Figure 1 shows the frequency response of the sensor; this response is slightly better than the response of the preliminary design, in the fact that it has a smaller drop at 10 kHz.

Figure 2 gives the directivity of a 12-in. long porous pipe at 5 frequencies: 0.5, 1, 2, 5, and 10 kHz. The directivity follows rather closely the directivity of an ideal line sensor of the same length; this is illustrated in Fig. 3 for the frequencies 5 and 10 kHz; the left hand side of Fig. 3 gives the directivity of the porous pipe sensor; the right hand side gives the directivity of the ideal line sensor. The main lobes are comparable. The minor lobes are somewhat different; while the minor lobes of the ideal sensor decrease gradually with increasing angle of incidence, the minor lobes of the porous pipe sensor tend to level off to approximately -25 dB. This effect is attributed to the irregularities of the porosity of the surface; it was discussed in Memo No. 1.

Figures 4 and 5 give the directivity of the porous strip sensor in an aerofoil; in the first set, Fig. 4, the main chord of the aerofoil is perpendicular to the plane of rotation, that is, the plane formed by the main axis of the sensor and a line directed to the sound source. In the second set, Fig. 5, the main chord of the aerofoil is parallel to the plane of rotation. The directivities of the main lobes are similar for the two orientations of the main chord; the details of the minor lobes are somewhat different but their level remain quite low over the full angular range. This success of maintaining a low level of the minor lobes for both orientations of the main chord of the aerofoil, is attributed to the symmetry of the design: two porous strips, one on each face of the aerofoil, which sum their contributions on the face of the condenser microphone.

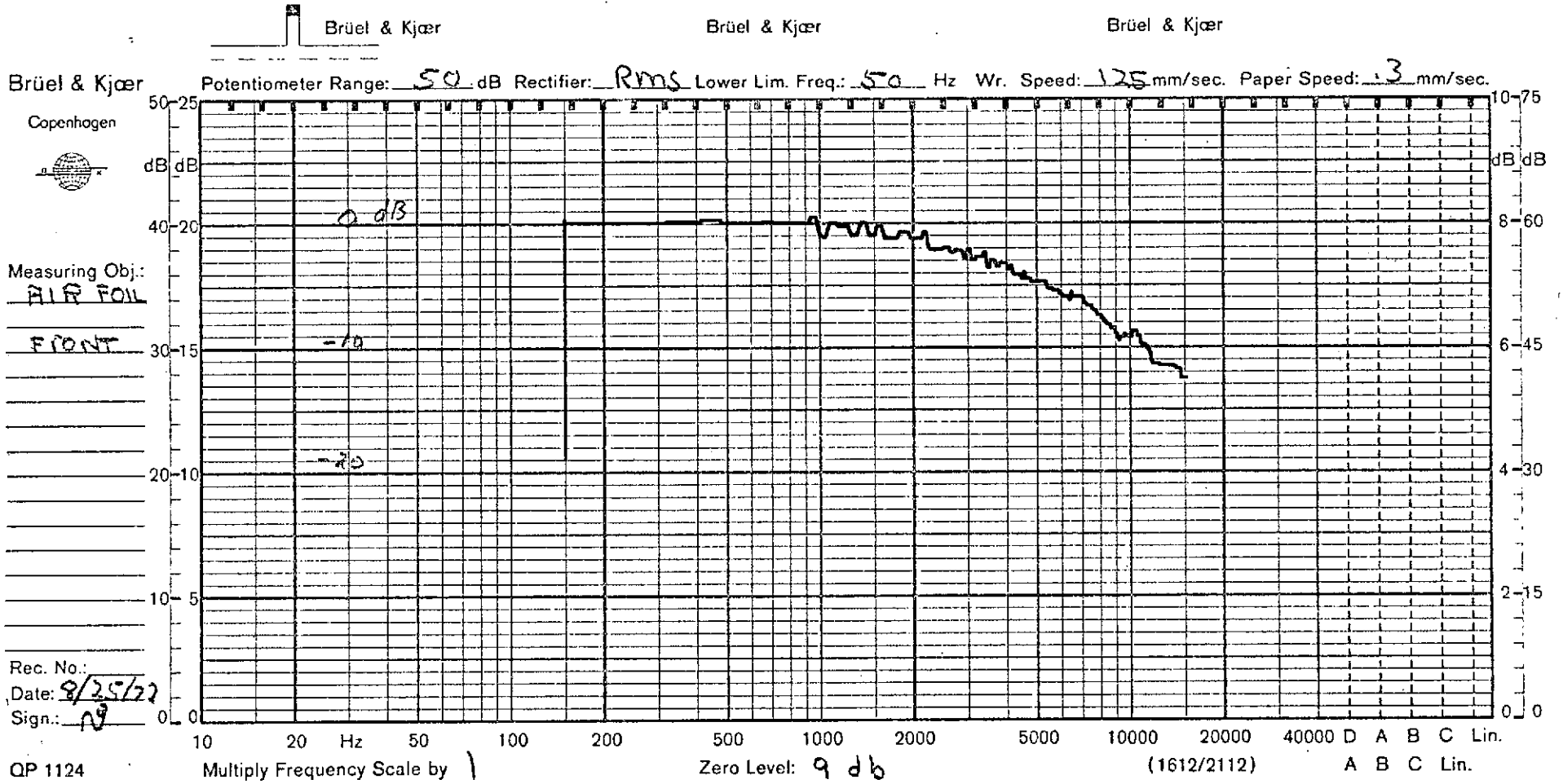


FIG 1A PRESSURE RESPONSE OF POROUS STRIP SENSOR
IN AN AEROFOIL ; L = 14 INCH ;
0° INCIDENCE .



Brüel & Kjær

Brüel & Kjær

Brüel & Kjær

Brüel & Kjær

Potentiometer Range: _____ dB Rectifier: _____ Lower Lim. Freq.: _____ Hz Wr. Speed: _____ mm/sec. Paper Speed: _____ mm/sec.

Copenhagen



dB dB

dB dB

Measuring Obj.:

AIR FOIL

BACK

50-25

40-20

30-15

20-10

10-5

0-0

10-75

8-60

6-45

4-30

2-15

0-0

Rec. No.:

Date: 8/25/72

Sign.: N^a

QP 1124

Multiply Frequency Scale by

Zero Level:

(1612/2112)

A. B C Lin.

FIG 1B. PRESSURE RESPONSE OF POROUS STRIP SENSOR
 IN AN AEROFOLIL; $l = 14$ INCH
 180° INCIDENCE.

CODEX BOOK COMPANY, INC. NORWOOD, MASSACHUSETTS, U.S.A.
NO. 3124, POLAR CO-ORDINATE.

30° 20° 10° 0 350° 340° 330°
330° 320° 310° 300° 290° 280° 270° 260° 250° 240° 230° 220°

Reproduced from
best available copy.

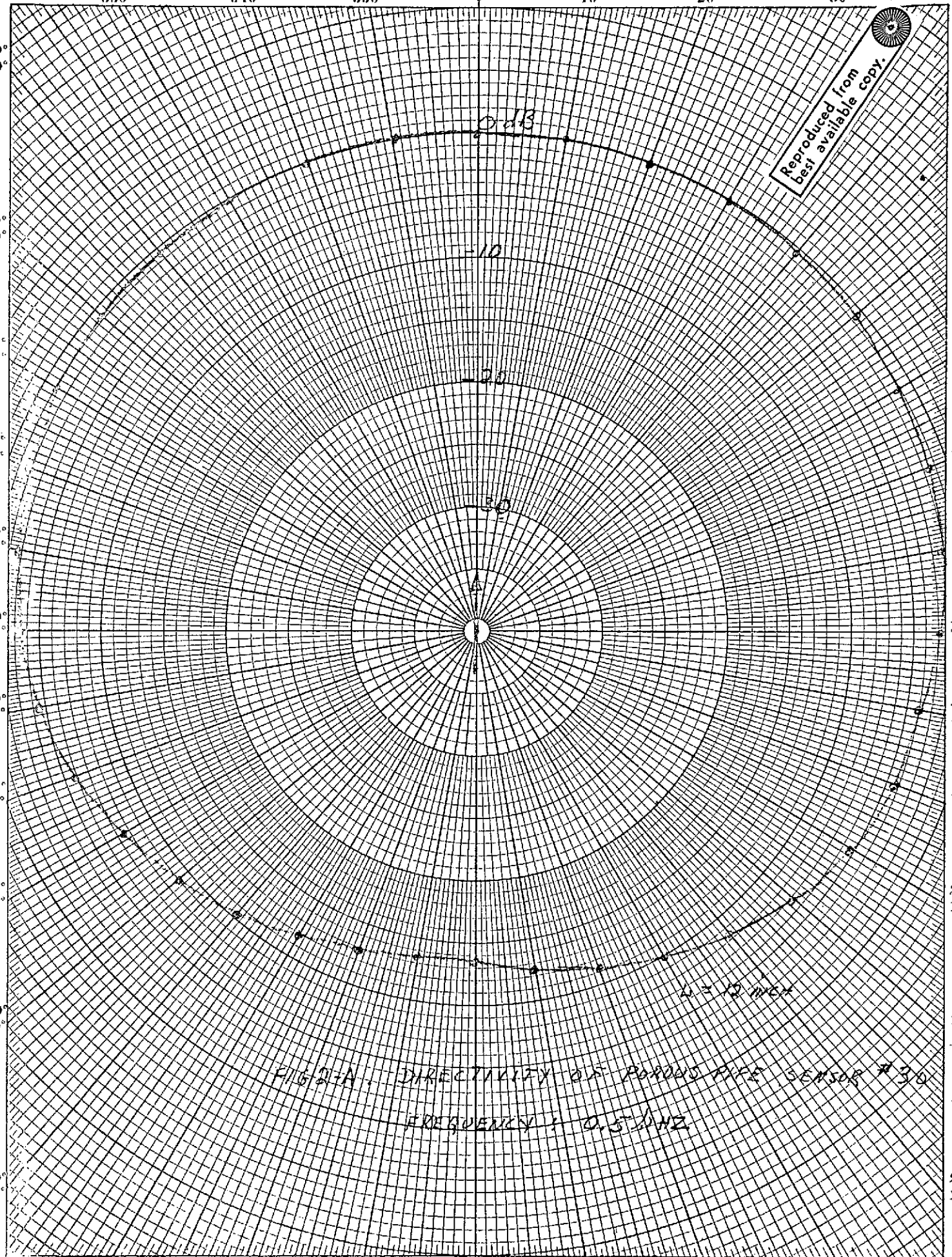


FIGURE A DIRECTIVITY OF PARASITIC SENSORS #30
FREQUENCY: 0.5 MHz

150° 160° 170° 180° 190° 200° 210°
210° 200° 190° 180° 170° 160° 150°

NO. 3124. POLAR CO-ORDINATE.
CODEX BOOK COMPANY, INC. NORWOOD, MASSACHUSETTS, U.S.A.

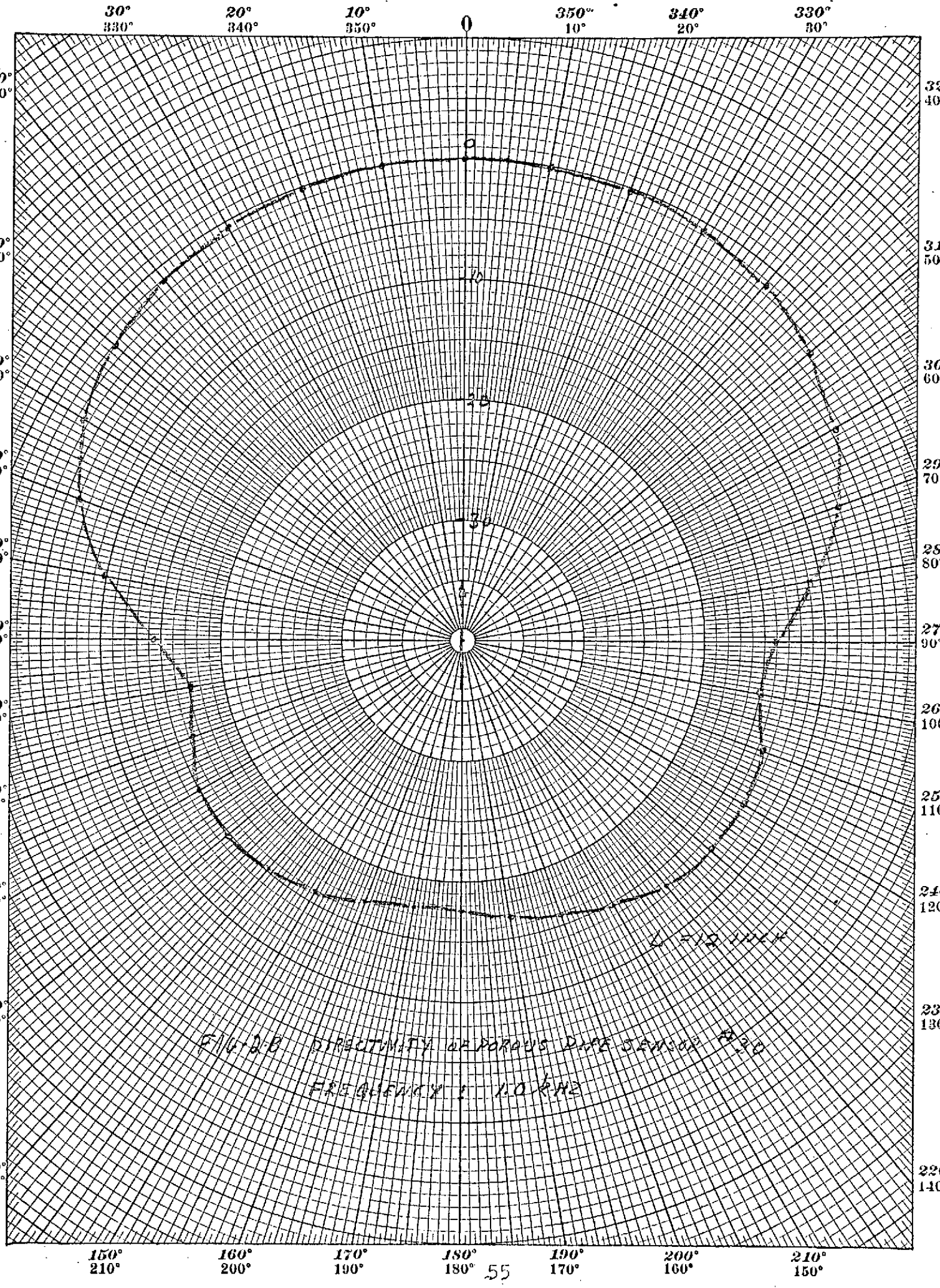


FIGURE DIRECTIVITY OF POROUS DOME ANTENNA
FREQUENCY 1.0 MHz

CODING BOOK COMPANY, INC. NORWOOD, MASSACHUSETTS, U.S.A.
NO. 3124. POLAR CO-ORDINATE.

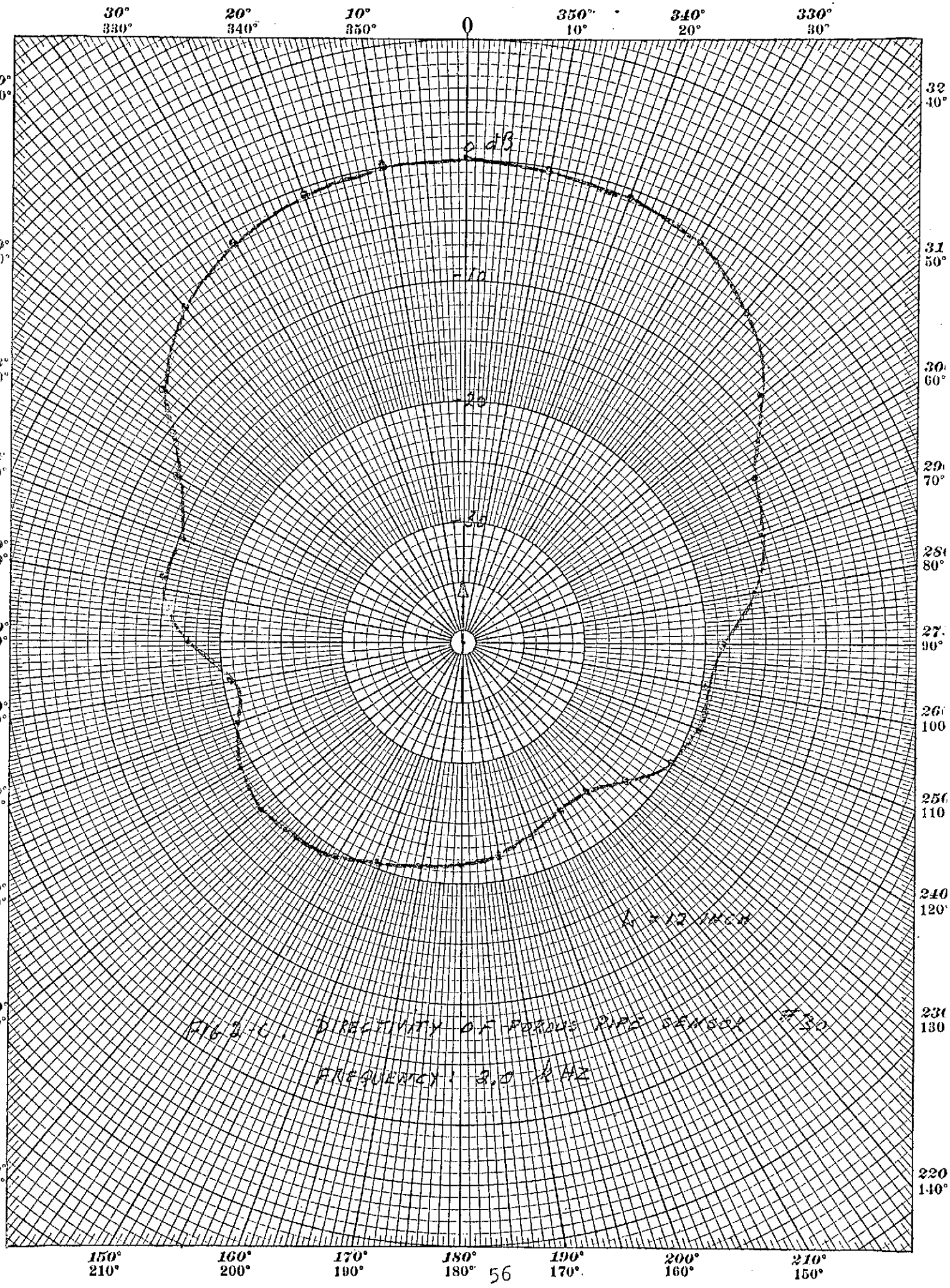


FIG. 2-16. DIRECTIVITY OF POROUS PIPE SENSOR $F=3.0$
FREQUENCY: 3.0 KHZ

30° 20° 10° 0 350° 340° 330°
330° 340° 350° 10° 20° 30°

Reproduced from
best available copy.

CODEX BOOK COMPANY, INC. NORWOOD, MASSACHUSETTS, U.S.A.
ND. 3124. POLAR CO-ORDINATE.

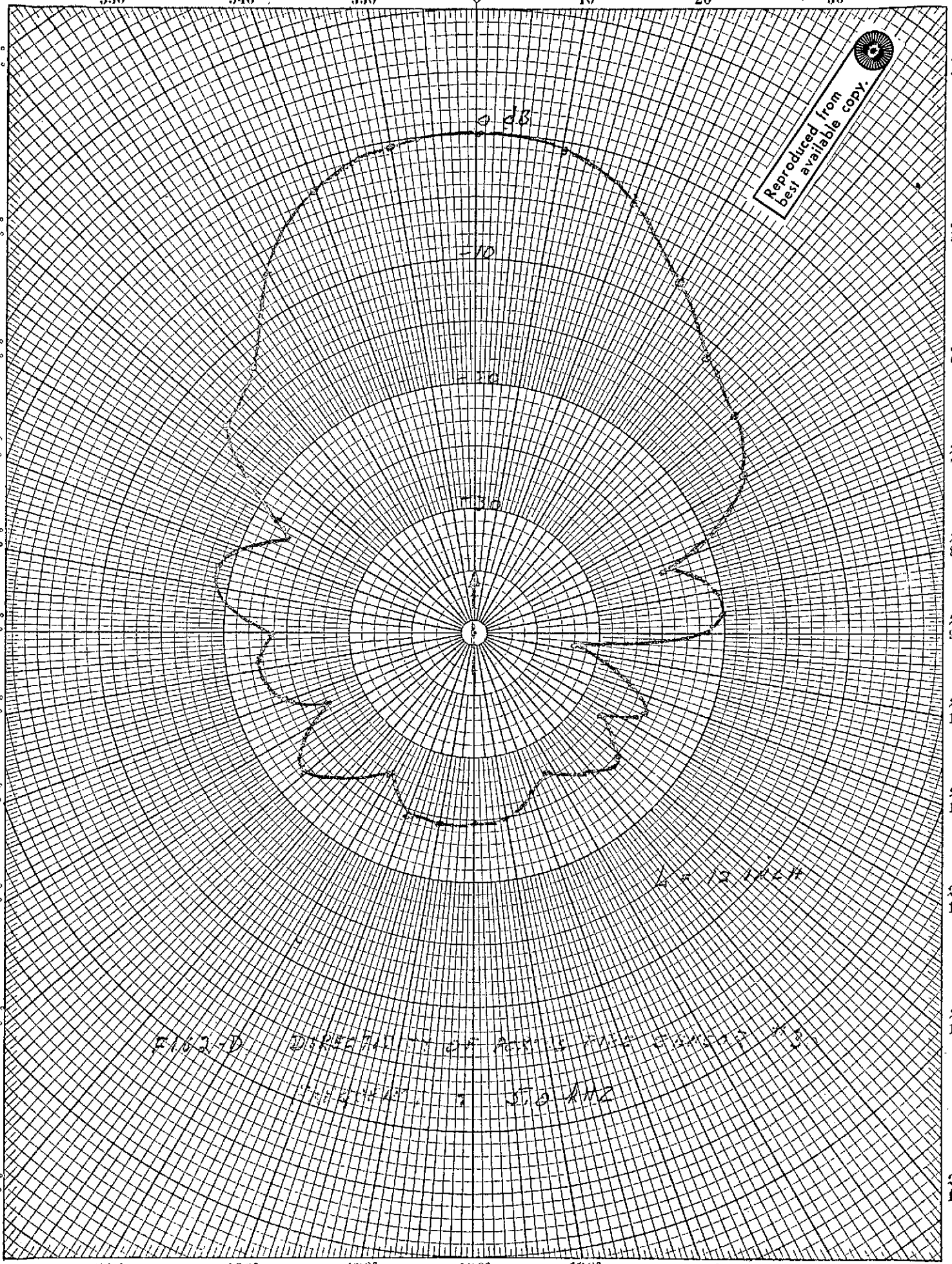


FIGURE 1
DIRECTION OF ARRIVAL OF SIGNALS
JANUARY 1 5 1942

150° 160° 170° 180° 190° 200° 210°
210° 200° 190° 180° 170° 160° 150°

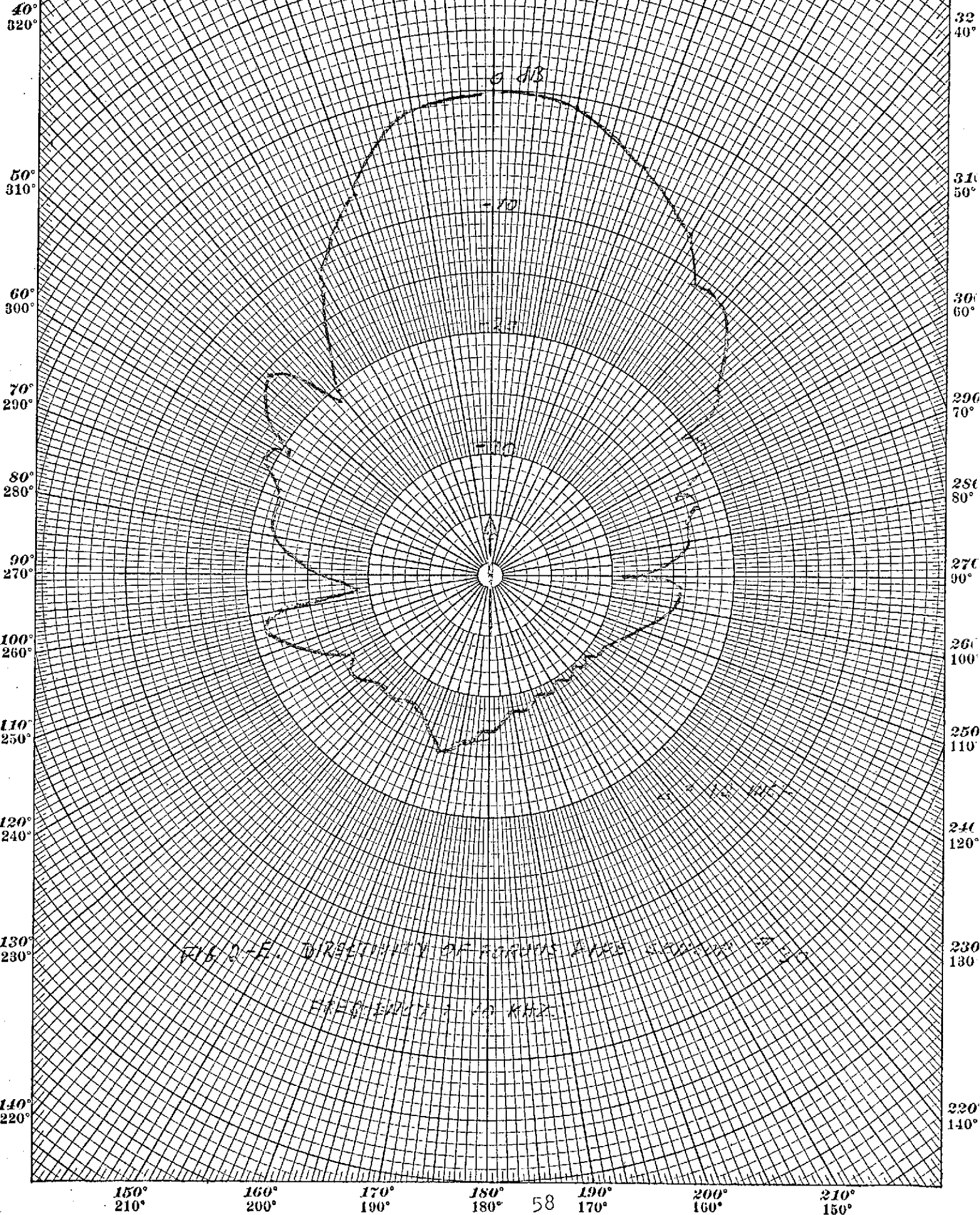
32
31
30
29
28
27
26
25
24
23
22

40°
320°
50°
310°
60°
300°
70°
290°
80°
280°
90°
270°
100°
260°
110°
250°
120°
240°
130°
230°
140°
220°

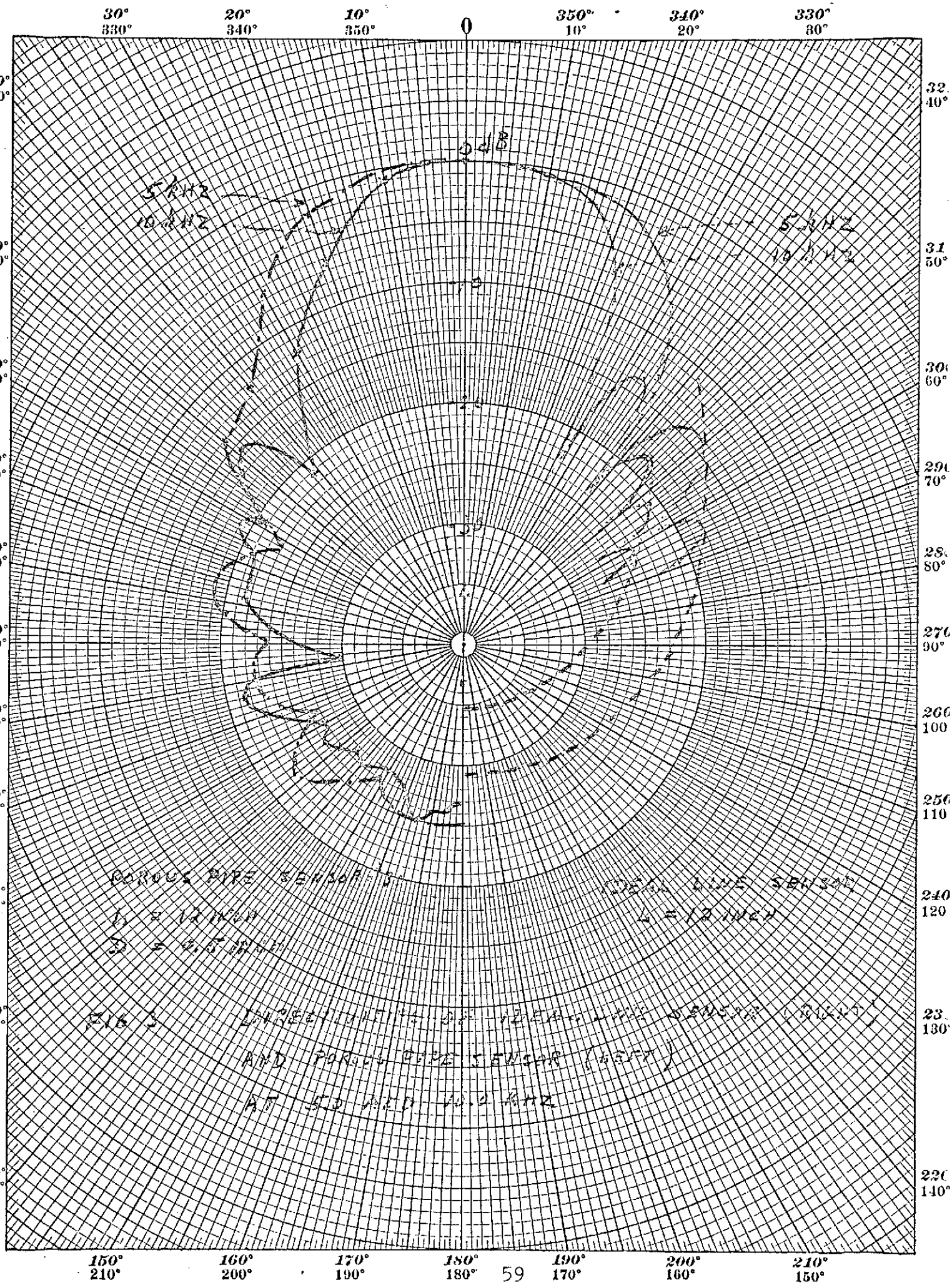
CODEX BOOK COMPANY, INC. NORWOOD, MASSACHUSETTS.

NO. 3124, POLAR CO-ORDINATE.

30° 20° 10° 0 350° 340° 330°
330° 340° 350° 10° 20° 30°



CODER BOOK COMPANY, INC. NORWOOD, MASSACHUSETTS.
U.S.
NO. 3124. POLAR CO-ORDINATE.

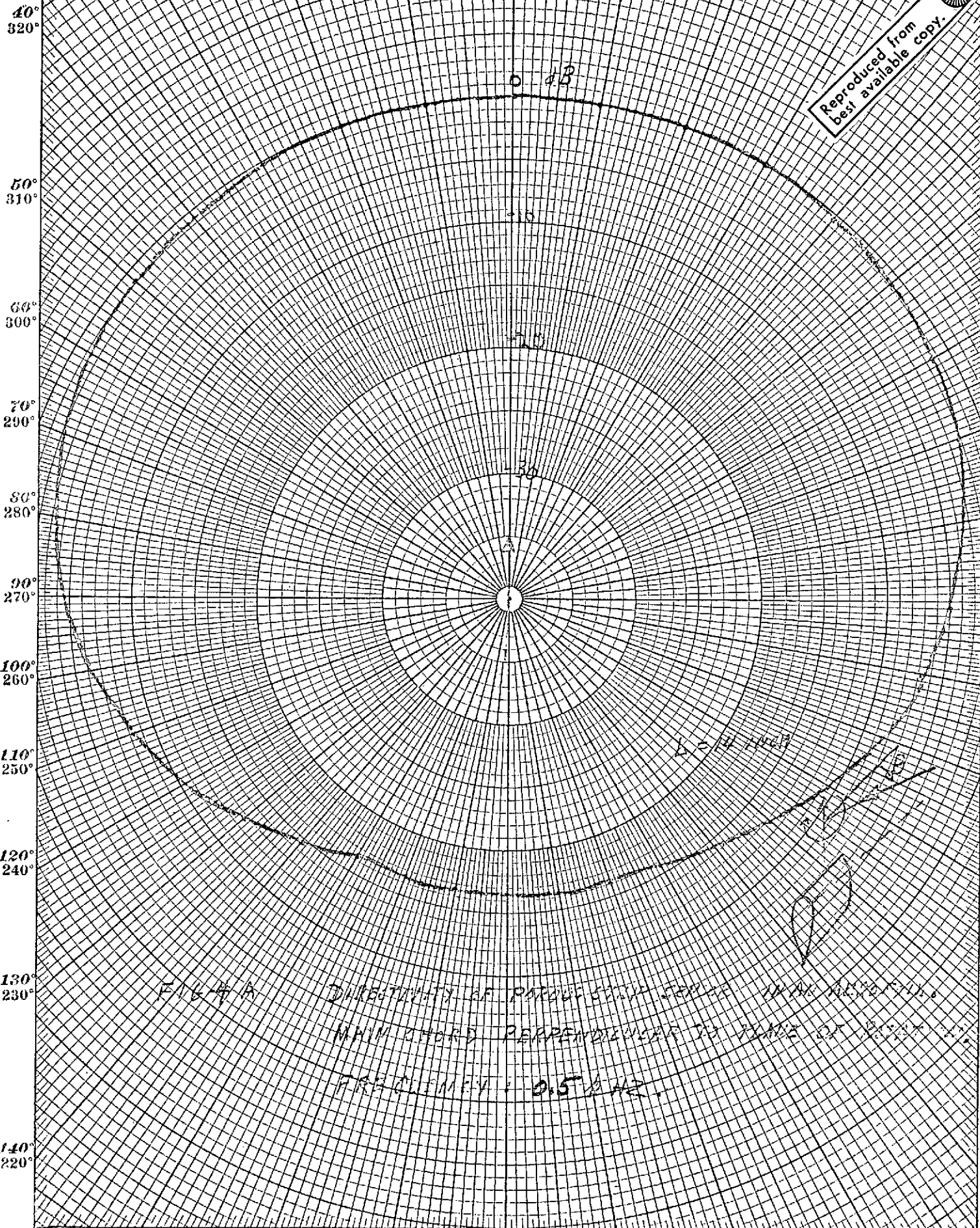


150° 210° 160° 200° 170° 190° 200° 210°
180° 59 170° 160° 150°

CODEX BOOK COMPANY, INC. NORWICH, MASSACHUSETTS U.S.A.

NO. 3124. POLAR CO-ORDINATE.

30° 20° 10° 0 350° 340° 330°
330° 340° 350° 10° 20° 30°



Reproduced from
best available copy.

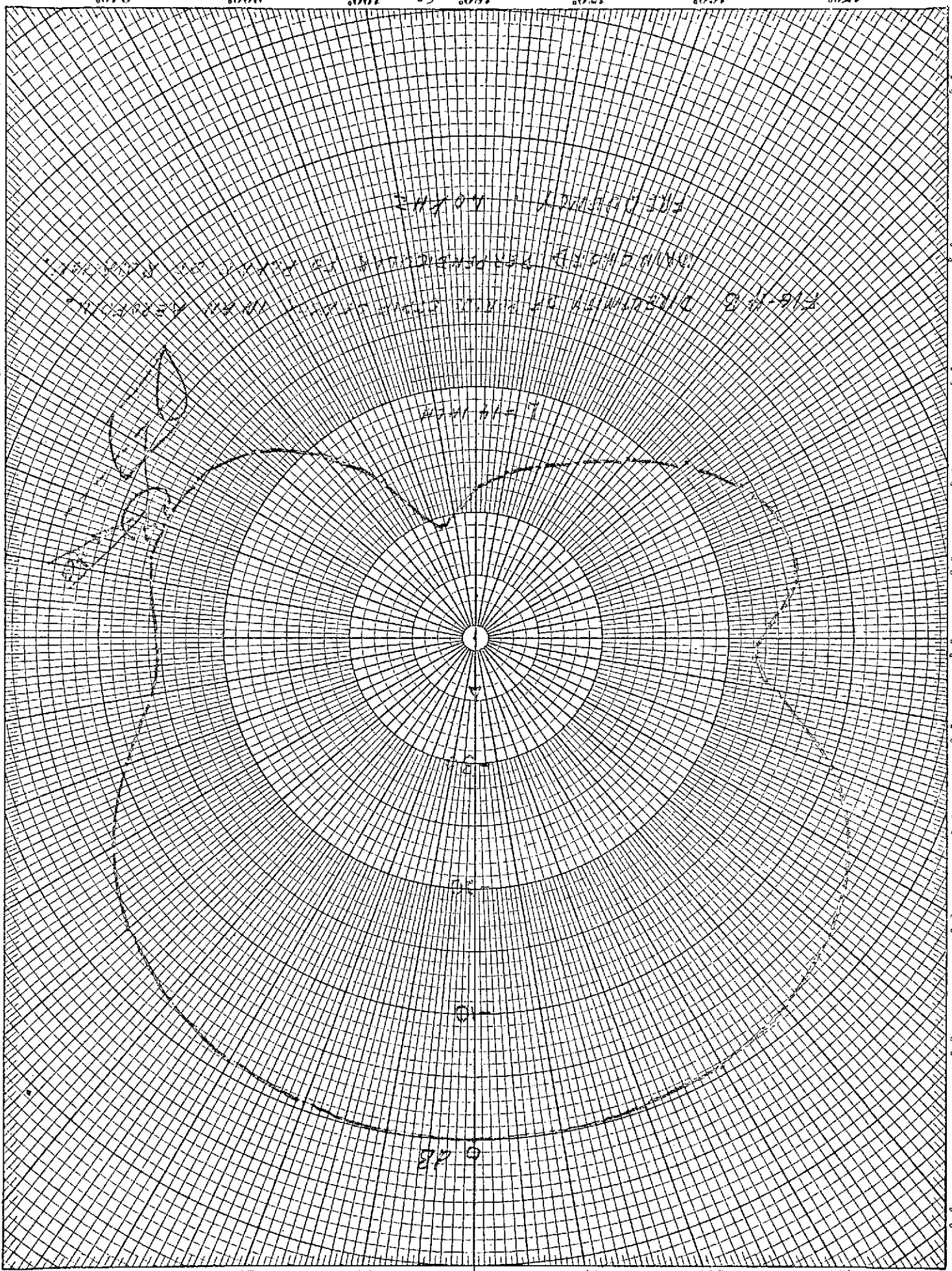
FIG. 4 A DIRECTIVITY OF PARABOLIC ANTENNA
MAIN LOBE PERPENDICULAR TO PLANE OF FEEDING
FREQUENCY = 0.5 GAZ

150° 160° 170° 180° 60 190° 200° 210°
210° 200° 190° 180° 170° 160° 150°

150° 210° 150° 170° 190° 180° 170° 190° 200° 210°

140° 130° 120° 110° 100° 90° 80° 70° 60° 50° 40°

170° 180° 190° 200° 210° 220° 230° 240° 250° 260° 270° 280° 290° 300° 310° 320°



330° 340° 350° 0 10° 20° 30° 40° 50° 60° 70° 80° 90° 100° 110° 120° 130° 140°

NO. 3124. POLAR CO-ORDINATE.

CODER BOOK COMPANY, INC. NORWOOD, MASSACHUSETTS, U.S.A.

CODING BOOK COMPANY, INC. NORWOOD, MASSACHUSETTS, U.S.A.
N.D. 3124. POLAR CO-ORDINATE.

30° 20° 10° 0 350° 340° 330°
330° 340° 350° 10° 20° 30°

Reproduced from
Best available copy.

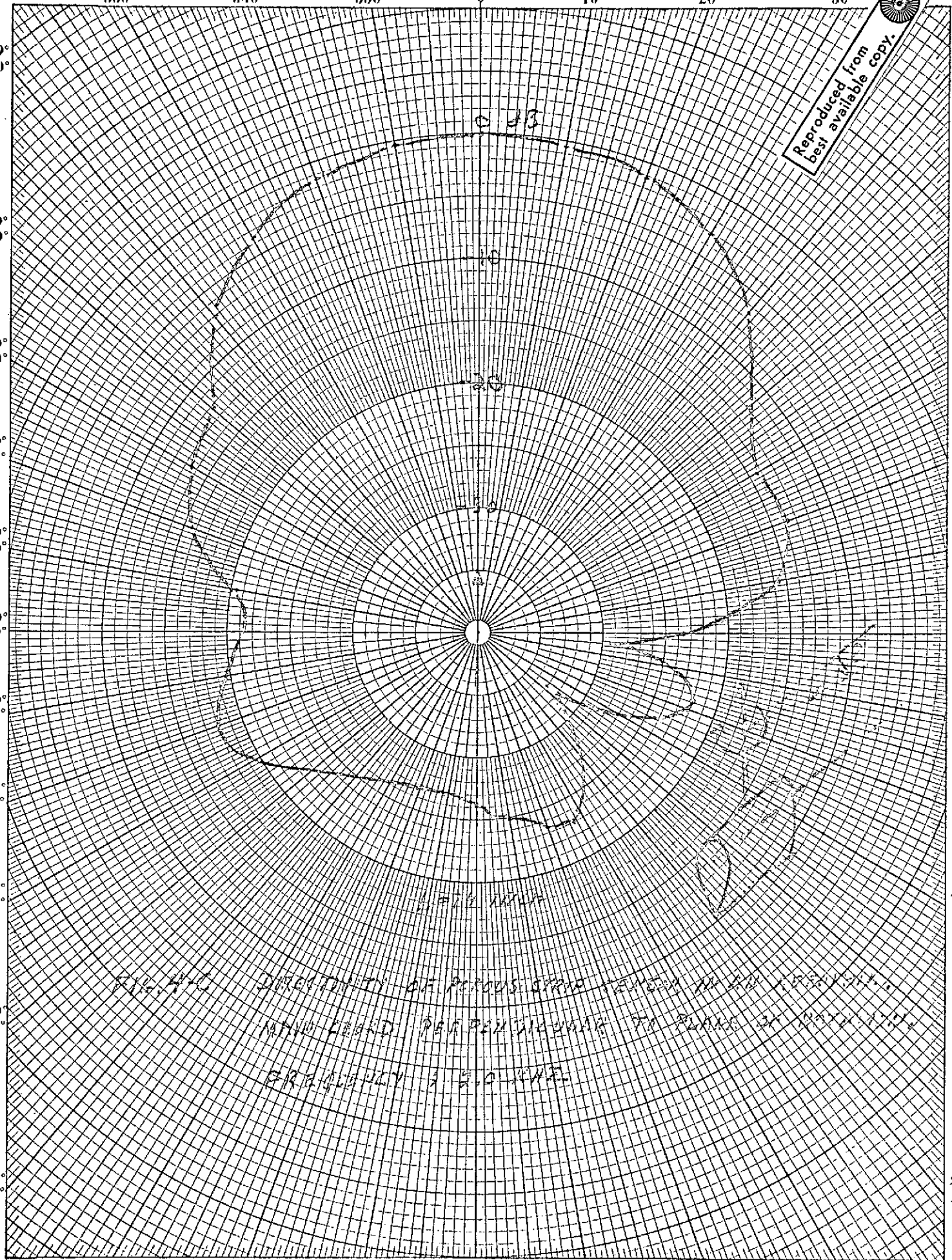


FIG. 47C DIRECTION OF FLOW OF SPINNING WHEELS IN THE
MOTOR LEAD PATENTING OFFICE TO BUREAU OF PATENTING
BUREAU OF PATENTING

150° 160° 170° 180° 190° 200° 210°
210° 200° 190° 62 180° 170° 160° 150°

210° 150°

CODEX BOOK COMPANY, INC. NEWWOOD, MASSACHUSETTS, U.S.A.
NO. 3124. POLAR CO-ORDINATE.

30° 20° 10° 0 350° 340° 330°
330° 340° 350° 10° 20° 30°

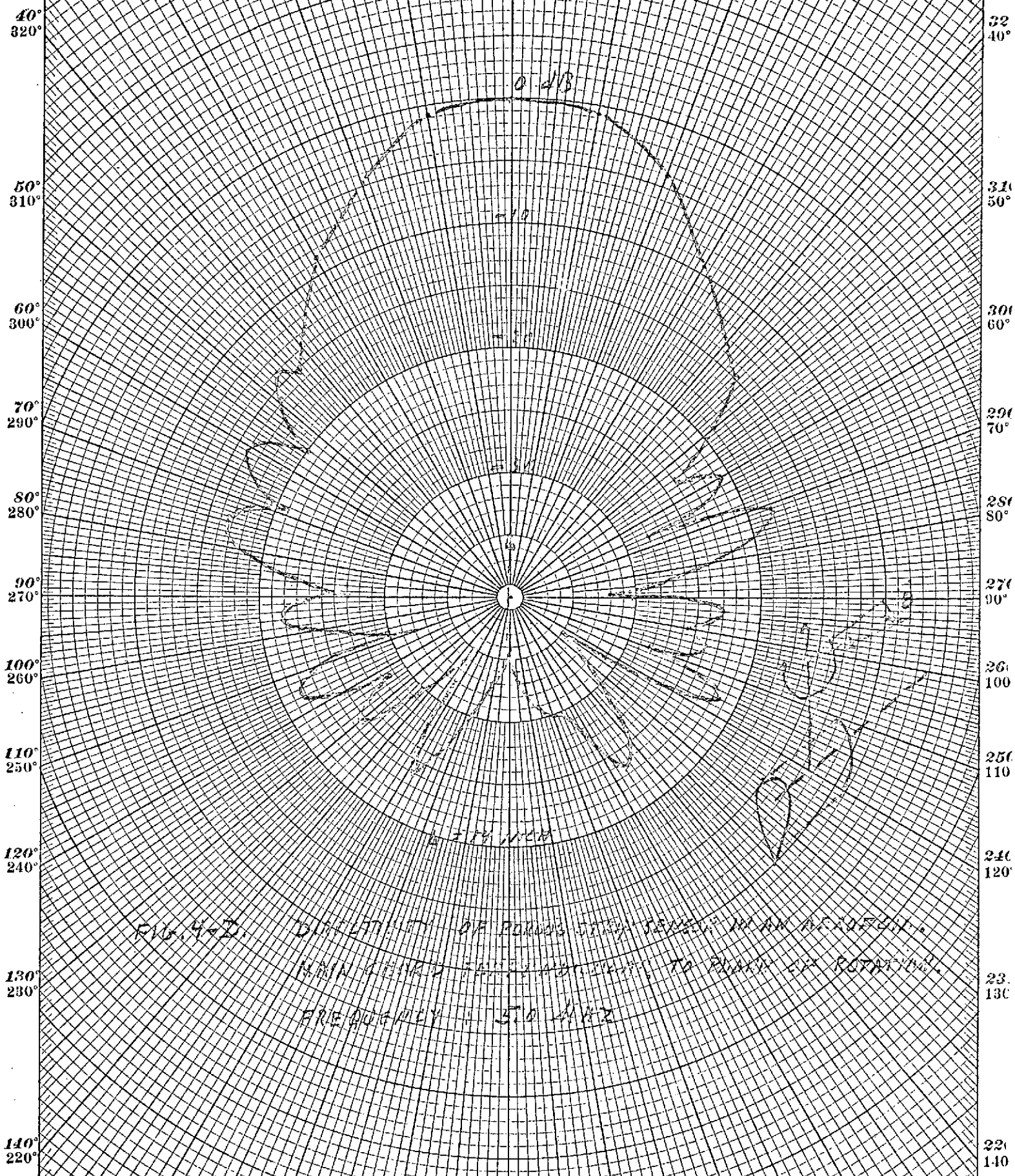


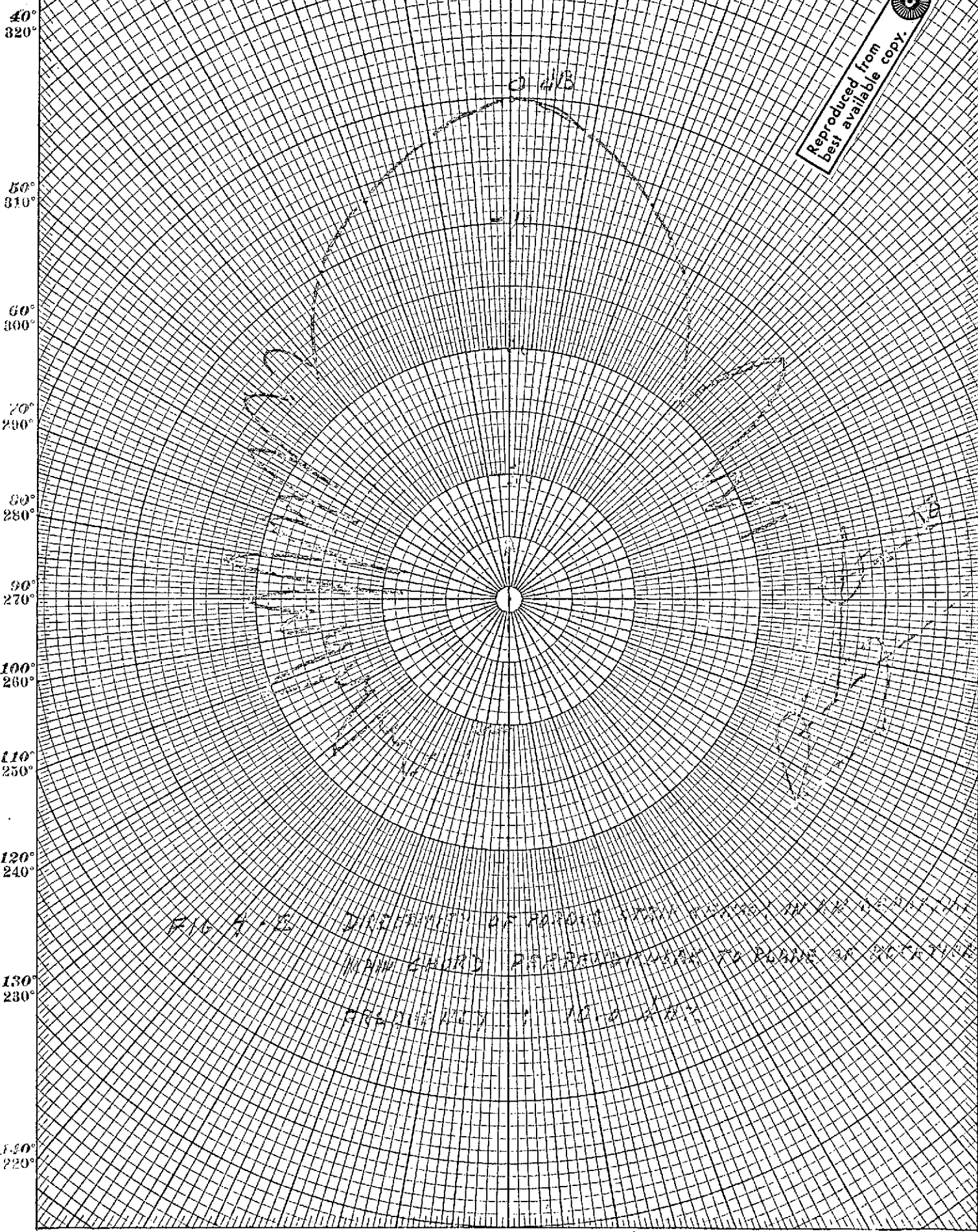
FIG. 4-D. DIRECTIONAL PATTERN OF POLAR DIRECTOR WITH REFLECTOR.
MAXIMUM GAIN, 14.5 DB, 100 WATT, 300 MC, 100 FT. ROTATIONAL
FREQUENCY = 370 MC

150° 160° 170° 180° 190° 200° 210°
210° 200° 190° 63 180° 170° 160° 150°

CODING COPY COMPANY, INC. NORWOOD, MASSACHUSETTS, U.S.A.

NO. 3124. POLAR CO-ORDINATE.

30° 330° 20° 340° 10° 350° 0 350° 10° 340° 20° 330° 30°



Reproduced from best available copy.

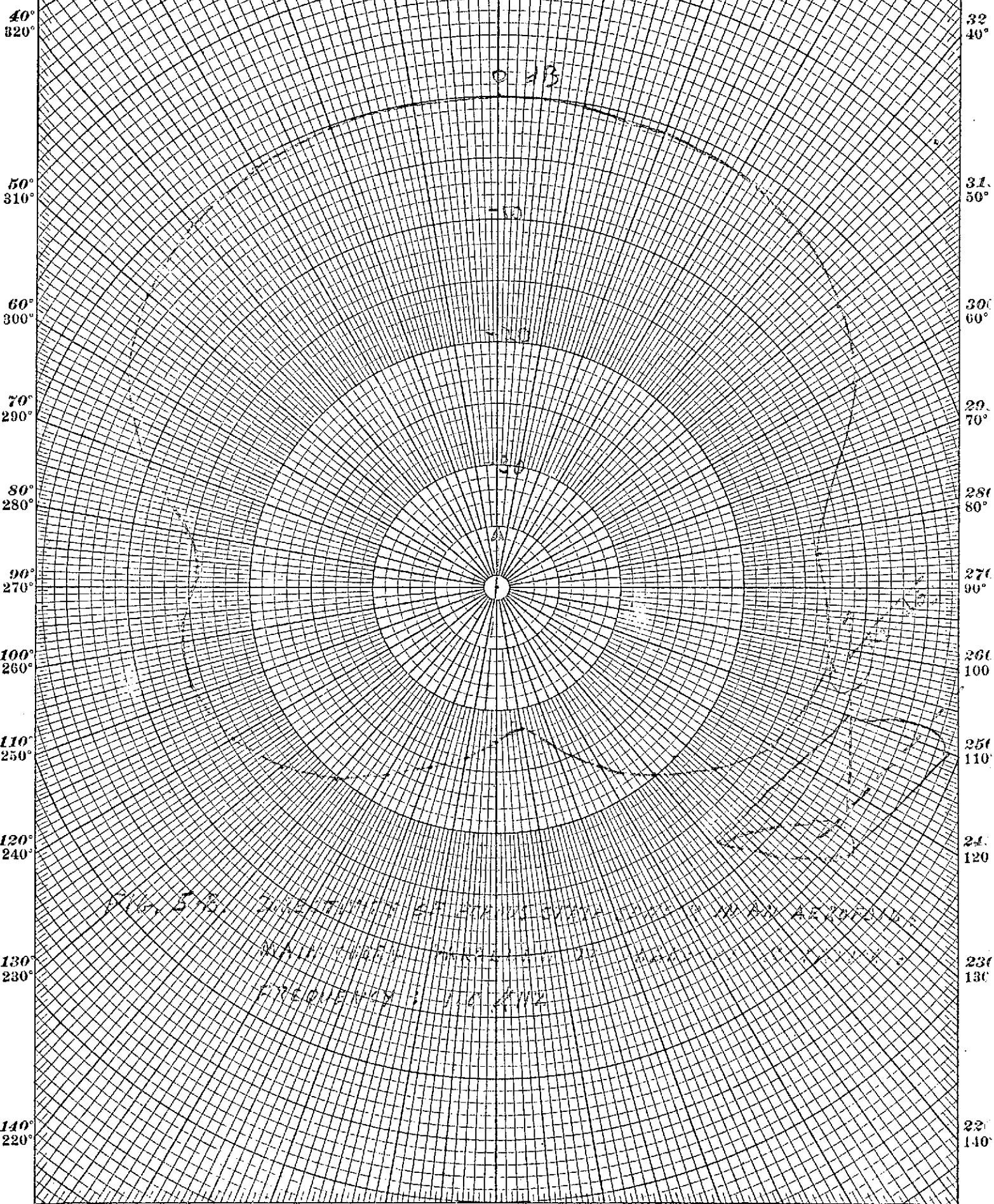
FIG. 4-12. DIFFERENCE OF SOUND PRESSURE LEVEL IN DB BETWEEN MAIN BEAM PRESSURE AND TO POINT OF OBSERVATION FREQUENCY = 1000 Hz.

150° 210° 160° 200° 170° 190° 180° 64 190° 170° 200° 160° 210° 150°

CODEX BOOK COMPANY, INC. NEW WOOD, MASSACHUSETTS, U.S.A.

NO. 3124. POLAR CO-ORDINATE.

30° 20° 10° 0° 350° 310° 330°
330° 340° 350° 10° 20° 30°

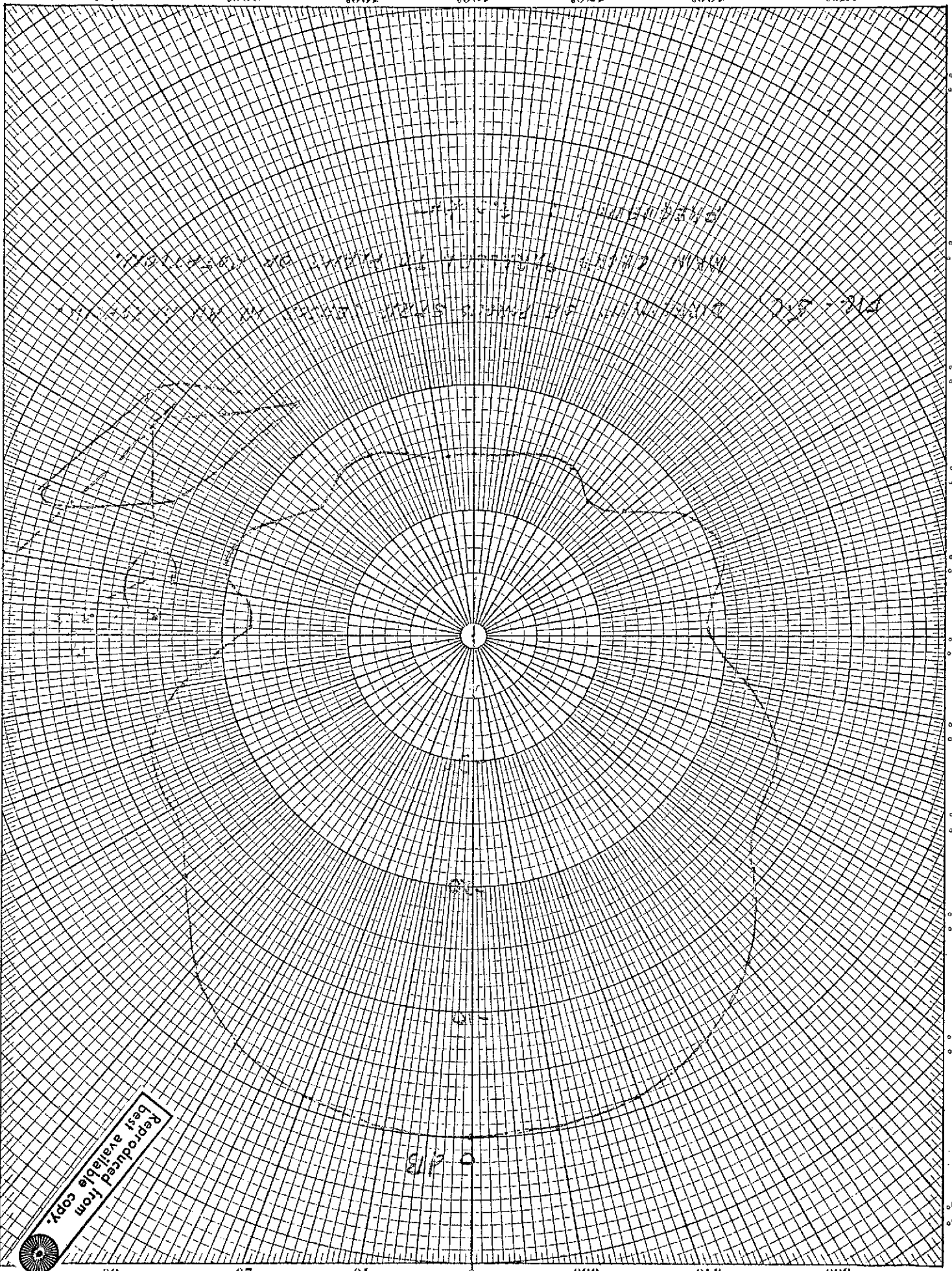


210° 200° 190° 180° 170° 160° 150°



110° 100° 90° 80° 70° 60° 50° 40°

110° 100° 90° 80° 70° 60° 50° 40°



Reproduced from
best available copy.



330° 340° 350° 0 10° 20° 30° 40°

NO. 3124. P-LAR CO-ORDINATE

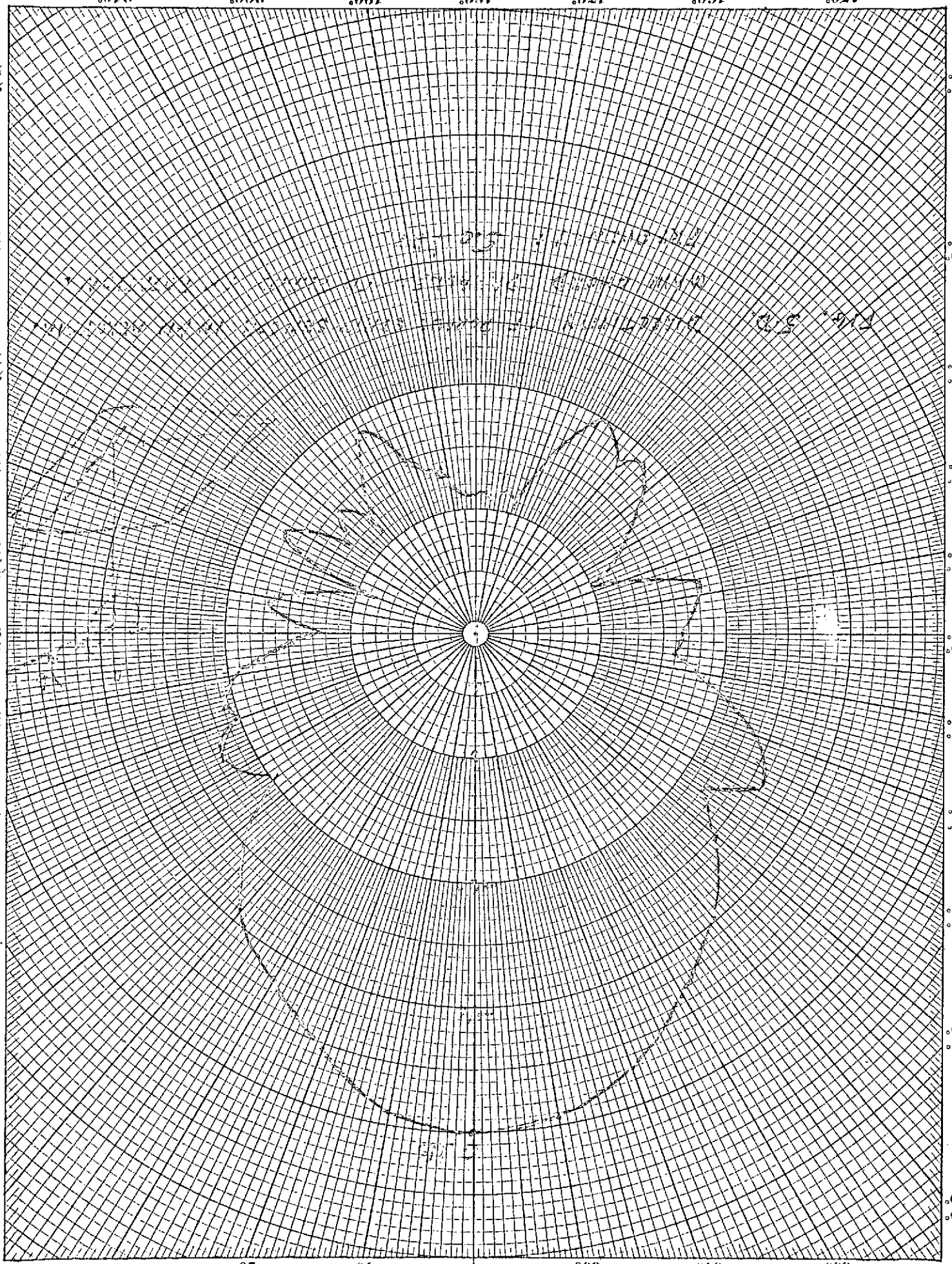
CODER BOOK COMPANY, INC. NORWOOD, MASSACHUSETTS

150° 210° 160° 200° 170° 180° 190° 200° 210°

110° 130° 150° 170° 190° 210° 230° 250° 270° 290° 310° 330°

110° 130° 150° 170° 190° 210° 230° 250° 270° 290° 310° 330°

330° 340° 350° 0 10° 20° 30° 40°



N.C. 3124. POLAR COORDINATE.

COPY BOOK COMPANY, INC., NEWBOD MASSACHUSETTS.

APPENDIX 6: WIND TUNNEL TESTS IN A QUIET FLOW

1. INTRODUCTION

The three types of microphones have been tested in the quiet BBN wind tunnel; these microphones are

- Bruel and Kjaer 1/2 inch condenser microphone with nose cone;
- Porous pipe sensor No. 32, 1/2 inch diameter, 12 inch long;
- Porous strip sensor in an aerodynamic shape.

The three microphones were tested at four angles* of incidence of the air flow with respect to their axes: 0°, 30°, 60° and 90°. The porous strip sensor was found to have a shape which caused some flow separation and the consequent excess noise at angles of incidence greater than 30°; the shape was modified to reduce the flow separation.

2. WIND TUNNEL

The wind tunnel has a 24 inch diameter nozzle; the air jet exhausts into a reverberant room. The maximum flow velocity is 74 feet per second.

The centers of the microphones were located on the axis of the air jet, 18 inch downstream from the face of the nozzle; for comparison, the microphones were also located "outside of the flow", 18 inches from the axis of the stream.

*The angle of incidence is the yaw angle at zero angle of attack.

The velocity and turbulence profile of the quiet jet at 74 ft/sec, shown in Fig. 1, were measured with a hot wire anemometer at 18 inches downstream from the face of the nozzle. The frequency spectrum of the quiet jet is shown in Fig. 3 of Memo No. 7. The turbulence inside the jet is defined as $\Delta U/U_0$ where U_0 is the free stream velocity and ΔU is the rms value of the velocity fluctuations. The overall turbulence in the free jet is 0.3% (or $20 \log_{10} \Delta U/U_0 = -50$ dB).

The microphones were tested at only the maximum flow velocity of the wind tunnel; even at this velocity some of the microphone data is limited by electronic noise.

The microphones, one at a time, are held in the flow by a pipe stand shown in Fig. 2. The pipe is 3/4 inch diameter; the microphone cable runs along and behind the pipe and both are covered by Arno tape to simulate an aerodynamic shape. The pipe with the tape creates some wind noise, although this noise is lower than the noise created by the pipe alone. This noise is likely to be negligible for the nose cone and the porous pipe microphones, because it is located at some distance away from the sensing surfaces; it may be significant for the Porous Strip Sensor because its sensing surface is closer to the pipe stand.

The base of the Porous Strip Sensor is not quite aerodynamic and creates some flow noise; for the purpose of the test the shape of the base was corrected where needed by a small amount of plastic clay which minimized the noise.

3. RESULTS

The flow noise sensed by each of the three sensors has been measured in third octave bands and normalized to the acoustic sensitivity of each sensor; the results appear in equivalent sound pressure levels in dB referred to 0.0002 microbar.

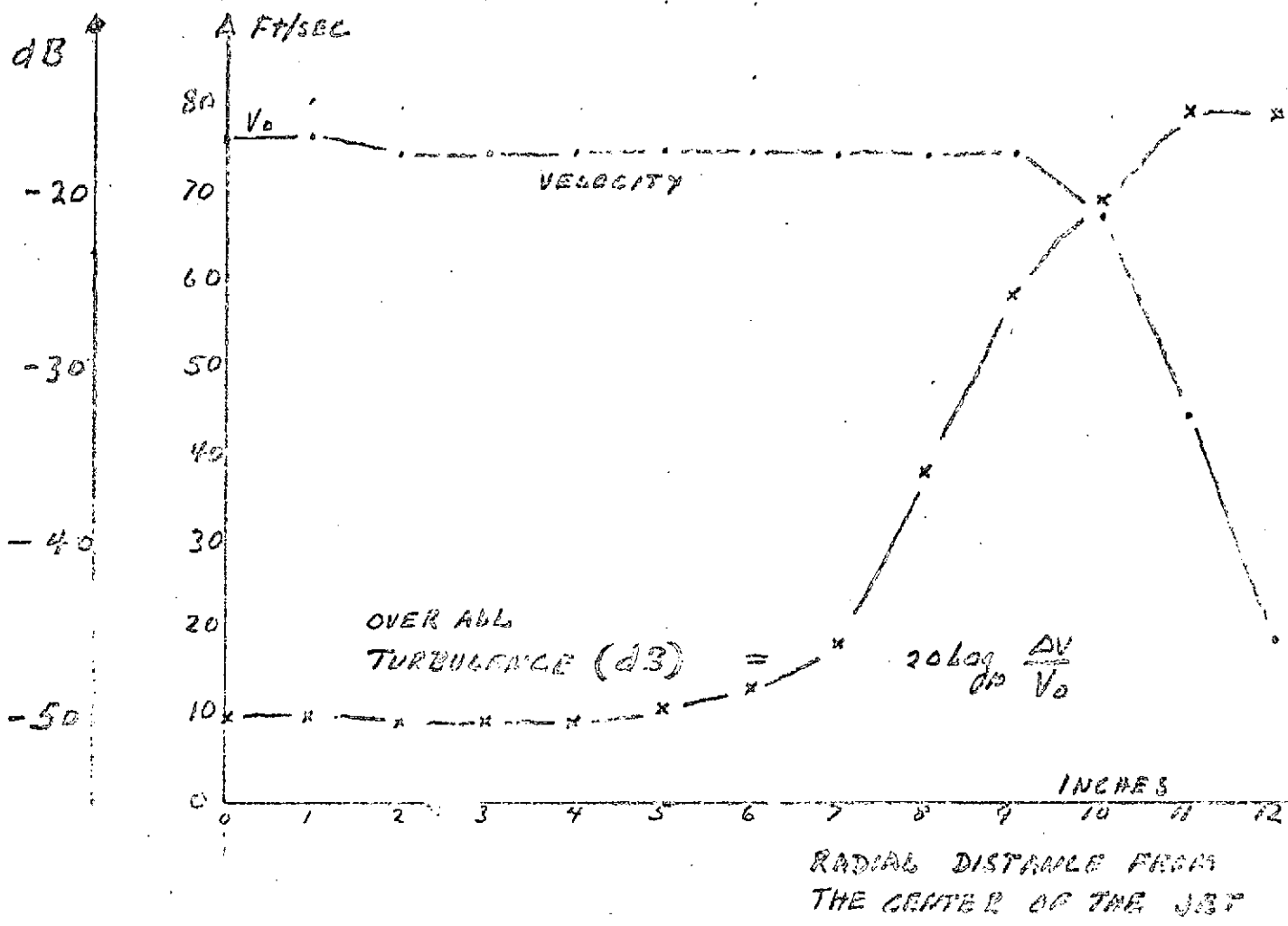


FIG. 1 : VELOCITY AND TURBULENCE PROFILES

OF FREE FLOW WIND TUNNEL;

NOZZEL DIAMETER : 24"

AXIAL DISTANCE FROM FACE OF NOZZLE : 18"

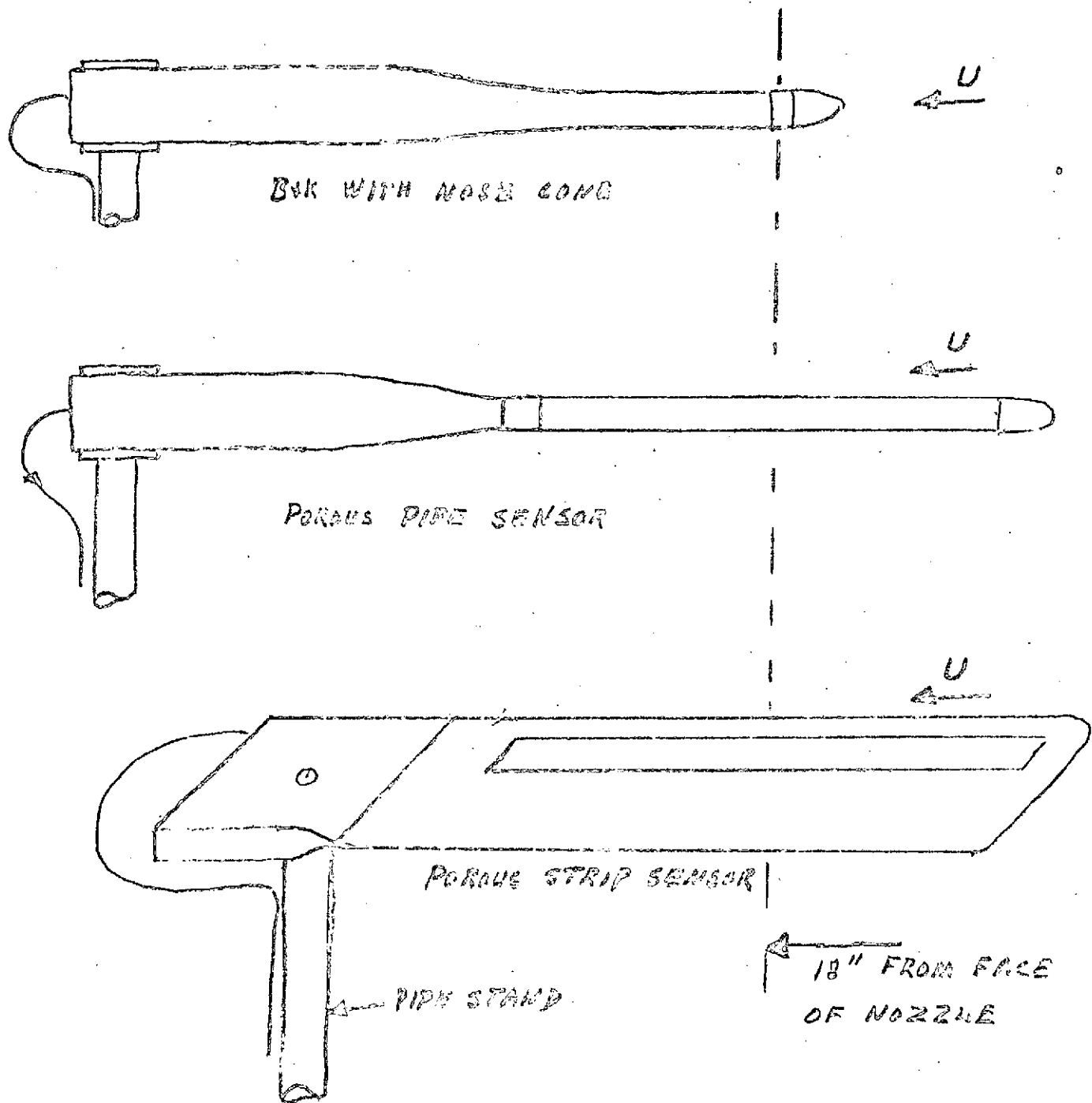


FIG 3 MOUNTING OF EACH SENSOR IN THE FLOW

The tests are made at a single flow velocity of $7\frac{1}{4}$ feet per second, which is the maximum available velocity; since some of the sensor data is limited by electronic noise at this maximum flow velocity, it would have been useless to make tests at lower flow velocities.

For each sensor there are five tests: one test is outside the flow at 18 inches away from the axis and 18 inches from the face of the nozzle; this test gives the acoustic noise generated by the tunnel and the jet and the reverberant level in the reverberant room. The other four tests are in the flow with the center of the sensing surface on the axis of the flow at 18 inches away from the face of the nozzle; the axis of the sensor makes an angle of 0° , 30° , 60° and 90° with respect to the flow.

a. Bruel and Kjaer 1/2 inch Microphone With Nose Cone

The condenser microphone is Type 4133 which, together with Type UA-0052 Nose Cone, gives an acoustic response at random incidence which is almost flat up to 15 kHz. A slight correction of 2 dB at 15 kHz could be added; however, in view of the uncertainty of the incidence the data is presented without any correction for the frequency response of the microphone.

The results are shown in Fig. 3.

b. Porous Pipe Sensor No. 32

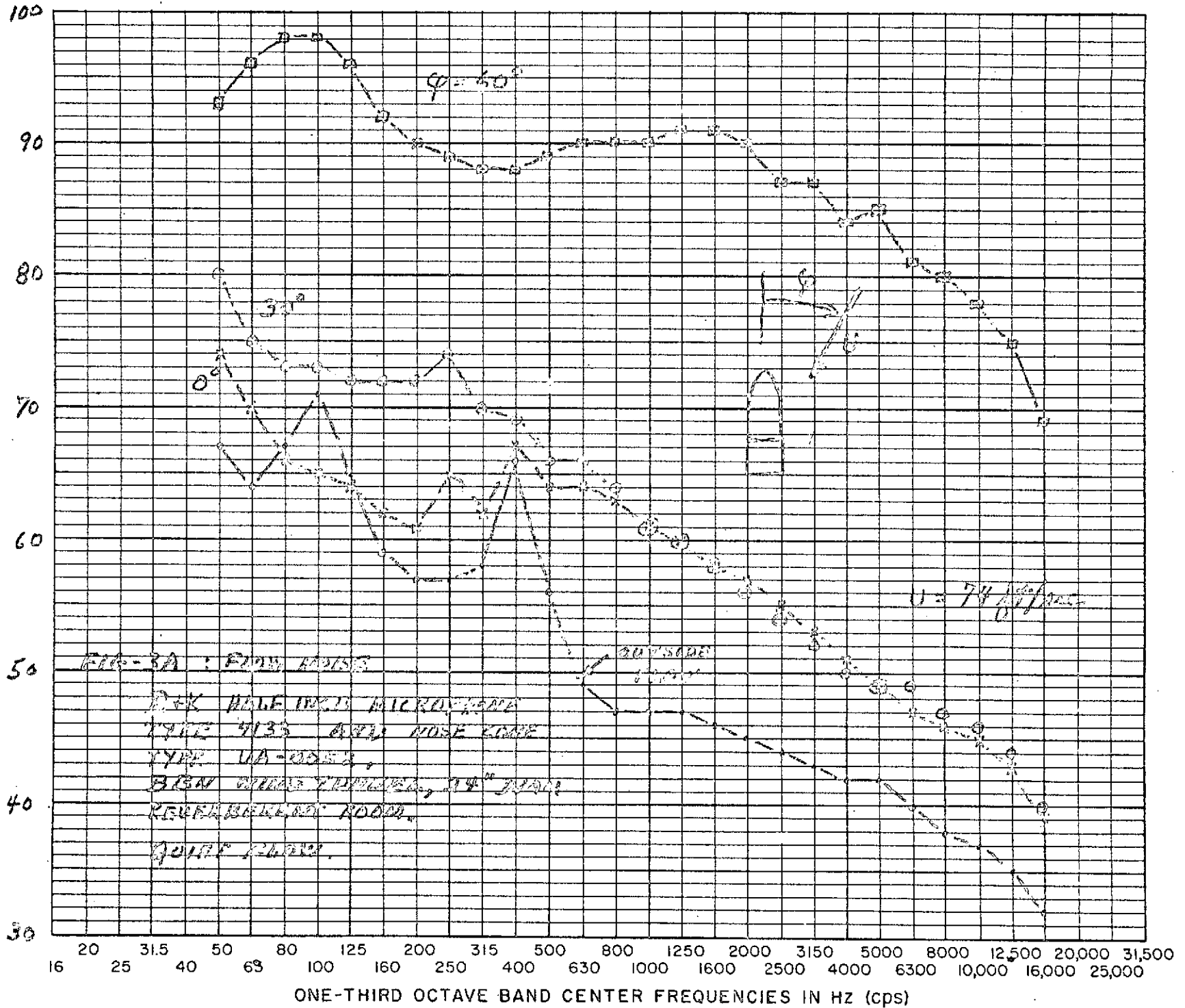
The Porous Pipe Sensor No. 32 was selected amongst the four pipe sensors calibrated and reported in Memo No. 2. This sensor is preferred to original sensor No. 3 because the former one has a smaller drop in frequency response at 10 kHz.

A half inch Bruel and Kjaer microphone type 4134 is inserted at the base of the Porous Pipe Sensor.

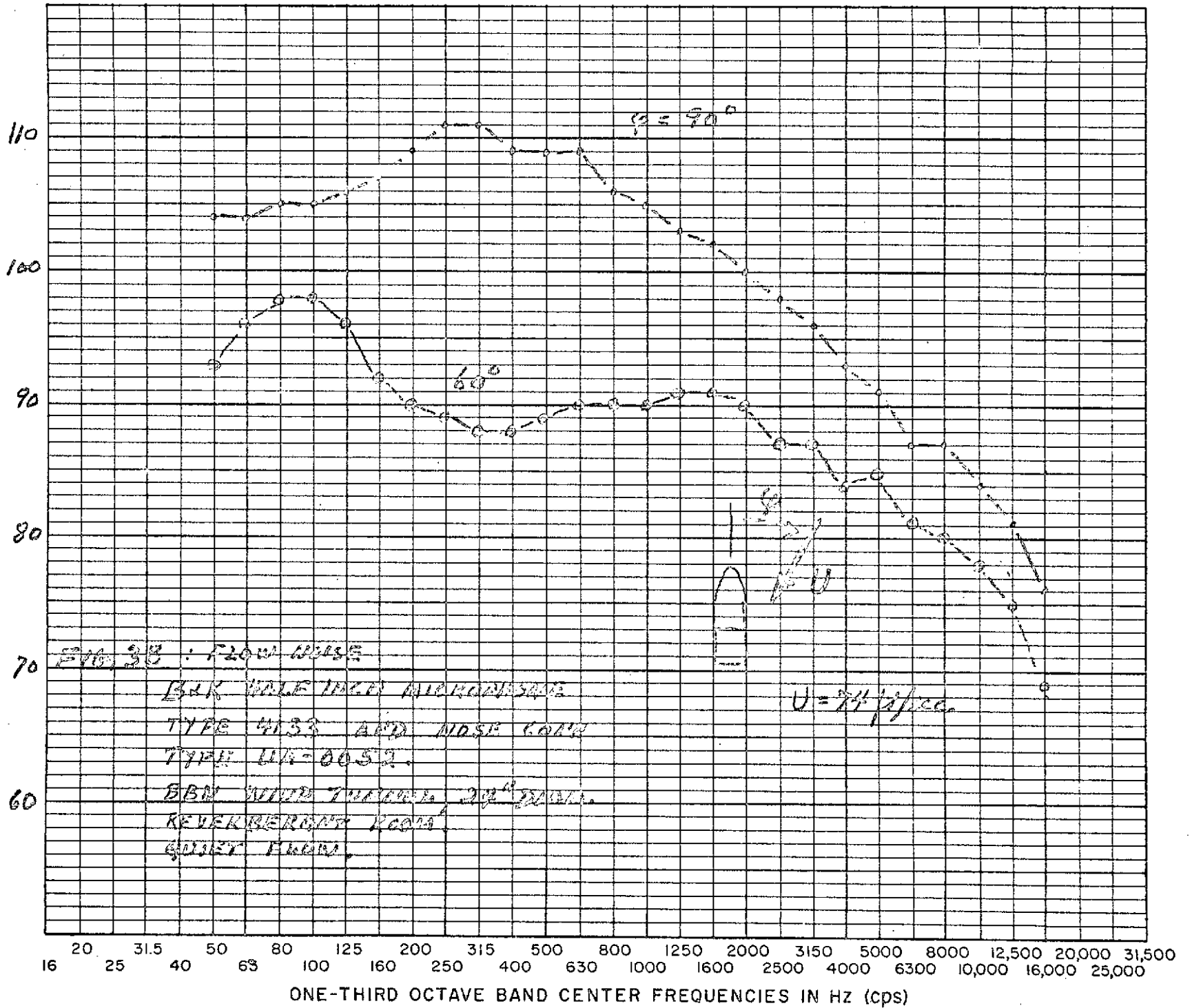
The wind noise data is corrected to equivalent sound pressure levels using the frequency response shown in Memo No. 2.

The results of the five tests are shown in Fig. 4. At frequencies above 4 kHz, the data is limited by electronic noise.

ONE-THIRD OCTAVE BAND SOUND PRESSURE LEVEL IN dB RE 0.0002 MICROBAR



ONE-THIRD OCTAVE BAND SOUND PRESSURE LEVEL IN dB RE 0.0002 MICROBAR



The flow noise is very low at angle of incidence $\phi=0^\circ$. At $\phi=30^\circ$ the flow noise increases considerably; however the spectrum is smooth indicating that the pipe causes some flow separation but that the vortices are not well developed. At $\phi=60^\circ$ and 90° definite vortex streets occur and audible tones are generated. At $\phi=90^\circ$ the first tone is at 400 Hz and its harmonic at 800 Hz, which are shown in Fig. 4. The fundamental tone corresponds to a Strouhal number of

$$\frac{fD}{U_0} = 0.23,$$

where f is the frequency in Hz and D is the diameter of the porous pipe.

Flow separation and the concurrent flow noise is inherent to a simple Porous Pipe Sensor at angles of incidence ϕ greater than a few degrees. At $\phi=0^\circ$ the porous pipe is very quiet.

c. Porous Strip Sensor (Before Modification)

The Porous Strip Sensor is described in Memos No. 4 and 5. A half-inch Bruel and Kjaer microphone Type 4134 is inserted in the sensor. The wind noise data is corrected by the frequency response shown in Memo No. 5, Fig. 1A, to give an equivalent sound pressure.

The results of the five tests are shown in Fig. 5.

The flow noise is consistently low for angles of incidence $\phi=0^\circ$ and 30° . At $\phi=60^\circ$ and 90° vortex shedding occurs and audible tones are generated. These tones are shown in Fig. 5 with fundamentals at 1250 Hz for $\phi=60^\circ$, and 1600 Hz for $\phi=90^\circ$. Harmonics of these tones are also present. These tones appear to be associated with the thickness of the boundary layer.

The Porous Strip Sensor (before modification) is slightly quieter than the Porous Pipe Sensor at $\phi=0^\circ$; it is much quieter than the Porous Pipe Sensor at $\phi=30^\circ$. At $\phi=60^\circ$ and 90° the Porous Strip Sensor could be made quieter than the Porous Pipe

ONE-THIRD OCTAVE BAND SOUND PRESSURE LEVEL IN dB RE 0.0002 MICROBAR

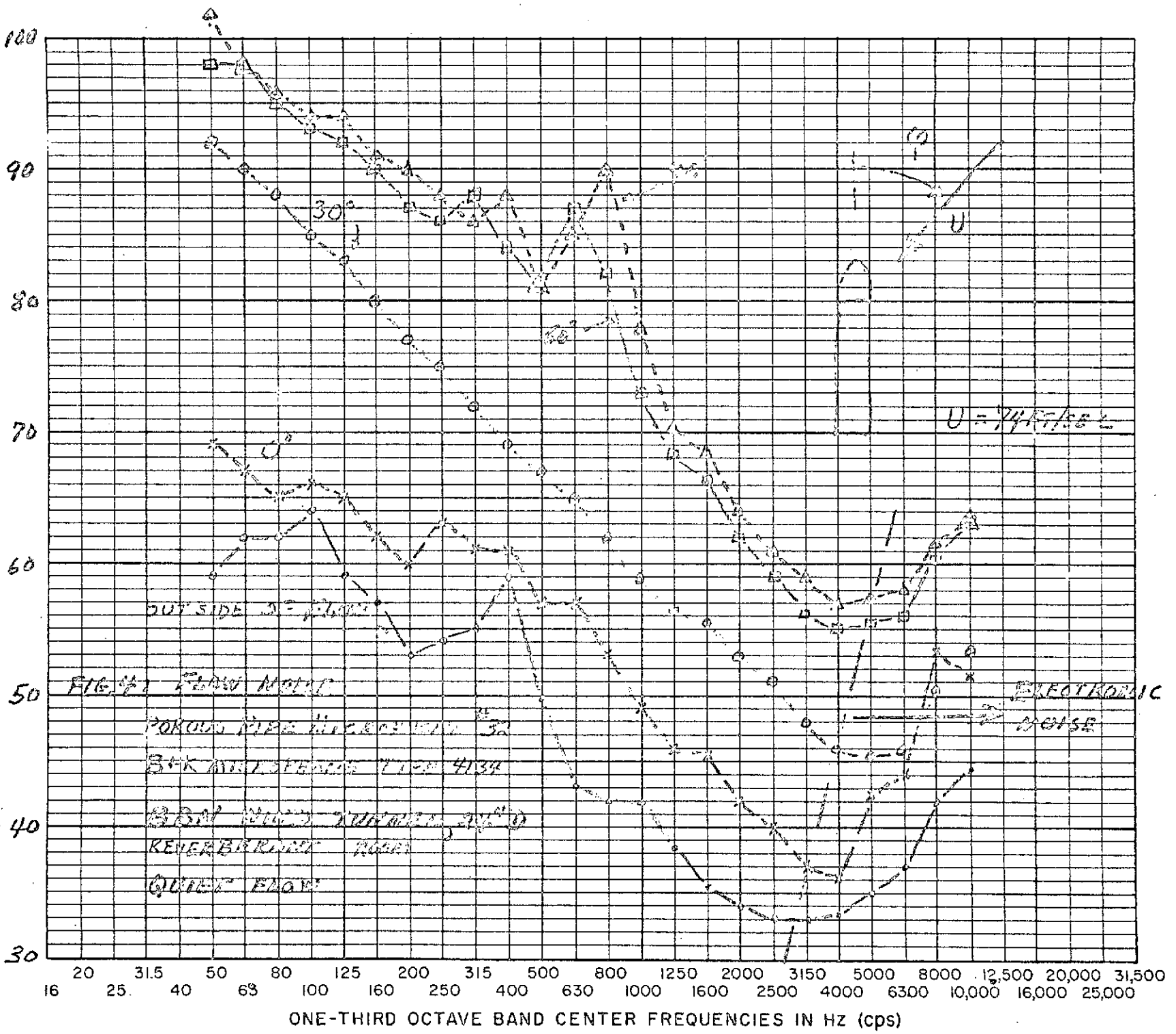
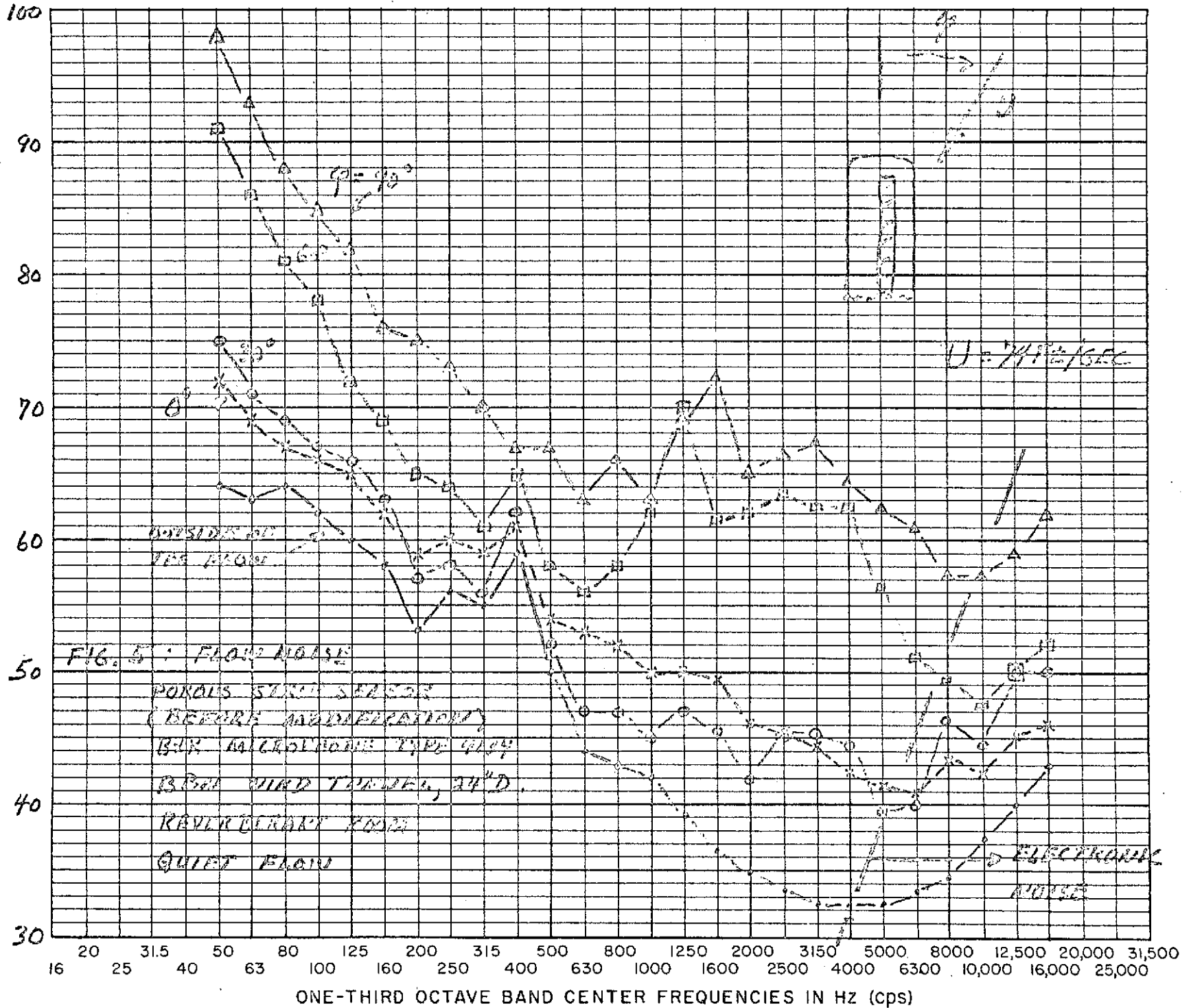


FIG. 47 FLOW NOISE
 POROUS PIPE MICROPHONE 32
 3K WITH FAN TYPE 4134
 BBN WITH TURBINE 4140
 REVERBERANT ROOM
 QUIET ROOM

ELECTRONIC NOISE

ONE-THIRD OCTAVE BAND SOUND PRESSURE LEVEL IN dB RE 0.0002 MICROBAR



by modifying its cross section in order to prevent the flow separation. This has been done and is reported in Part d.

d. Modified Porous Strip Sensor

The results of the preceding Part 3-c suggest that, if the aerofoil of the Porous Strip Sensor is modified to prevent flow separation, the flow noise would be reduced for angles of incidence ϕ of the flow, of 60° to 90° .

A partial correction of the original aerofoil is made by extending its trailing edge; the leading edge, which undoubtedly causes some of the flow separation, was left untouched. This modification reduces some of the flow noise at $\phi \geq 60^\circ$; it does not affect the frequency response as defined in Memo No. 5; it does not affect the directivity of the sensor when the main chord is parallel to the plane of rotation;* (see Fig. 5 of Memo No. 5); it will modify the directivity of the sensor when the main chord is perpendicular to the plane of rotation, (see Fig. 4 of Memo No. 5); however, this last directivity is less important than the first one.

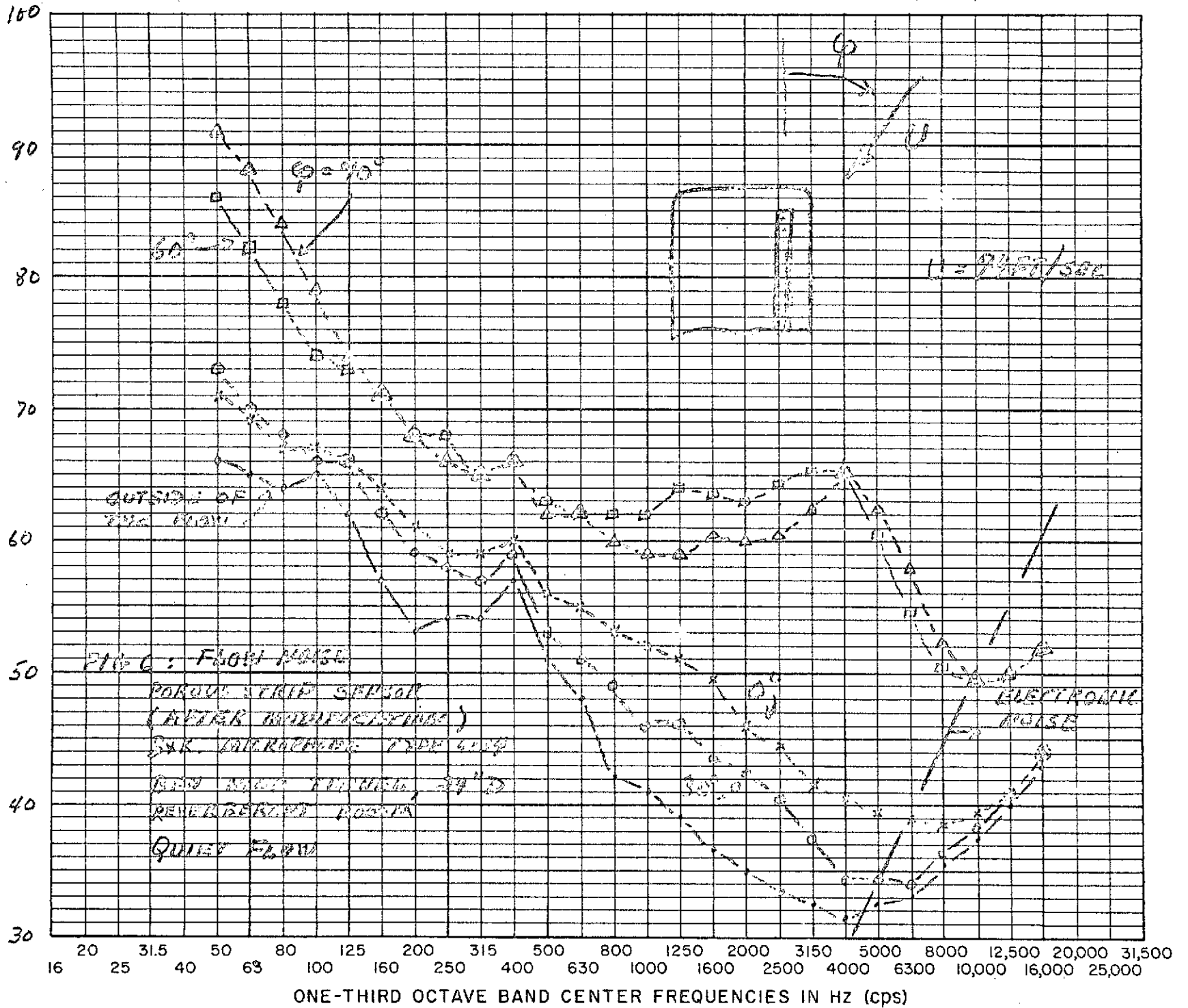
With this modification, which increases the main chord from 2.5 inches to 3.75 inches, the results of Fig. 6 are obtained. These results have been corrected for the frequency response shown in Memo No. 5, Fig. 1A.

Comparing the results of Figs. 5 and 6, it is shown that the noise at $\phi=0^\circ$ and 30° remain very low in both cases. For $\phi=60^\circ$ and 90° , the modified sensor has a lower noise; however some flow separation and its associated higher noise level is still apparent.

The modified Porous Strip Sensor is quieter than the Porous Pipe Sensor at angles of incidence $\phi \geq 60^\circ$, except in the frequency

* The plane of rotation is the plane made by the axis of the flow and the axis of the sensor when it rotated by an angle ϕ .

ONE-THIRD OCTAVE BAND SOUND PRESSURE LEVEL IN dB RE 0.0002 MICROBAR



region of 4 kHz. It is believed that a further modification of the leading edge of the Porous Strip Sensor would eliminate the excess noise in the region of 4 kHz.

4. CONCLUSION

a. Outside of the Flow

The very low acoustic noise generated by the wind tunnel is measured outside of the flow where the pressure field is almost the reverberant field of the room. Since the Bruel and Kjaer microphone with a Nose Cone is essentially omnidirectional for acoustic fields, it will measure the true acoustic pressure of the total reverberant field. In contrast, the porous sensors have a significant directivity and therefore will partially filter out some of the reverberant fields, retaining those components which have zero angle of incidence with the main axis. Hence, the acoustic pressures measured by the porous sensors outside of the flow are progressively lower at higher frequencies than those measured by the single B&K microphone with a nose cone. This is shown in the results of Figs. 3 to 6.

b. In the Flow: $\phi = 0^\circ$

When the angle of incidence $\phi=0^\circ$ inside the flow the porous sensors again have a progressively lower noise at higher frequency, than the B&K microphone with a nose cone. The reason for this difference is again the directivity of the porous sensors which is maintained even at subsonic wavenumbers; hence, the flow noise on the surface of the sensors is filtered out to a large degree.

c. In the flow: $\phi = 30^\circ$

The Porous Strip Sensor is the quietest of the three sensors, especially at high frequencies.

d. In the Flow: $\phi \geq 60^\circ$

At these large angles of incidence the modified Porous Sensors are quieter than the Bruel and Kjaer microphone with a nose cone; however it should be noted that the Bruel and Kjaer system would not be used at large angles of incidence because it is almost omnidirectional; it should always be oriented in the flow for $\phi \approx 0^\circ$.

The modified Porous Strip Sensor is quieter than the Porous Pipe Sensor, except in the region of 4 kHz. Further modification of the trailing edge and possibly of the leading edge of the aerofoils should reduce the flow noise in this frequency region.

APPENDIX 7: WIND TUNNEL TESTS IN A SPOILED FLOW

1. INTRODUCTION

The same tests made with a quiet flow in the BBN wind tunnel and reported in Memo No. 6 are repeated in a turbulent flow at the same maximum average flow velocity of 74 feet per second. The additional turbulence is created by a Flow Spoiler which is described in Section 2.

The purpose of these tests is to show that the porous sensors, which are designed to reject wavenumbers k other than the sonic one k_a ,

$$k_a = \omega/c_a$$

where ω is the frequency and c_a is the acoustic wave velocity, will therefore reject flow noise which, in a given frequency region ω and in subsonic flow, have a wavenumber spectrum which is predominantly subsonic: $k > k_a$.

In contrast the Bruel & Kjaer microphone with a nose cone does not have a significant directivity will hardly reject any flow noise associated with turbulence.

A comparison between the flow noise sensed by the Bruel & Kjaer microphone with a Nose Cone and the flow noise sensed by the porous sensors at $\phi=0^\circ$, in a turbulent flow will show that the first sensor is very much noisier than the latter one. In addition, the Porous Strip Sensor with the modified trailing edge is quieter than the Porous Pipe sensor for $\phi > 0^\circ$.

2. FLOW SPOILER

The purpose of the Flow Spoiler is to increase the turbulent pressure fluctuations in the flow while keeping the acoustic components of the pressure fluctuations at a relatively low level; indeed both components, the subsonic and the sonic components, will be increased but the ratio of the acoustic pressure to the total pressure fluctuations is to be kept small.

The Flow Spoiler consists of a rectangular grid of 1/8 inch diameter steel rods, with 4 inch spacing between rods, to which are soldered small triangular surfaces, their plane being inclined approximately 20° with respect to the flow. One tip of the equilateral triangles points towards the flow, while the side opposite to this tip is perpendicular to the flow*, (see Fig. 1). The array of small triangles covers the face of the nozzle. The Flow Spoiler is clamped on the face of the nozzle.

The Flow Spoiler modifies somewhat the profile of the flow velocity, as shown in Fig. 2, measured at a distance of 18 inches from the Flow Spoiler: the region on nearly constant flow is reduced from a diameter of 18 inches in the free flow (see Fig. 1, Memo No. 6) to a diameter of 16 inches in the spoiled flow. The overall turbulence of the spoiled flow across a section located 18 inches from the face of the nozzle is also shown in Fig. 2; the turbulence in the spoiled flow is roughly 5% compared with 0.3% in the free flow. The frequency spectra, in third octave bands of the velocity fluctuations in the free and in the spoiled flow is remarkably smooth; see Fig. 3.

The relative amount of acoustic noise in the spoiled flow has not been determined directly; it would require a detailed measurements of the spatial correlation of the velocity or pressure fluctuations, and a conversion of the correlation data (by Fourier transformation) into a wavenumber spectrum.

* This design was suggested by H. Heller of BBN.

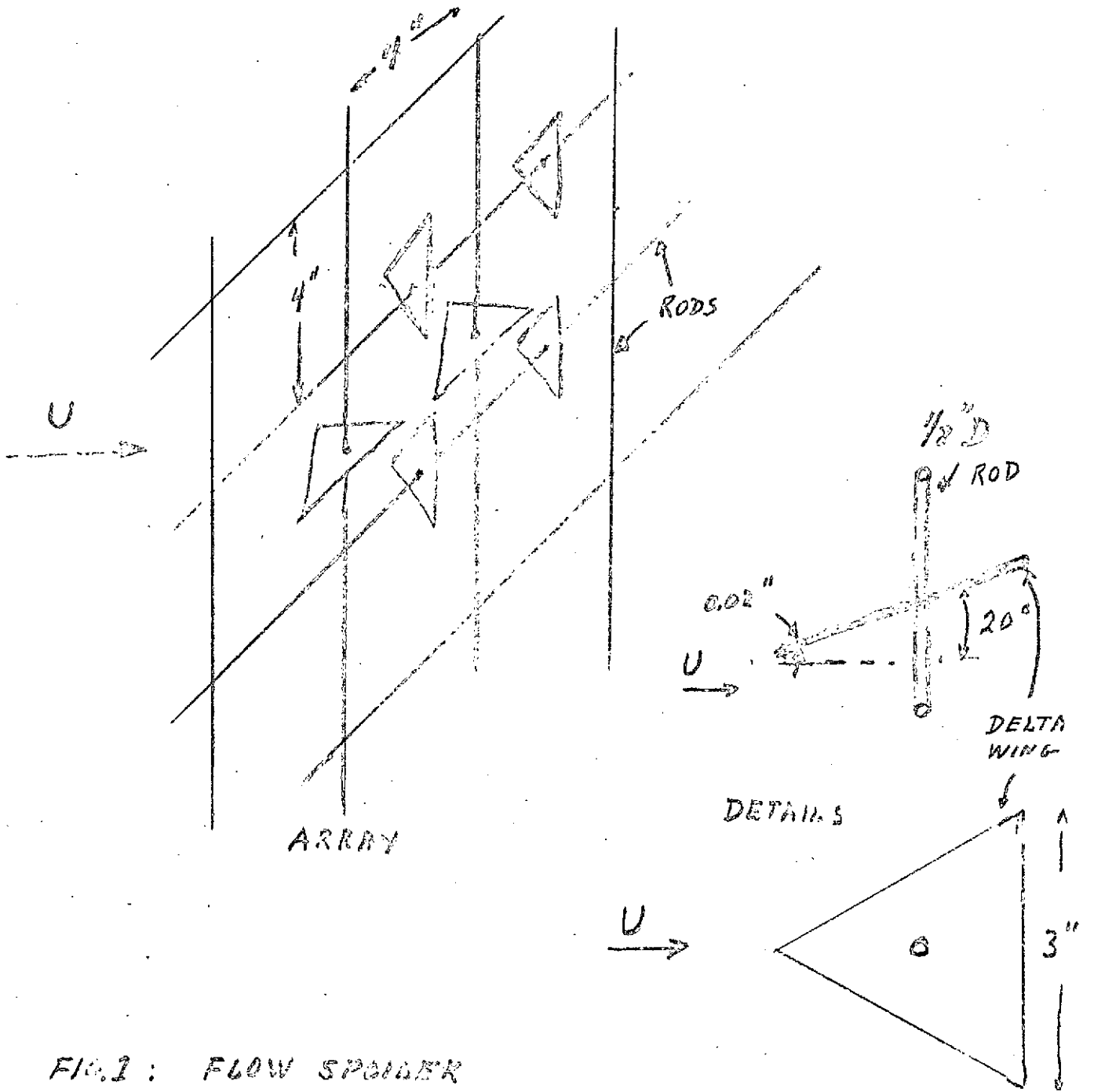


FIG.1 : FLOW SPOILER

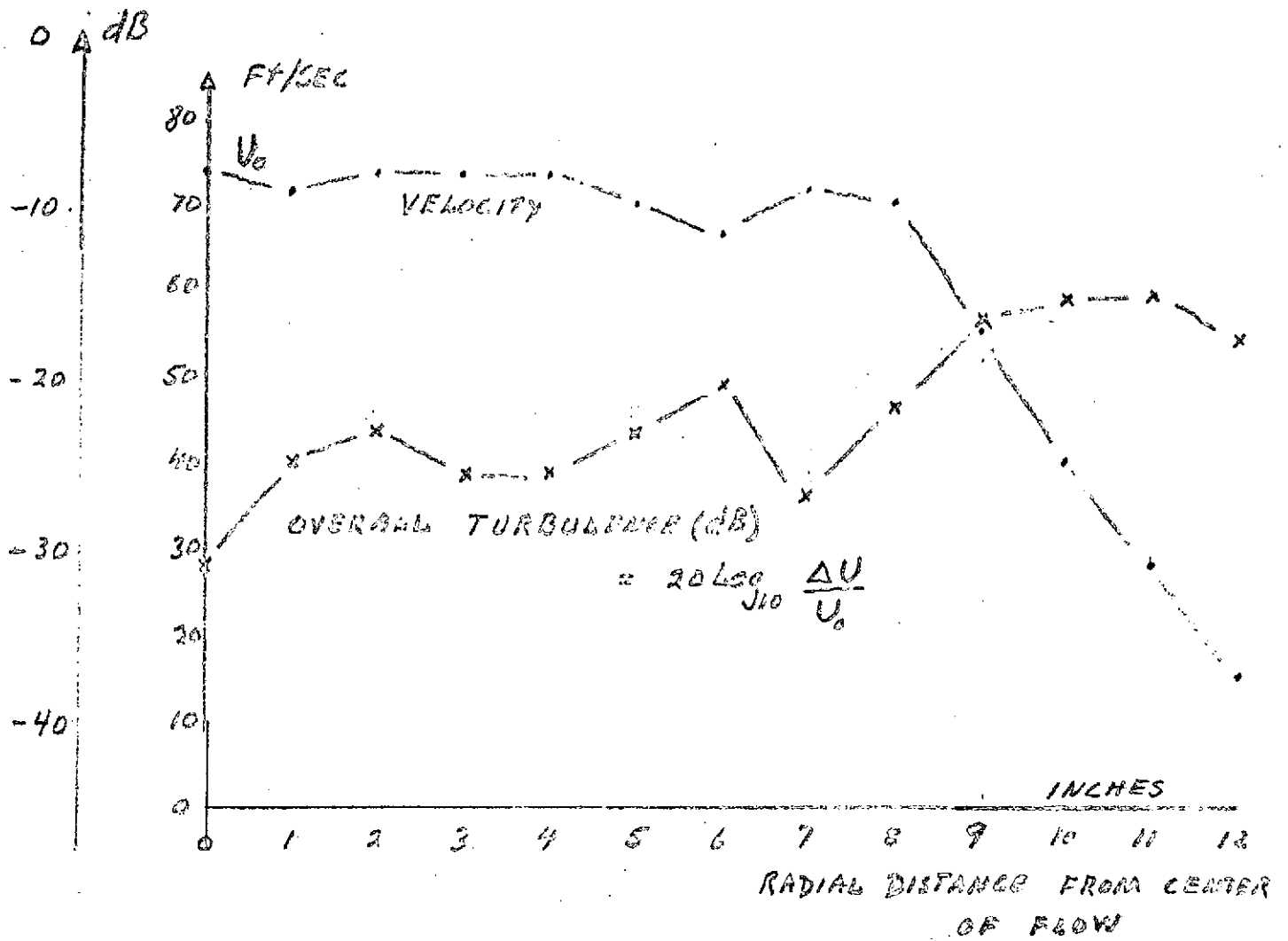


FIG. 2:

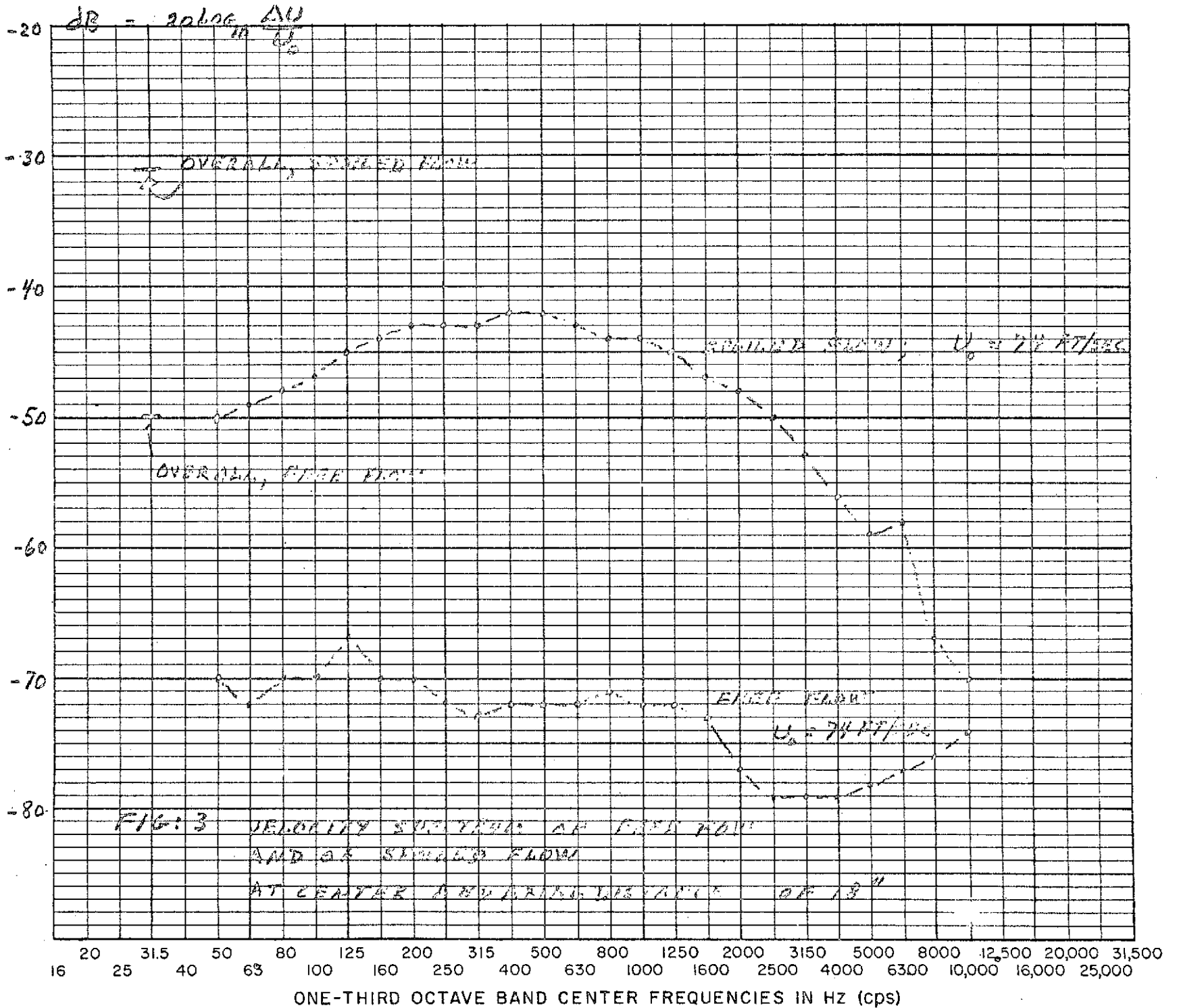
VELOCITY AND TURBULENCE PROFILES

OF SPOILED FLOW OF WIND TUNNEL;

NOZZLE DIAMETER: 24"

AXIAL DISTANCE FROM FACE OF NOZZLE: 18"

ONE-THIRD OCTAVE BAND SOUND PRESSURE LEVEL IN dB RE 0.0002 MICROBAR



The spatial filtering of a porous sensor would eliminate most of the non-acoustic (subsonic) pressure fluctuations while keeping the sonic components which have wavenumbers along the axis of the porous sensors. Therefore, a comparison of the pressure fluctuations measured by a porous sensor and by the B&K microphone with a Nose Cone would reveal the relative amount of acoustic signals, in an approximate way. This is indeed the converse of the purpose of these tests: either the spoiled flow is used to show that the porous sensors have a strong discrimination against subsonic components, or the porous sensors are assumed to have this discrimination and are therefore used to measure the acoustic components of the pressure fluctuations in the flow.

3. RESULTS

Except for the presence of the Flow Spoiler, the conditions of the microphone tests reported here are the same as those stated in Memo No. 6. The Porous Strip Sensor was left in its modified state and tested in this condition.

The results for the three microphones are shown in Figs. 4, 5 and 6.

4. DISCUSSION

a. Outside the Flow

Outside the flow, both the Porous Pipe and the modified Porous Strip Sensors have a lower output than the B&K microphone with a Nose Cone, the difference increasing with frequency. This is due to the directivity of the Porous Sensors.

The Porous Pipe and the modified Porous Strip Sensors have nearly the same output, the Porous Strip Sensor having a slightly smaller output because of its greater directivity.

b. Flow Noise at $\phi=0^\circ$

The flow noise measured by all three sensors is larger than the noise measured outside of the flow. The flow noise measured by the Porous Pipe and by the modified Porous Strip Sensors are equal.

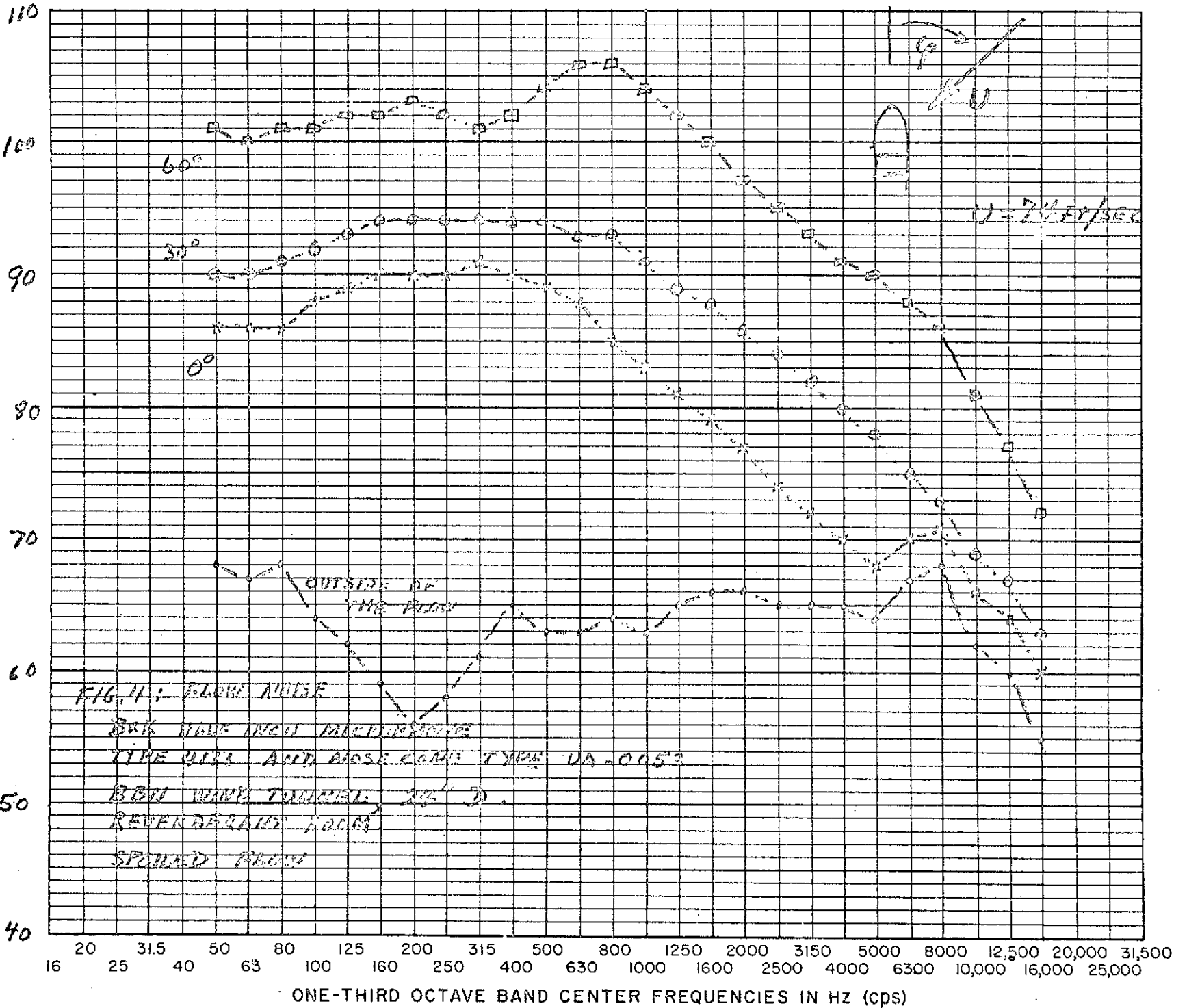
The flow noise measured by the B&K microphone with Nose Cone is dramatically higher than the noise measured by the Porous Sensors. The difference of the noise levels is shown in Fig. 7, in third octave bands. This is the main result of this memo.

The B&K microphone with Nose Cone having a very small sensing surface remains essentially omnidirectional up to high wavenumbers hence; it will measure as well acoustic and non-acoustic pressure fluctuations over a very broad range of wavenumbers.

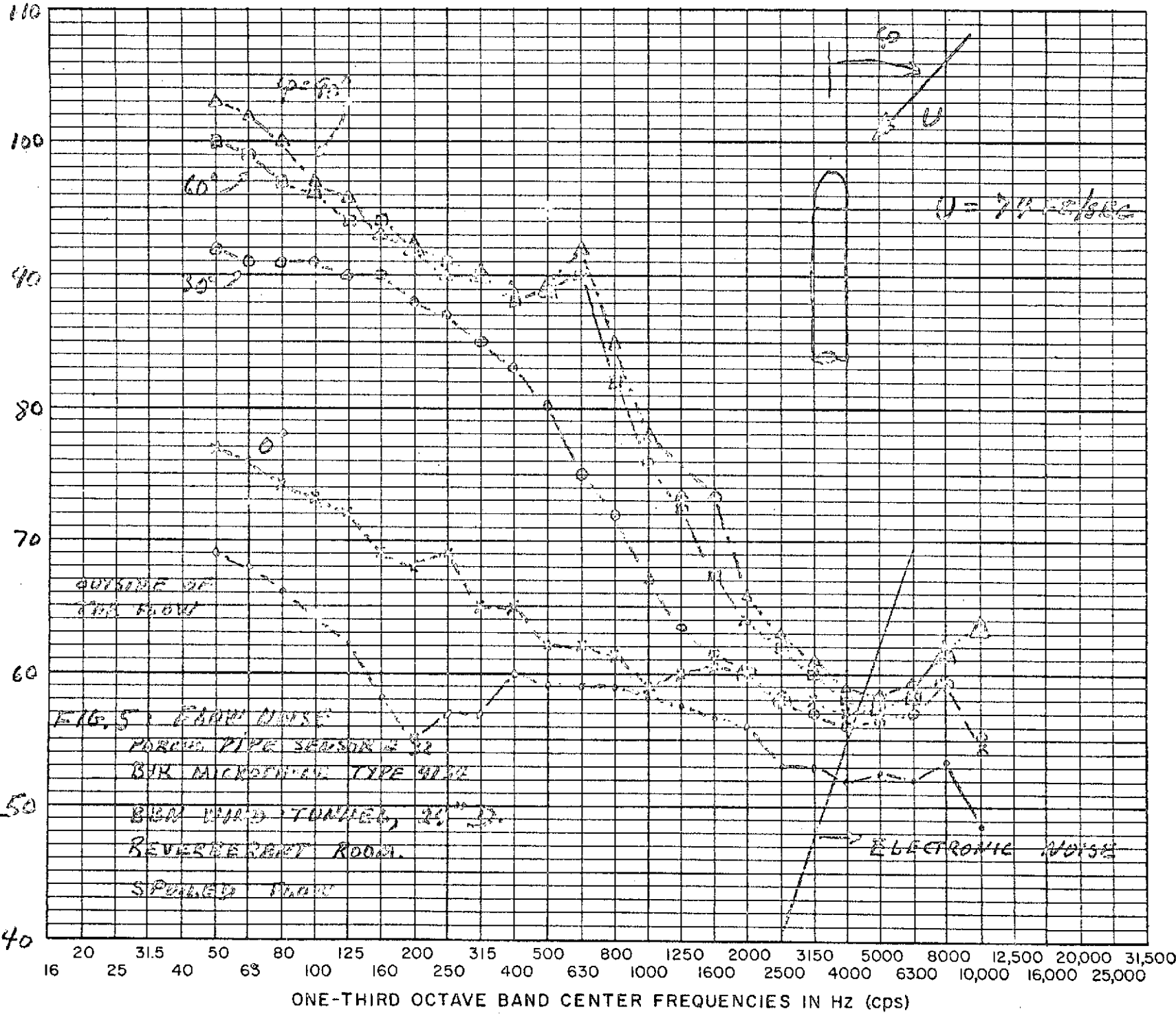
In contrast, the Porous Pipe and the Porous Strip Sensors are designed to accept sonic wavenumbers and reject subsonic wavenumbers; in other words the main lobe of the directivity pattern is centered at acoustic wavenumbers, and the directivity decreases progressively as the wavenumbers increase in the subsonic region. Hence, these Porous Sensors will filter out a major part of the turbulent pressure fluctuations present in the spoiled flow.

The difference in noise levels measured by the B&K microphone with Nose Cone and the Porous Sensors in a turbulent flow depend on the turbulence level and the scale of turbulence of the flow. If the turbulence level is low and its scale is large, the difference in noise levels measured by these two types of sensors will be small because the directivity of the Porous Sensors is not significant at low wavenumbers. The result of Fig. 7 means that in a turbulent flow of the type generated by the Flow Spoiler, the Porous Sensors will very effectively filter out the flow noise, which the B&K microphone with a Nose Cone will not.

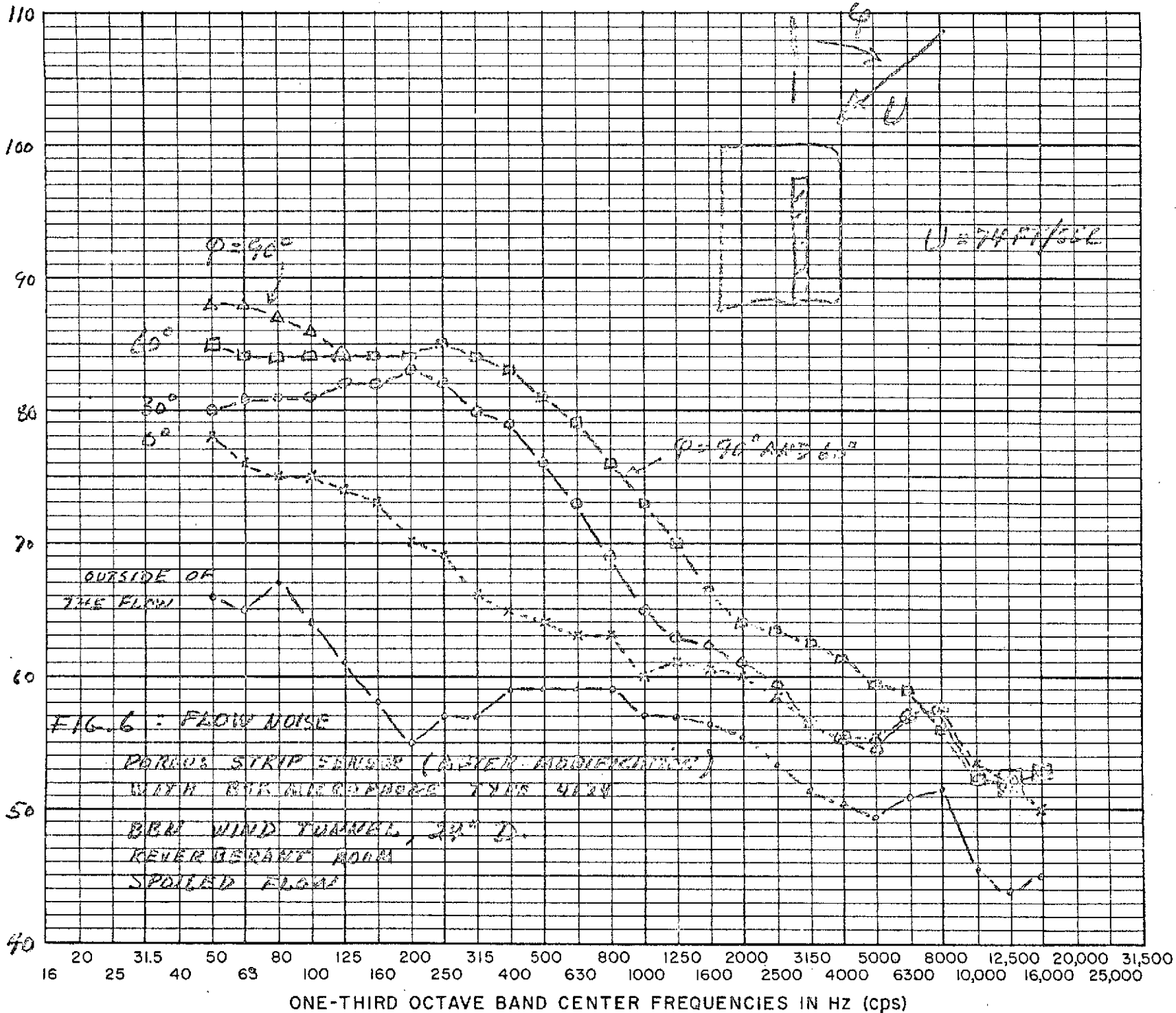
ONE-THIRD OCTAVE BAND SOUND PRESSURE LEVEL IN dB RE 0.0002 MICROBAR



ONE-THIRD OCTAVE BAND SOUND PRESSURE LEVEL IN dB RE 0.0002 MICROBAR



ONE-THIRD OCTAVE BAND SOUND PRESSURE LEVEL IN dB RE 0.0002 MICROBAR



Another way to show that the B&K microphone with Nose Cone tends to measure the total pressure fluctuations is to relate the pressure fluctuations measured by the B&K system to the velocity fluctuations $\Delta U/U_0$ measured by a hot wire anemometer; the frequency spectrum of $\Delta U/U_0$ is given in Fig. 3 for the spoiled flow. The total pressure fluctuation Δp is related to $\Delta U/U_0$ by

$$\Delta p = 2 \Delta U/U_0 (1/2\rho U_0^2)$$

The values of Δp calculated from this equation are compared in Fig. 8 with the pressure spectrum measured by the B&K system at $\phi=0^\circ$. The two curves show a strong correlation. The correlation may have been stronger if the three components of the velocity vector $\Delta \underline{U}$ had been measured (instead of only the axial component) and if a more complete model were used to relate Δp to $\Delta \underline{U}$ than the model given by the equation above.

Finally, the result of Fig. 7 suggests that the Flow Spoiler has been successful in increasing the turbulence level of the flow while keeping the level of acoustic components to a relatively low value.

c. Flow Noise at $\phi=30^\circ$

The B&K microphone with Nose Cone remains very much noisier than the Porous Sensors.

The modified Porous Strip Sensor is generally quieter than the Porous Pipe Sensor, especially at low frequencies up to 1250 kHz. Both are noisier at $\phi=30^\circ$ than at $\phi=0^\circ$ because the filtering action of the porous surface decreases with the angle of incidence of the flow.

d. Flow Noise at $\phi=60^\circ, 90^\circ$

The B&K microphone remains much noisier than the Porous Sensors.

The modified Porous Strip Sensor is significantly quieter than the Porous Pipe up to 1,000 Hz. Above 2 kHz their noise level are nearly equal because (1) the filtering action of each sensor decreases rapidly with angle of incidence and (2) both the Porous Pipe and the modified Porous Strip Sensors create noise of their own in the form of flow separation; moreover it appears that the flow noise sensed by either one of the two Porous Sensors is dominated by the turbulence of the spoiled flow, above 2 kHz.

5. CONCLUSIONS FROM THE TESTS IN THE SPOILED FLOW

1. In a turbulent flow the Porous Sensors can be much quieter than the B&K microphone with a Nose Cone.

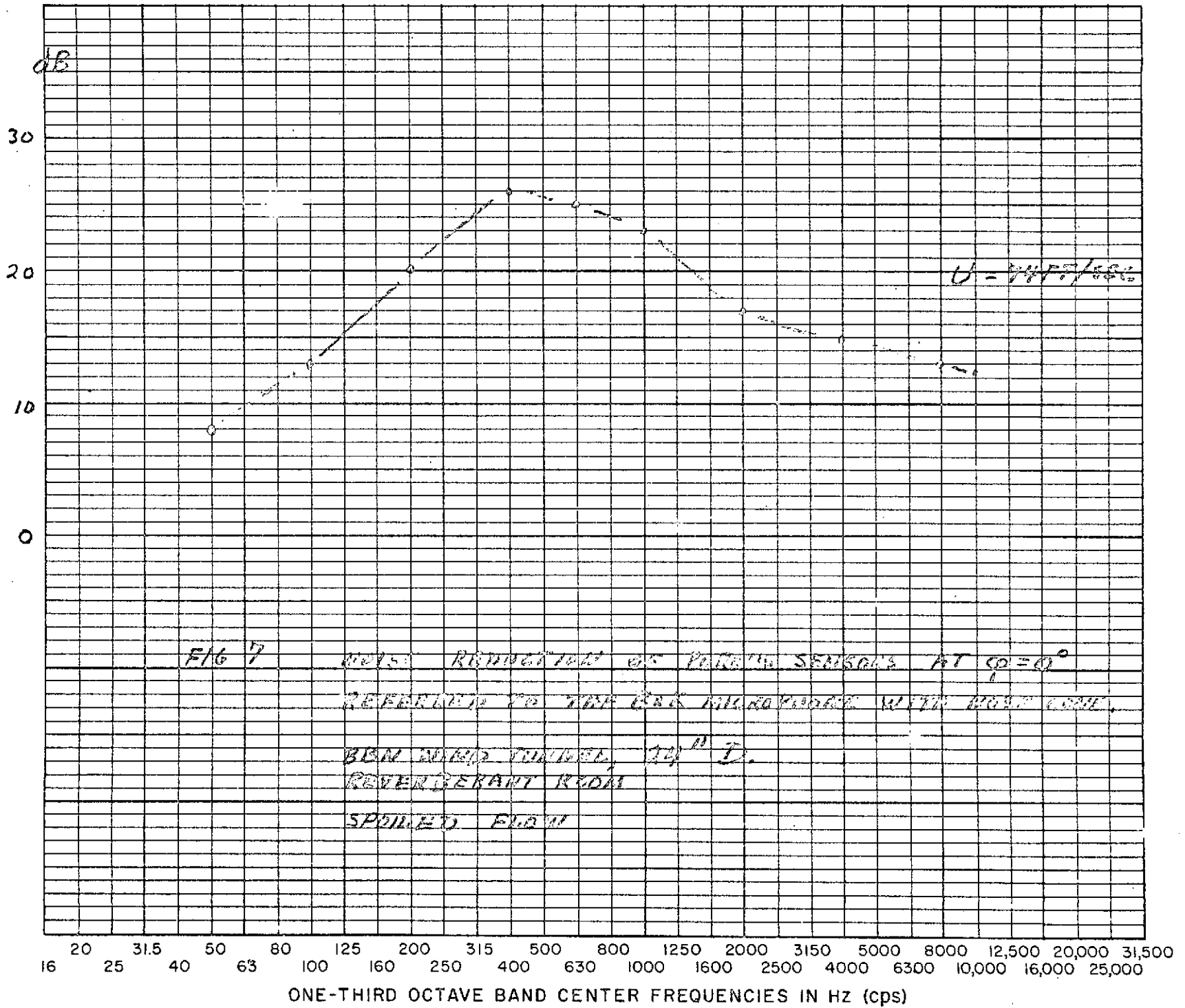
2. If, in the present spoiled flow, the B&K microphone with Nose Cone is operated only at $\phi=0^\circ$ while the Porous Strip Sensor is allowed to be rotated from $\phi=0^\circ$ to $\phi=90^\circ$, the Porous Strip Sensor will be everywhere quieter than the B&K microphone with a Nose Cone.

3. It is anticipated that a further modification of the airfoil of the Porous Strip Sensor will reduce the flow noise sensed at $\phi>60^\circ$, especially in a quiet air flow.

4. The directivity of the Porous Sensors is useful not only for rejecting flow noise but also for measurements in a reverberant room. In an isotropic reverberant field created by a sound source in a reverberant room, the distance from the source where the direct field is greater than the reverberant field is increased by a factor equal to the Directivity Factor¹ of the Porous Sensor.

¹ L.L. Beranek, Acoustics, McGraw Hill Book Co., p. 109.

ONE-THIRD-OCTAVE-BAND-SOUND-PRESSURE-LEVEL-IN-DB-RE-0.00002-MICROBAR



Reproduced from
best available copy.

ONE-THIRD OCTAVE BAND SOUND PRESSURE LEVEL IN dB RE 0.0002 MICROBAR

